

# Near Diffraction Limited High-Power Narrow-Linewidth Er<sup>3+</sup>-doped Fiber Amplifiers

— Developments Towards Laser Sources at 1.5  $\mu\text{m}$  —  
Wavelength for Gravitational Wave Astronomy

Von der Fakultät für Mathematik und Physik  
der Gottfried Wilhelm Leibniz Universität Hannover

zur Erlangung des Grades

Doktor der Naturwissenschaften

**Dr. rer. nat.**

genehmigte Dissertation

von

Dipl.-Phys. Vincent Kuhn

geboren am 12.02.1984 in Hannover

2011

Referent: Prof. Dr. rer. nat. Karsten Danzmann  
Korreferent: Prof. Dr. rer. nat. Michael Oestreich  
Tag der Promotion: 16.12.2011

*für Leo*





## Kurzzusammenfassung

Das Thema dieser Dissertation sind faserbasierte Laserverstärker für einfrequente Signale bei 1,5  $\mu\text{m}$  Wellenlänge. Die Arbeiten erfolgten im Rahmen der Erforschung von Laserquellen für die dritte Generation interferometrischer Gravitationswellendetektoren. Hier wird im Zusammenhang mit der Verwendung von Optiken aus kristallinem Silizium derzeit eine zukünftige Betriebswellenlänge um 1,5  $\mu\text{m}$  diskutiert. Grundanforderung an die benötigten Laserquellen sind hohe Ausgangsleistung bei einfrequentem Betrieb und (nahezu) beugungsbegrenzter Strahlqualität. Die Realisierbarkeit dieser Parameter mit  $\text{Er}^{3+}$ -dotierten Faserverstärkern wurde für die vorliegende Arbeit untersucht. In den Experimenten wurden sowohl nur mit  $\text{Er}^{3+}$ -dotierte Fasern als auch  $\text{Er}^{3+}:\text{Yb}^{3+}$ -kdotierte Fasern verwendet. Letztere haben den Vorteil einer erhöhten Pumplichtabsorption pro Faserlänge. Allerdings können die kodotierten  $\text{Yb}^{3+}$ -Ionen auch zu parasitären Laserprozessen bei 1,0  $\mu\text{m}$  Wellenlänge und damit zu einer Limitierung der möglichen Ausgangsleistung führen. Zudem werden für beide Dotierungsvarianten – mit einer Pumpwellenlänge um 980 nm – deutlich geringere Effizienzen als für  $\text{Yb}^{3+}$ -dotierte Fasern für Verstärker bei 1,0  $\mu\text{m}$  Wellenlänge erreicht.

Vor der Präsentation der Experimente werden wichtige theoretische Grundlagen und Entscheidungskriterien für die Entwicklung von Faserverstärkern vorgestellt und diskutiert. In der Beschreibung der durchgeführten Experimente wird zunächst auf die erstmalige Demonstration einer Leistungsskalierung von  $\text{Er}^{3+}:\text{Yb}^{3+}$ -kdotierten Faserverstärkern mit Hilfe eines zweiten Eingangssignals bei 1,0  $\mu\text{m}$  Wellenlänge eingegangen. Im Anschluss werden Experimente beschrieben, in denen erstmals der relative  $\text{TEM}_{00}$ -Anteil des Ausgangsstrahls einer neuartigen  $\text{Er}^{3+}:\text{Yb}^{3+}$ -kdotierten Multifilament-Kern Faser gemessen wurde. Die Faser wies eine sehr große Modenfläche von ca. 720  $\mu\text{m}^2$  auf und zeigte gleichzeitig einen relativen  $\text{TEM}_{00}$ -Anteil von über 90 %. Beide Werte liegen deutlich oberhalb derer von derzeit kommerziell erhältlichen  $\text{Er}^{3+}:\text{Yb}^{3+}$ -kdotierten Großkernfasern. Desweiteren wurden auch Experimente mit  $\text{Yb}^{3+}$ -freien  $\text{Er}^{3+}$ -dotierten Großkernfasern durchgeführt. Die Leistungsskalierbarkeit bis zu Werten von über 70 W Ausgangsleistung wurde erstmals mit Pumpstrahlung bei 980 nm Wellenlänge demonstriert. Hierfür wurden zunächst Simulationen zur Fasertemperatur im Hochleistungsbetrieb durchgeführt und eine Faserwärmesenke entwickelt. Diese wurde benötigt, um die thermisch empfindlichen Fasermäntel aus fluorinierten Polymeren – welche bei konventionellen Doppelkernfasern eingesetzt werden – vor Überhitzung zu schützen. Zudem wurde für die Experimente dieser Arbeit die erste  $\text{Er}^{3+}$ -dotierte Großkernfaser basierend auf dem Konzept photonischer Kristallfasern realisiert. Faserverstärker wurden basierend auf konventionellen Fasern sowie der photonischen Kristallfaser entwickelt. Ausgangsleistungen von 54 W bzw. über 70 W konnten mit annähernd beugungsbegrenzter Strahlqualität demonstriert werden. Für beide Fasertypen sind dies jeweils Rekordwerte für die genutzte Kombination aus Dotierung und Pumpwellenlänge.

**Schlagwörter:** Laser, Faserverstärker, Erbium-dotiert, einfrequent.

## Abstract

The topic of this thesis are fiber based single-frequency laser amplifiers at 1.5  $\mu\text{m}$  wavelength. The presented developments were made in the framework of the research on laser sources for the third generation of interferometric gravitational wave detectors. Here, the use of crystalline silicon for the mirror and beam splitter substrates is currently under discussion. The use of this substrate material would require a laser wavelength near 1.5  $\mu\text{m}$ . Fundamental requirements on the laser sources are high single-frequency output power levels and (almost) diffraction limited beam quality. The feasibility to reach these properties with  $\text{Er}^{3+}$ -doped fiber amplifiers has been studied in the course of this thesis. Purely  $\text{Er}^{3+}$ -doped as well as  $\text{Er}^{3+}:\text{Yb}^{3+}$ -codoped fibers have been investigated. Fibers codoped with  $\text{Yb}^{3+}$ -ions have the advantage of increased pump absorption per unit length. However, the  $\text{Yb}^{3+}$ -ions can also lead to output power limitations through parasitic emission and laser processes at 1.0  $\mu\text{m}$  wavelength. Moreover, for both dopant variants, the conventional pump wavelength around 980 nm leads to significantly lower values for the amplification efficiency than known from  $\text{Yb}^{3+}$ -doped amplifiers at 1.0  $\mu\text{m}$  wavelength.

First, fundamental properties of fiber amplifiers as well as several important design criteria will be introduced and discussed. Afterwards, experimental results with a novel amplifier scheme which employs an auxiliary seed signal at 1.0  $\mu\text{m}$  wavelength are presented. Using this scheme, significant output power scaling at 1.5  $\mu\text{m}$  wavelength could be demonstrated. Additionally, the spectral dependence on the auxiliary seed wavelength has been investigated. After the treatment of the novel power scaling scheme, experiments with the recently developed  $\text{Er}^{3+}:\text{Yb}^{3+}$ -codoped multifilament-core fibers are described. In these experiments, the fractional  $\text{TEM}_{00}$  content of the multifilament-core fiber output beam has been measured and compared to values obtained with a commercially available large mode area fiber. The multifilament-core fiber had a very large mode area of about 720  $\mu\text{m}^2$  and also surpassed the commercial fiber in terms of fractional  $\text{TEM}_{00}$  content with values above 90 %. Furthermore, also experiments with  $\text{Yb}^{3+}$ -free  $\text{Er}^{3+}$ -doped large mode area fibers have been performed. With a pump wavelength of 980 nm, output power levels up to 70 W have been demonstrated for the first time. For this, simulations of the temperature distribution inside of the fiber at high power levels have been performed and a fiber heat sink has been developed. This heat sink has been used to protect the fluorinated polymer fiber coatings of the conventional double-clad fibers, which are sensitive to elevated temperatures. For further experiments, also the first  $\text{Er}^{3+}$ -doped large mode area photonic crystal fiber has been manufactured. Fiber amplifiers based on conventional as well as the photonic crystal fiber have been realized and respective output power levels of 54 W and above 70 W could be reached with near diffraction limited beam quality. For both fiber types, these are the highest values ever reported for this combination of dopant and pump wavelength.

**Keywords:** Lasers, fiber amplifiers, erbium-doped, single-frequency.





# Contents

<b>1</b>	<b>Introduction</b>	<b>11</b>
<b>2</b>	<b>Laser Sources for Gravitational Wave Detection</b>	<b>15</b>
<b>3</b>	<b>Fundamentals of Optical Fiber Amplifiers &amp; Double-Clad Fibers</b>	<b>19</b>
3.1	Introduction to Waveguide Properties and Basic Design Considerations	19
3.2	Design Criteria for High Power Fiber Amplifiers . . . . .	24
3.2.1	Cross Sections and Optical Efficiency . . . . .	26
3.2.2	Requirements on Pump Source Brightness . . . . .	29
3.2.3	Thermal Considerations . . . . .	31
3.2.4	Feasibility of Fiber Designs . . . . .	35
3.2.5	Beam Quality Degradation . . . . .	40
3.2.6	Stimulated Brillouin Scattering . . . . .	41
3.2.7	Fiber End Facet Damage . . . . .	44
3.2.8	Estimation of Power Scaling Limits at 1.5 $\mu\text{m}$ Wavelength . . . .	45
3.3	Parasitic Emission from $\text{Er}^{3+}:\text{Yb}^{3+}$ -Codoped Fiber Amplifiers . . . . .	52
3.3.1	Introduction to $\text{Er}^{3+}:\text{Yb}^{3+}$ -Codoped Systems . . . . .	52
3.3.2	Numerical Simulations of Parasitic Emission . . . . .	55
<b>4</b>	<b>Experiments with <math>\text{Er}^{3+}:\text{Yb}^{3+}</math>-Codoped Fibers</b>	<b>67</b>
4.1	Experiments with Auxiliary Seed Signal at 1.0 $\mu\text{m}$ Wavelength . . . . .	67
4.1.1	Output Power Scaling with Auxiliary Seed Signal at 1064 nm . . . .	68
4.1.2	Influence of Auxiliary Seed Signal Wavelength Tuning . . . . .	75
4.1.3	Summary of Experiments with Auxiliary Seed Signal . . . . .	79
4.2	Study of Mode Content from Multifilament and Step-Index Fiber Cores	81
4.2.1	Mode Cleaning Cavity Setup . . . . .	83
4.2.2	Fiber Amplifier Setup . . . . .	84
4.2.3	Numerical Simulations of Fiber Mode Contents . . . . .	86
4.2.4	Experiments . . . . .	89

4.2.5	Summary of Mode Content Measurements . . . . .	93
<b>5</b>	<b>Experiments with Yb<sup>3+</sup>-free Er<sup>3+</sup>-doped fibers</b>	<b>95</b>
5.1	Transverse Temperature Distribution . . . . .	96
5.2	Power Scaling and Thermal Loading Experiments . . . . .	99
5.3	Conventional Near Single-Mode Fiber . . . . .	104
5.4	Photonic Crystal Fiber . . . . .	105
5.5	Summary of Experiments with Yb-free Er-doped Fibers . . . . .	111
<b>6</b>	<b>Conclusion</b>	<b>113</b>
<b>7</b>	<b>Outlook</b>	<b>117</b>
	<b>Table of Acronyms</b>	<b>119</b>
	<b>Bibliography</b>	<b>121</b>
	<b>Publications in Peer-Reviewed Journals</b>	<b>139</b>
	<b>Publications in Conference Proceedings</b>	<b>140</b>
	<b>Curriculum Vitae</b>	<b>142</b>
	<b>Danksagung</b>	<b>144</b>

# 1 Introduction

In the first and second generation of interferometric gravitational wave detectors (GWDs) – such as the LIGO (Laser Interferometer Gravitational Wave Observatory), VIRGO, GEO600 and TAMA300 observatories – single-frequency laser sources at 1064 nm wavelength have been used. The choice of this wavelength has been based on a trade-off between wavelength and power dependent sensitivity constraints for the GWD interferometers. Higher power levels as well as shorter wavelengths increase the GWD sensitivity, so that the very high output power levels reachable at 1064 nm led to the choice of this operating wavelength. In these interferometers, fused silica substrates are being used for the mirrors and beam splitters. However, with increasing sensitivity values, thermal noise from the fused silica substrates and their dielectric coatings becomes an increasingly important noise source within the detectors. Due to this, a change of the substrate material from fused silica to crystalline silicon is being considered for the planned third generation of GWD interferometers like, e.g., the Einstein Telescope (ET). Especially under cryogenic cooling conditions, crystalline silicon has superior thermo-optical properties like excellent heat conductivity, low thermal expansion and extremely low residual absorption in its transparency window. However, the spectral position of this absorption minimum lies around 1550 nm wavelength, while the material is not transparent for 1064 nm radiation. Thus, the development of GWD laser sources around 1550 nm wavelength is needed to allow for the realization of GWD interferometers with crystalline silicon based substrates.

In the course of this thesis, the feasibility to realize fiber based single-frequency sources with several 10 watts of output power and near diffraction limited beam quality was studied. For emission around 1550 nm wavelength,  $\text{Er}^{3+}$ -doped fibers need to be employed. With the typical pump wavelength of 980 nm, these fibers usually allow for optical-to-optical efficiency values of only about 20 % to 30 %. Also, the absorption cross section at 980 nm and the possible doping concentration of the  $\text{Er}^{3+}$ -ions are both about one order of magnitude lower than for  $\text{Yb}^{3+}$ -ions. These

## 1 Introduction

facts largely complicate the power scaling of  $\text{Er}^{3+}$ -doped fiber amplifiers compared to  $\text{Yb}^{3+}$ -doped ones. A possible approach to increase the pump absorption is the codoping with  $\text{Yb}^{3+}$ -ions, where a resonant transfer process from the  $\text{Yb}^{3+}$ - to the  $\text{Er}^{3+}$ -ions is exploited. This approach increases the pump absorption per unit length, but introduces new issues like parasitic  $\text{Yb}^{3+}$ -emission, high core numerical apertures and limited refractive index control inside of the fiber core. The experiments of this thesis thus focussed on various subject areas. Several achievements were made with  $\text{Er}^{3+}:\text{Yb}^{3+}$ -codoped as well as  $\text{Yb}^{3+}$ -free  $\text{Er}^{3+}$ -doped fiber amplifiers both in terms of power scaling and beam quality evaluation of novel fiber designs.

In chapter 2, the fundamental requirements and basic concepts of laser sources for interferometric GWD laser sources are discussed briefly. In chapter 3, the fundamental properties of optical fibers and basic design considerations of optical fiber amplifiers are introduced. Subsequently, a more detailed discussion of numerous output power limitations for single-frequency fiber amplifiers is given. Also a comparison of the impact of the treated effects for different active fiber dopants is made. Additionally, a formalism to estimate the maximum output power levels at  $1.5\ \mu\text{m}$  wavelength for different fiber core-to-cladding ratios is derived. Finally, numerical studies of  $\text{Er}^{3+}:\text{Yb}^{3+}$ -codoped fiber amplifiers are presented that allow for a better understanding of the parasitic  $\text{Yb}^{3+}$ -emission at  $1\ \mu\text{m}$  wavelength and its physical origins.

In chapter 4, experiments performed with  $\text{Er}^{3+}:\text{Yb}^{3+}$ -codoped fiber amplifiers are described. First, experiments performed with a novel kind of stabilization scheme are described. In this scheme, an auxiliary seed signal at  $1.0\ \mu\text{m}$  wavelength in addition to the conventional seed signal at  $1.5\ \mu\text{m}$  wavelength is used. This auxiliary signal extracts excess energy from the  $\text{Yb}^{3+}$ -ions and thus inhibits the onset of parasitic laser processes in the  $\text{Yb}^{3+}$ -ion emission band. Different experiments demonstrating significant and stable power scaling at  $1.5\ \mu\text{m}$  wavelength as well as showing the dependence on the wavelength of the auxiliary seed signal are presented. In the second part of this chapter, experiments performed with the recently developed  $\text{Er}^{3+}:\text{Yb}^{3+}$ -codoped multifilament-core fibers are described. In these experiments, the fractional  $\text{TEM}_{00}$  content of the multifilament-core fiber output was analyzed for the first time. The measured values are also compared with the results obtained with a more conventional step-index large mode area core design.

In chapter 5, power scaling and thermal loading experiments with  $\text{Yb}^{3+}$ -free  $\text{Er}^{3+}$ -

doped fiber amplifiers pumped around 980 nm are presented. First, a cooling scheme for high power amplifiers with large quantum defect and its demonstration utilizing an  $\text{Er}^{3+}$ -doped multi-mode fiber with increased pump absorption through a large core-to-cladding ratio are presented. In the following, power scaling experiments performed with a conventional near single-mode large mode area double-clad  $\text{Er}^{3+}$ -doped single-frequency fiber amplifier are described. Finally, experiments with the first large mode area  $\text{Er}^{3+}$ -doped photonic crystal fiber are presented. This fiber has allowed for the highest output power levels and simultaneously highest fractional  $\text{TEM}_{00}$  content of all  $\text{Yb}^{3+}$ -free  $\text{Er}^{3+}$ -doped fibers.

Finally, in chapters 6 and 7, the main results of this thesis are summarized and an outlook on possible future developments and experiments is given.



## 2 Laser Sources for Gravitational Wave Detection

As a fundamental requirement, a laser source suitable for the usage in the current interferometric gravitational wave detector (GWD) concepts needs to have a transversely and longitudinally single-mode output beam. The demand for diffraction limited beam quality is somewhat relaxed by the fact that the higher order TEM modes contained in a laser beam can be filtered out in non-confocal cavities (so-called "mode-cleaners") [1, 2]. These mode-cleaners are generally used before a laser beam enters the actual GWD interferometers. Thus, several percent of power in higher order modes can be tolerated in the current generation of GWD laser sources (see, e.g., Refs. 3 and 4). Nevertheless, to rule out, e.g., excessive amplitude noise of the mode-cleaner throughput and to maximize the optical power inside of the interferometers, low relative and absolute higher order mode power is naturally highly favorable. The requirements on the frequency noise and spectral linewidth properties of the single-frequency radiation are more rigorous. Thus, typically low-noise sources with an initial linewidth of about 1 kHz are employed and afterwards further frequency-stabilized to meet the GWD requirements.

Additionally, very high output power levels are needed in order to reduce the influence of shot-noise in the GWDs (see, e.g., Refs. 3, 5 and 6). Currently, the US based LIGO detectors are equipped with solid state laser systems delivering almost 200 W of frequency-stabilized and mode-filtered cw (continuous wave) output power at 1064 nm [4]. This laser system is considered to be an important contribution for realizing the second GWD generation. The research performed for this thesis was executed in the framework of the laser source development for the planned third generation of GWDs [5, 6]. For this upcoming generation, laser output power levels of up to 1 kW at 1064 nm and up to  $> 100$  W around 1550 nm are under consideration.

Due to the demanding requirements on frequency stability and phase noise, a typical concept for GWD laser sources is the usage of either injection-locked lasers [4] or the master-oscillator power-amplifier (MOPA) scheme [7]. In the injection locking

scheme, the properties of a stable low power laser are transferred to a high power laser by use of active stabilization and feedback techniques. In the MOPA scheme, a relatively low power laser source with the desired output beam quality and spectral properties is amplified to higher output power in one or several single-pass amplification stages. This concept allows for reaching the necessary output power levels, while it is in principle also capable of (in large part) preserving the other characteristics of the initial input – the so-called seed signal. For 1064 nm GWD sources, typically a Nd:YAG based non-planar ring oscillator (NPRO) [8] with up to 2 W of output power is used as initial seed source (see, e.g., Ref. 9). Around 1550 nm, low-noise single-frequency fiber laser systems seem to be suitable candidates for the seed source (see, e.g., Ref. 10).

Optical fibers are especially suitable for MOPA schemes because of their very high single-pass small signal gain values of up to  $> 30$  dB together with low gain saturation power levels. These result from the large product of pump light intensity and long interaction length of pump and signal in the actively doped section of fiber [11]. Thus – in contrast to bulk solid state laser systems – injection-locking schemes are typically not necessary for fiber based systems. Nevertheless, injection-locked fiber lasers have been demonstrated at low power levels [12, 13]. However, the highly reduced system complexity makes fiber based MOPA configurations almost generally preferable.

Up to now, GWD laser sources have been operated at 1064 nm. All of these systems have been based on Nd<sup>3+</sup>-doped yttrium aluminum garnet (YAG) and/or yttrium vanadate (YVO<sub>4</sub>) laser crystals [4, 7, 14]. An important reason for this approach has been the well understood bulk solid state laser technology that allowed for the development of reliable long-term stable high power laser systems. However, further power scaling becomes very challenging for the current GWD laser source output power levels of about 200 W. The maximum diffraction limited output power per utilized laser crystal is limited through effects like thermal lensing aberrations [14, 15]. While an increase of system output power through usage of multiple crystals is possible [4], this approach also implies an increase of system and alignment complexity.

There have also been reports on watt-level bulk solid-state lasers in the spectral range about 1.5  $\mu\text{m}$ . These have been based on, e.g., Er<sup>3+</sup>-doped YAG [16–18] and sesquioxide [19] laser crystals. Compared to typical 1.0  $\mu\text{m}$  systems, resonant pumping around 1530 nm might lead to similar thermal properties for 1.5  $\mu\text{m}$  bulk solid-state lasers. By pumping an Er<sup>3+</sup>:YAG laser with an Er<sup>3+</sup>:Yb<sup>3+</sup>-codoped fiber laser, Kim et



al. [17] could demonstrate up to 60 W of output power at 1645 nm with a  $M^2$  value of  $> 3$ . The output beam quality was limited by thermal lensing effects for high output power levels. With additional efforts and by use of the injection-locking scheme, bulk solid state lasers might become an alternative for fiber based MOPA systems at 1.5  $\mu\text{m}$ . However, the above mentioned limits to power scaling of diffraction limited laser systems at 1.0  $\mu\text{m}$  naturally also apply for 1.5  $\mu\text{m}$  wavelength. Therefore, high power diffraction limited output will typically result in the need for more complex and expensive laser systems compared to fiber MOPA systems with comparable output parameters.



## 3 Fundamentals of Optical Fiber Amplifiers & Double-Clad Fibers

This chapter deals with important properties of optical fibers as well as fiber based amplifiers. First, a general introduction into the waveguide properties will be given in section 3.1. In the following section 3.2, several properties and design criteria of fiber based amplifiers will be discussed in more detail and compared for different active fiber dopants. Finally, the issue of parasitic emission at 1  $\mu\text{m}$  wavelength from  $\text{Er}^{3+}:\text{Yb}^{3+}$ -codoped fiber amplifiers will be treated in special detail in section 3.3.

### 3.1 Introduction to Waveguide Properties and Basic Design Considerations

In conventional optical fibers, light is guided in a region with raised index of refraction, which is called the "fiber core" (see Fig. 3.1). Typical fiber core diameters are in the order of several micrometers, leading to discrete transverse electro-magnetic fiber core modes. The shape, dimension and number of these modes in a specific fiber core can be determined by solving the following differential equation [20]:

$$\frac{d^2F}{d\rho^2} + \frac{1}{\rho} \frac{dF}{d\rho} + \left( n^2 k_0^2 - \beta^2 - \frac{m^2}{\rho^2} \right) F = 0, \quad (3.1)$$

where  $\rho$  is the distance from the fiber core in transverse cylindrical coordinates,  $F(\rho)$  is the transverse electromagnetic field distribution,  $n(\rho)$  is the transverse refractive index distribution,  $\beta$  is the propagation constant (effective index) of a specific fiber mode,  $k_0$  is the vacuum wavenumber at the signal wavelength and  $m$  is an integer parameter giving information on the radial symmetry of the specific resulting fiber modes.

There are also alternative possibilities of creating a fiber core, to which belong periodic lower refractive index structures (photonic crystal fibers [21], leakage channel

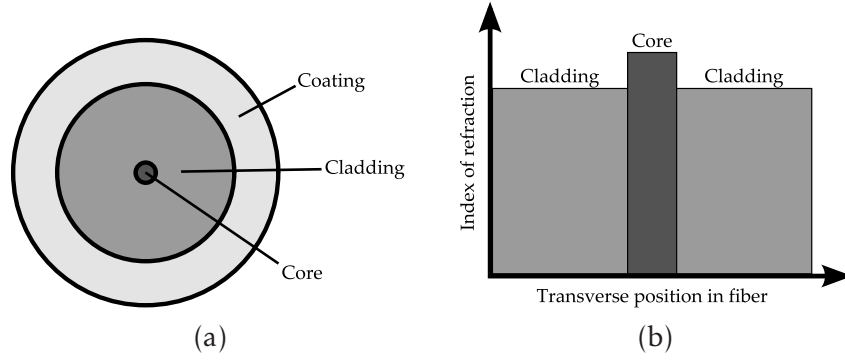


**Figure 3.1:** (a): Schematic depiction of the transverse profile of a step-index optical fiber. (b): Depiction of transverse refractive index distribution in an optical fiber with step-index profile.

fibers [22]) and transverse Bragg structures (Bragg fibers [23, 24]). It is even possible to make a fiber core of optically active material without using any refractive index variations (pure chiral fibers [25]) or use gain guiding instead of index guiding [26].

Conventional step-index fibers are made of fused silica, where the core is made by codoping with rare-earth elements like, e.g., germanium (Ge), boron (B), phosphorous (P) and fluorine (F). Ge and P lead to an increased index of refraction, while B and F lead to a decrease. Also laser active dopants can be brought into the fiber core. The first demonstration of a fiber laser has been as early as 1964 [27]. To date, the most important active fiber dopants are  $\text{Yb}^{3+}$ ,  $\text{Er}^{3+}$  and  $\text{Tm}^{3+}$ -ions with emission at 1  $\mu\text{m}$ , 1.5  $\mu\text{m}$  and 2  $\mu\text{m}$  wavelength, respectively.

The parameters most important for determining the number of potentially guided optical modes in a step-index fiber are the fiber core radius  $r_{\text{core}}$  and the numerical aperture (NA) of the core, together with the wavelength of operation  $\lambda$ . These parameters are used to define the so-called V number as

$$V = \frac{2\pi}{\lambda} \cdot r_{\text{core}} \cdot \text{NA}, \quad (3.2)$$

where the core NA can be calculated from  $\text{NA} = \sqrt{n_{\text{core}}^2 - n_{\text{clad}}^2}$ , with  $n_{\text{core}}$  and  $n_{\text{clad}}$  being the respective refractive indices of fiber core and cladding. The V number is a figure of merit for the number of optical eigenmodes supported by the fiber. For  $V \leq 2.405$  an ideal step-index fiber only supports one – the fundamental – mode [20]. This mode is denoted as  $\text{LP}_{01}$ -mode. Its overlap with a Gaussian shaped mode depends

on the exact fiber parameters [28], but the overlap with the best matched Gaussian-shaped  $TEM_{00}$ -mode typically exceeds 99 %. The small deviation from a perfect theoretical overlap with a Gaussian mode results from the fact that the transverse shapes of the LP-modes are given by composite expressions of Bessel functions  $J_m$  (in the core region) and modified Bessel functions  $K_m$  (in the cladding region). In order to obtain predominant  $TEM_{00}$  output from a conventional step-index fiber laser system the  $LP_{01}$  content needs to be maximized. With increasing V number more and more different modes with little  $TEM_{00}$  mode content can be guided. Further details on higher order modes in step-index fibers can be found, e.g., in Refs. 29 and 30.

Strictly single-mode fibers with active dopants can typically not be realized for core diameters larger than 10 to 15  $\mu\text{m}$ . Increasing the mode area while sustaining single-mode properties implies the reduction of the core NA. This reduction leads to further trade-offs. With conventional manufacturing techniques, the NA can typically not be decreased below respective values of about 0.06 for  $Yb^{3+}$ - and about 0.1 for  $Er^{3+}$ - and  $Tm^{3+}$ -doped step-index fibers. Typical step-index large mode area (LMA) fibers with core diameters of  $> 20 \mu\text{m}$  are not intrinsically single-mode fibers. However, such core diameters typically have to be used for high power fiber systems in order to minimize nonlinear effects. As will be treated in more detail in the course of this thesis, this leads to the need to analyze and optimize the modal content of specific fibers. Also, several novel fiber designs, capable of extending single-mode core sizes, will be discussed.

In high power fiber laser systems, it is often inconvenient to launch the pump radiation directly into the signal waveguide, if an output beam with almost diffraction limited beam quality is needed. In such a scheme, it would be mandatory for the pump radiation to also have near diffraction limited beam quality. Especially diode lasers, which serve as pump source in most fiber laser systems, are to date limited to output power levels of about 1 W from single-mode fibers. However, they can, e.g., emit nearly 1 kW of output power from a 300  $\mu\text{m}$  core diameter fiber with a NA of 0.22 [31]. Therefore, so-called "double-clad" fibers are better suited for (directly diode pumped) high power fiber amplifiers with the requirement of high output beam quality [32, 33]. These fibers are typically coated with special fluorinated polymers that have a lower refractive index than fused silica. Thus, they allow for the pump light to be guided in the fiber cladding instead of the fiber core. As previously mentioned, LMA fiber cores typically have a NA of 0.1 and lower, in order

to allow for large core sizes and simultaneously decent beam quality. In contrast, cladding waveguides mostly have a NA of 0.46 and diameters of hundreds of micrometers. This allows for the coupling of radiation from high power diode lasers whose minimum focal spot sizes are significantly above the diffraction limit. Naturally, the cladding guided pump light can only be absorbed where it is crossing the core during its propagation. Thus, the absorption per unit length scales roughly with  $r_{\text{core}}^2/r_{\text{clad}}^2$ , where  $r_{\text{core}}$  and  $r_{\text{clad}}$  are the respective radii of fiber core and cladding. A more precise prediction can be made by a rigorous numerical calculation of the light propagation in the multi-mode cladding waveguide [34]. This typically leads to a slight decrease of the predicted absorbed power per unit length. It is also noteworthy that in circular fiber claddings light can be guided in helical modes, which have no overlap with the fiber core. This can result in up to several 10 % of non-absorbable pump light [35, 36]. In order to avoid this effect, actively doped double-clad fibers typically have non-circular – e.g., octagonally or D-shaped – pump claddings (see Fig. 3.2(a)). These lead to mode-mixing effects in the pump waveguide which effectively suppress stable guidance in the undesired helical modes [37, 38]. However, for polarization maintaining fibers usually a circular cladding shape can be used, because these fibers incorporate boron-doped elements to introduce mechanical stress into the fiber, which also lead to the required mode-mixing effects.

The value of the  $M^2$  beam quality factor [39, 40] of the multi-mode pump sources is typically considerably larger than 100. Thus, in some fiber laser experiments an impressive improvement by more than a factor of 10000 has been reached when comparing the brightness of the input pump to the output signal radiation [33]. Here, the brightness is defined as the optical power emitted per area and solid angle. Experimental brightness improvements naturally depend on the core to cladding ratio and optical-to-optical efficiency of a specific fiber.

A drawback of the double-clad fiber approach is that the utilized low-index polymers do not have the same mechanical and thermal robustness as typical coatings of single-clad fibers. Therefore, the fiber should, e.g., not reach temperatures above 80 °C [41] in long term operation or be brought into sustained contact with water as this can diffuse into the coating and deteriorate the fiber properties [42]. It is possible to avoid the need for low-index coatings by several approaches. More robust coating materials can be used, when no regard has to be paid to their optical properties. One technique is thus to create an additional multi-mode waveguide – an "inner cladding"

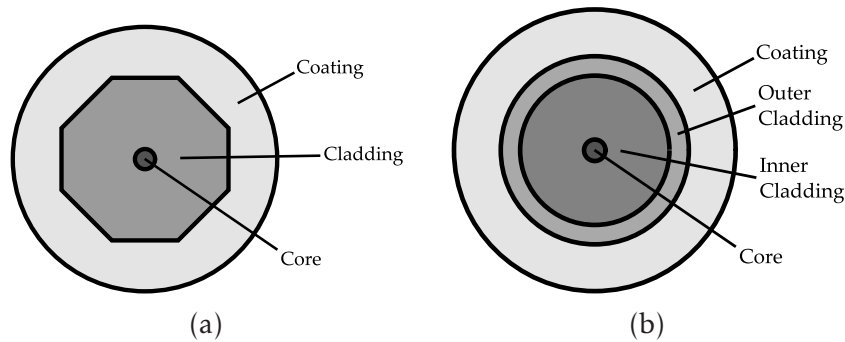


**Figure 3.2:** Depiction of double-clad optical fibers with (a) octagonally shaped pump cladding and (b) all-glass inner cladding pump waveguide.

– around the fiber core via additional fiber doping, as shown in Fig. 3.2(b). However, typically no pump guide NAs larger than 0.22 can be obtained for these fibers as the refractive index of the host glass cannot easily be modified by a larger amount. It is also difficult to make non-circular inner claddings which again can lead to problems with efficient absorption of pump radiation. Another approach for inner claddings is the introduction of a so-called "air-cladding" into the fiber [43–45]. This consists of a ring of several micrometer wide air holes around the inner cladding. These air holes are separated by some hundred nanometers thick glass bridges. The air enclosed in the fiber allows for high NA pump waveguides from about 0.55 up to 0.8 due to its near unity refractive index. The exact value of the pump NA depends on the thickness of the silica bridges. Air-clad fibers with relatively thick bridges and accordingly lowered pump NAs have shown high thermal robustness and are suitable for high power fiber amplifiers [46]. Although the fiber claddings are almost round, the pump absorption is typically not reduced by the presence of helical cladding modes. This has been accounted to the induction of chaotic mode-mixing effects by the sub-wavelength sized air-clad structures [47]. The main drawback of this type of fiber is the impossibility of making robust fusion connections (so-called "splices") to other fibers. The necessary heating would lead to a collapse of the air hole structure and thus to a local destruction of the pump waveguide.

In addition to pumping double-clad fibers with high power diode lasers, it is also possible to pump one fiber laser system by another one operating at a suitable wavelength. This approach is known as "tandem pumping" and allows, e.g., for higher pump brightness in the main amplifier stage and distribution of the overall thermal load on several systems. Also favorable amplified spontaneous emission (ASE) prop-

erties can be achieved by usage of long wavelength high brightness pump lasers [48]. Tandem pumping has shown to be helpful in high power fiber laser systems, but of course leads to an increase in overall system complexity. Nevertheless, this technology is crucial especially in the development of multi-kW high power fiber lasers. Here, optimized distribution of the overall generated heat becomes mandatory due to the extreme power levels and densities [49, 50].

## 3.2 Design Criteria for High Power Fiber Amplifiers

The three main spectral regions of operation for fiber laser systems are around 1  $\mu\text{m}$ , 1.5  $\mu\text{m}$  and 2  $\mu\text{m}$ , which are accessed by doping the active fibers with  $\text{Yb}^{3+}$ -,  $\text{Er}^{3+}$ - and  $\text{Tm}^{3+}$ -ions, respectively. However, even between these more or less well established fiber dopants significant differences in maturity in fiber as well as fiber component fabrication exist. The reasons for this mostly lie in different motivations for the commercial usage of the different active fiber dopants. The commercial interests are, e.g., influenced by the possible optical-to-optical efficiencies with direct diode pumping, the spectral loss properties of fused silica or the relatively eye-safe nature of radiation with wavelengths longer than 1.5  $\mu\text{m}$ .

Due to the low quantum defect,  $\text{Yb}^{3+}$ -doped fibers allow for optical-to-optical efficiencies of more than 80 % with direct diode pumping in a broad absorption region between 915 and 976 nm. The low thermal load per extractable unit of optical power – together with the general superior thermal robustness of the fiber laser concept – has consequently led to massive commercial interest in high power  $\text{Yb}^{3+}$ -doped fiber lasers and amplifiers. This motivated impressive developments in  $\text{Yb}^{3+}$ -doped LMA fiber as well as 915 to 976 nm GaAs diode laser technology. These were in turn a key part for reaching output powers of up to 10 kW from single-mode and even up to 50 kW from multi-mode optical fibers in commercial systems [49, 50]. These output power levels were made possible by using the previously mentioned tandem pumping scheme, in which a fiber amplifier is pumped by another laser source with relatively high brightness. However, also with a direct diode pumped  $\text{Yb}^{3+}$ -doped LMA fiber laser more than 2 kW of output power and near diffraction limited beam quality have been demonstrated [51]. For single-frequency fiber amplifiers, more than 500 W of output power at 1064 nm were demonstrated with near-diffraction limited beam quality by three different groups [52–54].



### 3.2 Design Criteria for High Power Fiber Amplifiers

In the 1.5  $\mu\text{m}$  region, the main commercial motivation for  $\text{Er}^{3+}$ -doped fiber development has been the propagation loss minimum of fused silica at about 1550 nm wavelength [55], which leads to the possibility of operating long-haul optical fiber links for telecommunication purposes. Therefore, sophisticated commercial fibers with extremely low transmission losses (below 0.20 dB/km [55, 56]) and very reliable and well-understood  $\text{Er}^{3+}$ -doped single-mode fibers exist for this spectral region (see, e.g., Ref. 57). However, the technology of high power LMA fibers is far less mature than for  $\text{Yb}^{3+}$ -doped fibers. This is most probably due to the typically far lower achievable optical-to-optical efficiency values, doping concentrations and obtainable pump absorption values per unit length. As a consequence, still substantial work is necessary to identify the best ways to reach the required output parameters of future GWD laser sources in this spectral range. Nevertheless, several approaches for the power scaling of fiber laser systems at 1.5  $\mu\text{m}$  already exist and numerous successful experiments have been performed in the past. These will be covered in more detail in later parts of this thesis.

In years passed, there was a relatively brief period of interest in high power  $\text{Er}^{3+}$ -doped fiber amplifiers for "eye-safe" ranging and directed energy applications. In this context "eye-safe" means that no radiation can be transmitted directly to the human retina. Recently, the interest in these systems has been subsequently shifted to  $\text{Tm}^{3+}$ -doped fiber amplifiers in the 2  $\mu\text{m}$  wavelength range. A main reason for this has been the relatively high optical-to-optical efficiency of about 50 %, achievable with reliable and well understood pump diodes operating at 792 nm. In addition, absorption values of several dB/m without the need for codoping are also a main benefit when compared to systems operating at 1.5  $\mu\text{m}$ . These properties have contributed to the possibility of demonstrating a kW-class fiber laser [58] and more than 600 W of single-frequency output [59] at this also relatively eye-safe wavelength.

The most important fiber properties with regard to power scalability of (near) diffraction limited single-frequency fiber amplifiers are discussed in the following. Also a comparison of 1.5  $\mu\text{m}$  wavelength systems with systems operating in the other two spectral regions is performed. In parallel, quantitative estimates of the contribution of several effects to the output power limitation of fiber amplifiers at given fiber lengths and core sizes are provided. The output power limitations for specific core sizes and fiber lengths are then presented for 980 nm pumped  $\text{Er}^{3+}$ -doped fiber amplifiers in section 3.2.8. This model largely follows the work of Dawson et al. [60], but

is for the first time adapted to 980 nm pumped  $\text{Er}^{3+}$ -doped fiber amplifiers. Compared with the work of Ref. 60, also the treatment of thermal limitations is modified and extended.

The power scaling of systems based on  $\text{Er}^{3+}:\text{Yb}^{3+}$ -codoped fibers is typically limited by parasitic emission at 1  $\mu\text{m}$  wavelength. The occurrence and behavior of this emission depends on several fiber parameters. These are, e.g., the codoping concentration of the  $\text{Yb}^{3+}$ -ions and the  $\text{Er}^{3+}$ -to- $\text{Yb}^{3+}$  doping ratio [61]. Consequently, the power scalability of  $\text{Er}^{3+}:\text{Yb}^{3+}$ -codoped systems cannot be treated easily in a quantitative way. Therefore,  $\text{Er}^{3+}:\text{Yb}^{3+}$ -codoped amplifiers are only treated briefly in the calculations of section 3.2.8, where it is assumed that parasitic emission is overcome by suitable techniques. Some possible suppression schemes are discussed in section 3.3. Here, also the issue of parasitic emission at 1  $\mu\text{m}$  wavelength is treated in detail for exemplary fiber parameters. Accordingly, the idea of section 3.3 is to give a fundamental understanding of the parasitic emission's origins, as well as to introduce ways to suppress it to some extent.

#### 3.2.1 Cross Sections and Optical Efficiency

Due to the low quantum defect of only slightly more than 10 %,  $\text{Yb}^{3+}$ -doped fiber amplifiers have successfully been operated with optical-to-optical efficiencies of up to about 80 %. However, typical efficiency values are often slightly lower. Nevertheless, limited commercially available pump power is today no longer an inhibiting factor for the power scaling of  $\text{Yb}^{3+}$ -doped single-frequency MOPAs. Representative absorption and emission cross sections for  $\text{Yb}^{3+}$ -doped glass fibers are shown in Fig. 3.3(a). The level scheme of  $\text{Yb}^{3+}$ -doped fibers is relatively simple and involves only the  $^2\text{F}_{7/2}$  ground and  $^2\text{F}_{5/2}$  excited level manifolds [62]. The absorption at 976 nm is – depending on the exact composition of the host glass – typically more than three times higher than at 915 nm. However, this spectrally narrow higher absorption peak with only about 5 nm FWHM (full width at half maximum) is relatively challenging to exploit to full extent, because of increased demands on spectral width and stability of the used pump sources.

High power  $\text{Tm}^{3+}$ -doped fiber laser systems are typically pumped with 790 nm radiation. Here, a cross relaxation process is exploited that results in the creation of two photons at 2  $\mu\text{m}$  wavelength from only one photon at 790 nm. This mechanism leads

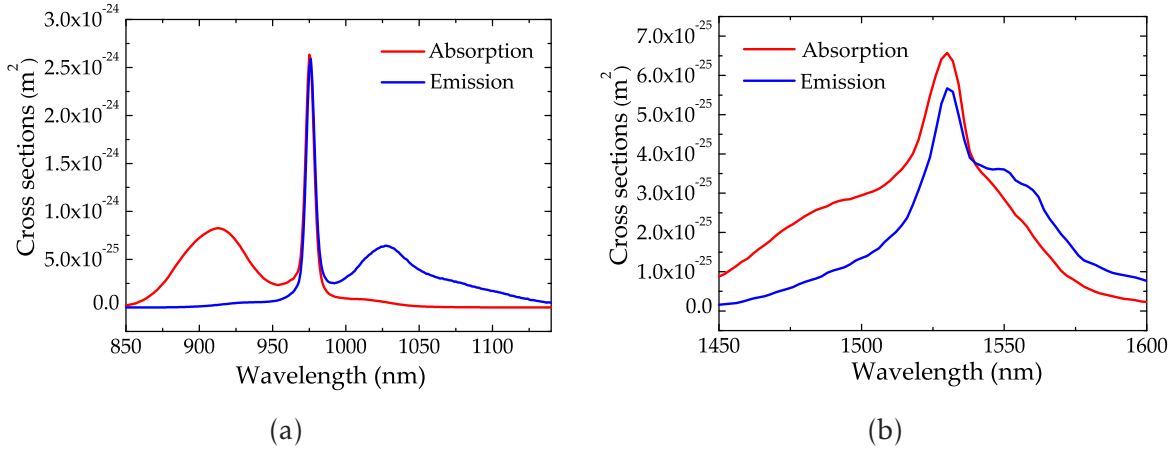


**Figure 3.3:** (a): Absorption and emission cross sections of Yb<sup>3+</sup>-doped germanosilicate fibers. (b): Absorption and emission cross sections of Er<sup>3+</sup>-doped aluminophosphosilicate fibers. The data has been taken from Refs. 62 and 63, respectively.

to a quantum efficiency above unity and decent direct diode pumping efficiencies of about 50 % [64].

As an example for typical cross sections of Er<sup>3+</sup>-ions, data from aluminophosphosilicate glass is shown in Fig. 3.3(b). The level scheme of the manifolds most important for the 1.5  $\mu\text{m}$  laser transition is shown in Fig. 3.4. In comparison with Tm<sup>3+</sup>- and Yb<sup>3+</sup>-ions the feasible doping concentration of Er<sup>3+</sup>-ions in glass is about a magnitude lower, if suitable optical-to-optical efficiencies of at least 20 to 30 % are to be reached. The main reason for this is the tendency of Er<sup>3+</sup>-ions to form detrimental clusters during the doping process [65–67]. The probability for this process increases nonlinearly with the average doping concentration of the ions. Inside of the clusters, an ion-ion interaction process, in which energy is transferred from one excited ion to another already excited counterpart, is highly efficient. By this, one ion returns to its <sup>4</sup>I<sub>15/2</sub> ground state, while the other one briefly doubles its excitation energy before returning to the <sup>4</sup>I<sub>13/2</sub> state on a  $\mu\text{s}$ -scale. As the desired laser process takes place on the ms-time scale of the Er<sup>3+</sup>-ions' fluorescence life time, this upconversion process is a quasi instantaneous loss mechanism for the laser process. All ions bound inside of an individual ion cluster – which typically are significantly more than just one interacting pair [66] – are subject to this parasitic ion-ion interaction. Effectively only one of these ions can be excited at a given time without almost instantaneously losing its excitation energy. Another parasitic effect that increases nonlinearly with the Er<sup>3+</sup> doping concentration is excited state absorption from the Er <sup>4</sup>I<sub>13/2</sub> level [67]. As ex-

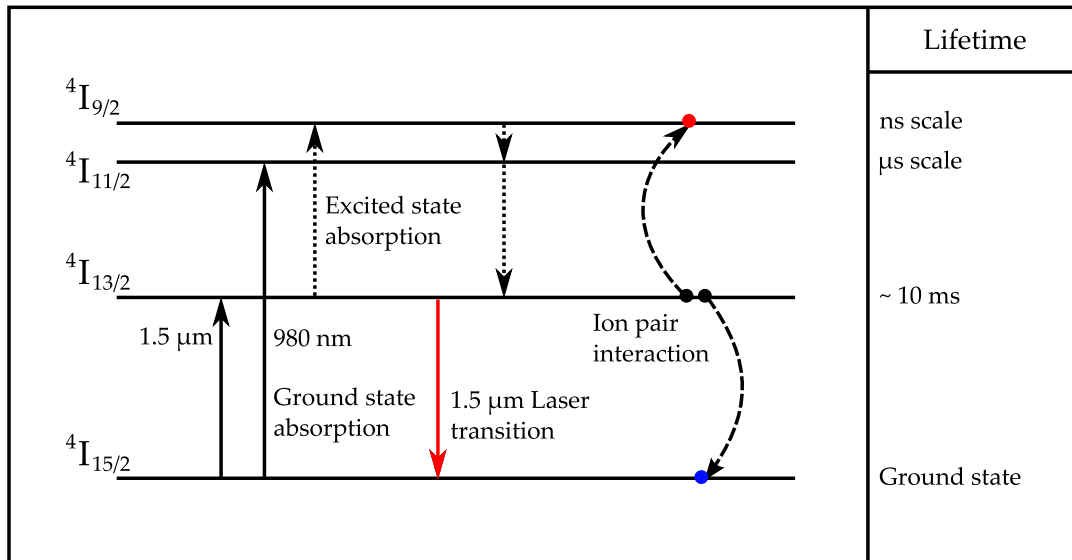


**Figure 3.4:** Depiction of simplified level scheme and important transitions of  $\text{Er}^{3+}$ -ions. Shown are the manifolds and transitions most important for laser emission at  $1.5 \mu\text{m}$  wavelength together with their characteristic lifetimes.

cited state absorption also leads to the excitation of energy levels with short lifetimes, both effects lead to a non-bleachable loss component in fibers with clustered ions.

The upconversion induced loss adds to the quantum defect of the optical pumping process, which leads to typical optical-to-optical efficiencies of about 30 % for 980 nm pumping and moderate doping concentrations. The reduction of the optical efficiency with increasing doping concentration can be seen in Fig. 3.5 [68]. Here, the results of amplifier experiments with  $\text{Er}^{3+}$ -doped single-clad fibers with different doping concentrations are presented. The input seed and pump power levels were held constant at 45 mW at 1556 nm and 1.7 W at 1480 nm, respectively. The small signal core absorption value at 1530 nm varied from 30 to 110 dB/m in the used fibers (first number in the legend of Fig. 3.5). The amplifier length was varied by subsequently cutting back the active fibers from initially slightly longer than optimum efficient lengths. It can be clearly observed that the maximum obtainable amplified signal output decreases with increasing core absorption and, hence, doping concentration. It is also interesting to note that two fibers with identical small signal core absorption but different core diameters showed differences in their overall efficiency values. The  $4 \mu\text{m}$  core diameter version of this fiber (Er80-4/125) showed clearly higher optical-to-optical efficiency than the version with  $8 \mu\text{m}$  core diameter (Er80-8/125). This underlines the importance of optimized fiber core compositions

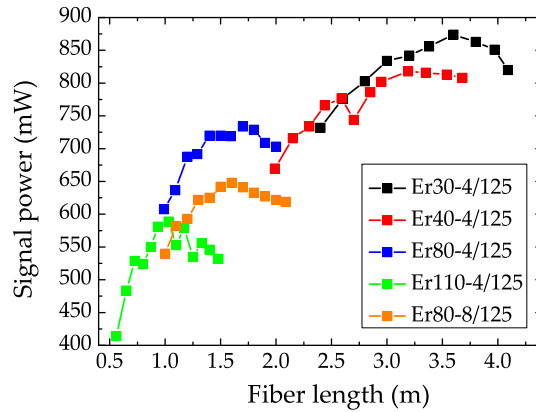


**Figure 3.5:** Output power levels of single-frequency fiber amplifiers with different Er-doping concentration and varied fiber length. The input seed and pump power levels were 45 mW at 1556 nm and 1.7 W at 1480 nm, respectively. The data of this graph has been taken from Ref. 68.

and shows that the optical efficiency does not depend on the  $\text{Er}^{3+}$ -ion concentration alone.

An especially important codopant in typical  $\text{Er}^{3+}$ -doped fibers is Aluminum (Al). The efficiency of  $\text{Er}^{3+}$ -doped fibers is typically optimized by codoping them with Al, as this reduces the extent of cluster formation [63]. Therefore, typical  $\text{Er}^{3+}$ -doped fibers – and also the ones used to obtain the data of Fig. 3.5 – use aluminosilicate host materials for optimized optical efficiency and absorption. However, codoping with Al increases the refractive index of the fiber core, which is part of the difficulty to make efficient  $\text{Er}^{3+}$ -doped fiber cores with NAs smaller than 0.1 [69]. In  $\text{Er}^{3+}$ -doped fibers the described limitations in possible doping concentration coincide with the relatively low absorption cross sections. When compared to  $\text{Tm}^{3+}$ - and  $\text{Yb}^{3+}$ -doped fibers with similar core to cladding ratio, these two effects lead to an about two orders of magnitude lower pump absorption in  $\text{Er}^{3+}$ -doped double-clad fibers.

### 3.2.2 Requirements on Pump Source Brightness

The brightness of a laser source is defined as the emitted optical power divided by the size of the emitting area and the irradiated solid angle. Thus, it has the dimension of  $\text{W}/(\text{Sr} \cdot \text{m}^2)$ . When pumping fiber laser systems with diode lasers, mostly a passive delivery fiber is used to facilitate the pump coupling and homogenize the pump

beam. Therefore, the brightness of the pump source is typically defined by the diameter and numerical aperture of this delivery fiber. High power diode laser bars have elliptical output beams with unequal beam quality on their respective fast and slow axis. The beam quality behind the delivery fiber is largely determined by the worse slow axis beam quality of the emitting diode laser. This is due to the necessity for a fiber core diameter suitable for an efficient diode-to-fiber radiation transfer for both axes. Inside of the delivery fiber, mode-mixing effects occur so that after several meters of propagation the beam quality of all axes is comparable to the slow axis beam quality of the initial diode laser (see, e.g., Ref. 33). In the experiments of section 5, a high power diode laser source was used that emitted up to 500 W at 976 nm out of a delivery fiber with 200  $\mu\text{m}$  diameter and NA of 0.22. The solid angle  $\Omega$  illuminated by this fiber is related to its NA by  $\Omega = \pi \cdot \text{NA}^2$ . This leads to a calculated brightness value of

$$b_{\text{pump}} = \frac{500}{(100^2 \cdot \pi) \cdot (\pi \cdot 0.22^2)} \frac{\text{W}}{\text{Sr} \cdot \mu\text{m}^2} = 0.105 \frac{\text{W}}{\text{Sr} \cdot \mu\text{m}^2}, \quad (3.3)$$

which is used in calculations of section 3.2.8. This value is assumed to be the current upper limit for commercially available high power diode lasers. Thus, if this brightness value has been reached, the available output power can only be scaled up by increasing the emitter size – i.e., using delivery fibers with larger core diameters and worse beam quality. Thus, for delivery fibers of different diameters, the highest available diode laser module output power levels vary, while the corresponding source brightness values typically remain roughly constant.

In general, the pump brightness limited output power of a fiber laser system can be estimated as follows [60]:

$$P_{\text{brightness}} = \eta_{\text{laser}} \cdot b_{\text{pump}} \cdot (\pi \cdot r_{\text{clad}}^2) \cdot (\pi \cdot \text{NA}_{\text{clad}}^2), \quad (3.4)$$

where  $\eta_{\text{laser}}$  is the optical-to-optical laser efficiency and  $\text{NA}_{\text{clad}}$  and  $r_{\text{clad}}$  are NA and radius of the active fiber's pump cladding, respectively. The pump brightness limited output power scales thus linearly with the laser efficiency, the available pump brightness, the cladding area and the squared numerical aperture of the pump cladding. To be able to determine the pump brightness requirements for a given core size and fiber length, it is convenient to express the pump cladding radius  $r_{\text{clad}}$  in terms of these quantities. With a known core absorption per unit length  $\alpha_{\text{core}}$ , the correspon-

ding approximate absorption of cladding launched light  $\alpha_{\text{clad}}$  is given by:

$$\alpha_{\text{clad}} = \alpha_{\text{core}} \cdot \frac{r_{\text{core}}^2}{r_{\text{clad}}^2}. \quad (3.5)$$

Please note that by using this calculation method, a slight overestimation of the absorption value for light in the multi-mode cladding waveguide (see discussion on pages 22 ff.) is neglected for reasons of simplicity. For fiber amplifiers, usually fiber lengths leading to an overall pump absorption  $A$  of about 15 dB are chosen. By using the relation  $A = \alpha_{\text{clad}} \cdot L$ , one obtains the relation

$$r_{\text{clad}} = r_{\text{core}} \cdot \sqrt{\frac{\alpha_{\text{core}} \cdot L}{A}}, \quad (3.6)$$

which defines  $r_{\text{clad}}$  in dependence of the core radius  $r_{\text{core}}$  and the fiber length  $L$  for a given small signal core absorption and overall pump absorption value. By inserting eq. (3.6) into eq. (3.4), one obtains the brightness limited output power in dependence of  $r_{\text{core}}$  and  $L$ :

$$P_{\text{brightness}} = \eta_{\text{laser}} \cdot b_{\text{pump}} \cdot \pi^2 \cdot \text{NA}_{\text{clad}}^2 \cdot \frac{\alpha_{\text{core}}}{A} \cdot L \cdot r_{\text{core}}^2. \quad (3.7)$$

It can be seen that – for a fixed value of the fiber length  $L$  –  $P_{\text{brightness}}$  scales linearly with  $\alpha_{\text{core}}$ . Thus, limited pump brightness is a far more important obstacle for power scaling of Yb<sup>3+</sup>-free Er<sup>3+</sup>-doped fiber laser systems than for the other popular dopants. This is because the significantly lower pump absorption in these fibers can typically only partly be compensated by increased fiber lengths due to nonlinear effects.

#### 3.2.3 Thermal Considerations

Double-clad optical fibers are in general well suited for the handling of significant thermal loads. A main reason for this is the high surface-to-volume ratio that allows for efficient heat dissipation [70]. Thermal problems occurring with double-clad fibers are typically linked to the temperature of their fluorinated low index polymer coatings. This temperature should not exceed about 80 °C in long term and 120 °C



in short term operation [41], respectively. Heat loads of several W/m can be tolerated for the industry standard fiber diameter of 125  $\mu\text{m}$  under the condition of free convection. Larger values can usually be tolerated by several hundred micrometers thick LMA fibers as the thermal resistance of their acrylate coatings is reduced by the increased inner coating diameters with maintained overall coating layer thickness. Nevertheless, the significant fraction of heat load per unit of absorbed pump power in  $\text{Er}^{3+}$ -doped fiber amplifiers can lead to thermally induced damage of the fiber coating already at relatively low pump power. High power cw systems at 1.5  $\mu\text{m}$  and 2.0  $\mu\text{m}$  wavelength need to be designed carefully with respect to thermal management. For example, often no uncooled parts of the fiber can be tolerated (see, e.g., Ref. 59). However, even by applying only passive cooling mechanisms, the threshold for thermally induced damage can be significantly increased. Passive cooling techniques can allow for thermal loads of at least several 10 W/m, as is, e.g., demonstrated in section 5 on pages 95 ff. Specific values for tolerable heat loads per unit length naturally depend on the chosen cooling mechanism and the outer diameter of the fiber.

The issue of thermal damage to the widely used fluorinated low-index coatings is very important for the power scaling of conventional double-clad fibers. However, it has not been included in the discussion of output power limiting effects in Ref. 60. Instead, the authors discuss several interesting – but not easily applicable – ideas to improve the thermal robustness of fiber pump waveguides and coatings. A rough estimation of output power limitations imposed by thermal damage of fluorinated polymer coatings will be derived in the following. For the evaluation of the thermal load on the pump coupling end of the fiber, an exponential pump light depletion along the fiber is assumed. The maximum tolerable thermal load  $Q_{\text{lim}}$  in W/m at the fiber tip of the pump end is then related to the maximum reachable signal power  $P_{\text{coating}}$  by:

$$Q_{\text{lim}} = \ln(2) \cdot \frac{\alpha_{\text{clad}}}{3} \cdot \frac{\eta_{\text{heat}}}{\eta_{\text{laser}}} \cdot P_{\text{coating}}, \quad (3.8)$$

where the factors of  $\ln(2)$  and 3 result from the assumption of an exponential pump light depletion and  $\eta_{\text{laser}}$  and  $\eta_{\text{heat}}$  are the respective fractions of pump power being converted to signal power and heat. Thus, for an approximately known value of  $Q_{\text{lim}}$ , the maximum tolerable output power  $P_{\text{coating}}$  can be calculated easily. A very important parameter for the maximum tolerable heat load is the heat transfer coefficient



$h$ , which has the dimension of  $W/(m^2 \cdot K)$  and represents the conductivity for the heat flow out of the fiber. Experimental experience as well as the thermal simulations of section 5 lead to estimated values of  $Q_{lim,10/62.5} = 5 W/m$  for  $h = 50 W/(m^2 \cdot K)$  and  $Q_{lim,10/62.5} = 100 W/m$  for  $h = 1000 W/(m^2 \cdot K)$  for a fiber with  $r_{core} = 10 \mu m$ ,  $r_{clad} = 62.5 \mu m$  and  $L = 15 m$  ( $\alpha_{clad} \simeq 1 dB/m$ ). A value of  $h = 50 W/(m^2 \cdot K)$  roughly applies for free convection at slightly elevated temperatures and  $h = 1000 W/(m^2 \cdot K)$  is a rather conservative approximation of the effect of applying thermally conductive paste. Calculations performed with the model used for the thermal simulations of the conductive fiber heat sink in section 5 suggest a roughly linear increase of  $Q_{lim}$  with  $r_{clad}$  for constant  $r_{clad}/r_{core}$ . For an unchanged core absorption value, this results in an approximate maximum tolerable output power of

$$P_{coating} = Q_{10/62.5}^{lim} \cdot \frac{3}{\ln(2) \cdot A} \cdot \frac{\eta_{laser}}{\eta_{heat}} \cdot \frac{L^{3/2}}{\sqrt{15m}} \cdot \frac{r_{core}}{10^{-6}m}. \quad (3.9)$$

The factors of  $\sqrt{15m}$  and  $10^{-6}m$  result from the calculation relative to  $Q_{10/62.5}^{lim}$ . For a given value of  $L$  an overall pump light absorption of about 15 dB is assumed so that the thermal load per unit length increases linearly with decreasing fiber length. The assumed linear dependence on  $r_{clad}$  results in the additional factor of  $\sqrt{L}$  which can be easily be seen from eq. (3.6). From the same equation, the linear dependence on  $r_{core}$  can be deduced. Due to the influence of various effects like, e.g., thermal radiation and convection mechanisms this equation can only give an estimate of the tolerable power in terms of coating temperature. Nevertheless, already this estimate is useful to determine whether thermal issues are expected to be an important output power limit.

When the pump radiation is not guided by the coating layer, more thermally and mechanically robust coatings or even all-glass fibers can be used, which can be operated at far higher temperatures. In these cases, also thermal limitations of the glass waveguide itself can become important. An effect that came to increasing attention in recent years due to massively increasing fiber laser output power is the so-called "fiber fuse" effect [71–73], which occurs, when a laser signal and local heating of the fiber core up to about 1000 °C (see, e.g., Ref. 74) lead to a chemical reaction. This causes the formation of plasma propagating along the fiber core at a velocity of typically several m/s. As this destroys the fiber core, it is important not to operate fiber amplifiers at such massively increased temperature levels. Also monitoring the fibers

for small defects that may result in massive local heating might be helpful for preventing fiber fuses. Methods to detect and terminate occurring fiber fuses have been demonstrated, which are helpful in minimizing the damage caused by this effect after its ignition [75, 76].

In Ref. 60 the melting temperature of the core (approx. 1983 K) is given as the limiting temperature for the operation of fiber laser systems. It is noteworthy that this assumption implies to have overcome any problems related to elevated fiber coating temperatures. However, even then the typical ignition temperature for the fiber fuse effect is about 1300 K. Thus, the fiber core temperature must not be increased beyond this point and the estimated core temperature limit of Ref. 60 should be changed accordingly. The estimated output power limitation due to this effect then becomes:

$$P_{\text{fuse}} = \frac{\eta_{\text{laser}}}{\eta_{\text{heat}}} \cdot \frac{4\pi \cdot k \cdot (T_f - T_c)}{1 + \frac{2k}{b \cdot h} + 2 \cdot \ln\left(\frac{r_{\text{clad}}}{r_{\text{core}}}\right)} \cdot L, \quad (3.10)$$

where  $k = 1.38 \text{ W/m}$  is the thermal conductivity coefficient of fused silica [60],  $T_f = 1300\text{K}$  is the approximate ignition temperature of the fiber fuse effect and  $T_c = 300\text{K}$  is the environmental (coolant) temperature.

For air-clad fibers, there have also been investigations regarding the stability of the glass bridges in presence of thermally induced mechanical stress [77]. The authors of Ref. 77 came to the conclusion that at least relatively thick and short bridges should allow for kW-level systems at  $1 \mu\text{m}$  wavelength. The use of such robust air-cladding implies numerical apertures of the pump waveguides between 0.5 and 0.6. However, especially fibers with delicate air containing core structures are naturally more prone to alteration of their waveguide properties through mechanical stress. This means that it is, e.g., not obvious that they remain transversely single-mode under significant thermal loads. For large quantum defects, this could naturally also play a role at accordingly lower output power levels and therefore remains an interesting subject for further investigations.

Also the possibilities of fiber rupture due to a transverse temperature gradient and thermal lensing have been theoretically predicted [60]. Although the effect of thermal lensing is typically of no concern in fiber based devices, it could theoretically occur in very large fiber cores under significant thermal loads. The critical power  $P_{\text{lens}}$  for

this effect in a single-mode fiber can be estimated as follows [60, 70]:

$$P_{\text{lens}} = \frac{\eta_{\text{laser}}}{\eta_{\text{heat}}} \cdot \frac{\pi \cdot k \cdot \lambda^2}{2 \cdot \frac{dn}{dT} \cdot r_{\text{core}}^2} \cdot L, \quad (3.11)$$

where  $\frac{dn}{dT}$  is the change of refractive index with temperature. Thermal lensing will be included into the calculations of the following subsection, although it does not play an important role for the power scalability of current fiber laser systems.

The critical power for the effect of fiber rupture through thermally induced stress can be estimated as follows [60]:

$$P_{\text{rupture}} = \frac{\eta_{\text{laser}}}{\eta_{\text{heat}}} \cdot \frac{4\pi \cdot R_m}{1 - \frac{r_{\text{core}}^2}{2r_{\text{clad}}^2}} \cdot L, \quad (3.12)$$

where  $R_m = 2460 \text{ W/m}$  [60] is the rupture modulus of fused silica. The critical power decreases with fiber length as again a constant amount of pump absorption – and accordingly changing thermal load per unit length – is assumed. Due to the high threshold powers of this effect, fiber rupture seems not to be a truly realistic limit for the power scalability of (current) fiber laser systems.

### 3.2.4 Feasibility of Fiber Designs

LMA technology of active fibers is significantly more advanced for  $\text{Yb}^{3+}$ -doping than for all other active fiber dopants. A main reason is that very small refractive index steps from cladding to core – and thus very small NA values – can be achieved with relative ease. The lower limit for the NA of conventional step-index fibers is usually set by finite homogeneity and flatness of the core's refractive index (see, e.g., Refs. 69 and 78). Thus, if the targeted core NA is chosen too small, refractive index variations might lead to a significantly blurred core structure if their magnitude is in the range of the core-to-cladding index step. In commercial  $\text{Yb}^{3+}$ -doped step-index LMA fibers minimum core NA values of about 0.06 can be reached (see, e.g., Ref. 79), which enables near diffraction limited operation of step-index fiber amplifiers with  $20 \mu\text{m}$  diameter cores [80]. Near single-mode operation can even be extended to  $25 \mu\text{m}$  cores, if care is taken to preferentially excite the fundamental mode [81–83]. In addition, there is also the possibility to increase the mode field area by using special refractive

index profiles to flatten the fundamental mode (see, e.g., Ref. 84). However, this leads to strong pointing fluctuations of the fiber output. It is also possible to increase the beam quality of near single-mode fibers by coiling them to diameters of typically several centimeters. Here, the positive effect on beam quality is due to stronger bending losses for higher order modes than for the  $LP_{01}$  [85]. However, usually a trade-off between higher order mode suppression and excess loss for the fundamental mode is needed (see, e.g., Ref. 86). Moreover, for very low core NA step-index LMA fibers, the fundamental mode area is significantly decreased even for moderate bending diameters [87, 88].

In  $Er^{3+}:Yb^{3+}$ -codoped fibers strong codoping with phosphorous is needed for achieving suitable optical efficiency values [69]. As a consequence, the core refractive index profile is usually especially hard to control in  $Er^{3+}:Yb^{3+}$ -codoped fibers, because the P-codoping typically leads to pronounced refractive index dips in the center of the core and strong refractive index oscillations towards the core-cladding boundary [78]. Due to this, it is at the very least challenging to reduce the core refractive index close to the value of fused silica via additional codopants. Therefore, a small refractive index step from the core to its environment can typically only be achieved by raising the refractive index of the material surrounding the core. Typically, this is done by creating a so-called "refractive index pedestal" around the core by codoping with germanium [69]. By this, the core NA can be reduced from the typical value of 0.2 to about 0.1, which leads to a reduction of the V number by a factor of two. Again, the lower limit of the core NA is set by incomplete control of the refractive index profile.

A drawback of the pedestal technique in double-clad optical fibers is that the pedestals are able to serve as a waveguide for high brightness components of cladding launched pump radiation. As the pedestals are typically round, they support stable helical modes and thus potentially lead to an unabsorbable fraction of pump light. This fraction can be decreased by reducing the pedestal's diameter. However, this typically also leads to a decrease in output beam quality as the modes inside of the pedestal are increasingly overlapping with the actively doped core. The higher this overlap, the larger becomes the amount of amplification that is experienced by pedestal modes instead of core modes. The presence of light in the pedestal modes can also not be fully avoided, as in the course of the amplification process always a fraction of the core light is coupled into the pedestal. This is due to, e.g., imperfect

fiber launching conditions, scattering at core refractive index inhomogeneities and bending induced coupling between core and pedestal modes. A solution for problems related to pedestal modes might be to use a pedestal with an index step to the core but a smoothly decreasing index at the transition to the fused silica cladding. This could weaken the influence of pedestal modes, but also significantly increase the complexity and cost of the manufacturing process for a specific fiber. It might also be feasible to use Ge-doped glass instead of pure fused silica for the cladding, i.e. expanding the pedestal over the whole pump cladding. However, this would also massively increase the fiber manufacturing costs and possibly alter the mechanical properties.

As demonstrated in recent years, it is also possible to control the core refractive index by creating nano-scale composite fluorine- and rare earth-doped structures (see, e.g., Ref. 89). For structures smaller than the laser wavelength, the radiation experiences an averaged refractive index. Thus, nano-structured cores allow for very precise refractive index tailoring by using defined amounts of higher and lower index materials. This has allowed for a refractive index control in the order of  $10^{-5}$  for  $\text{Yb}^{3+}$ -doped fibers, which is about one order of magnitude more precise than conventional manufacturing techniques. In recent years, this superior refractive index control has been a main reason for the successful developments in  $\text{Yb}^{3+}$ -doped photonic crystal LMA fibers. In photonic crystal fiber (PCF) cores, the NA is not solely determined by a dopant induced index step but also by a surrounding air-hole structure [21]. To be able to fully exploit the possibilities of PCF cores, the refractive index of the core material needs to be lower or ideally identical to that of its fused silica environment [90]. Theoretically, PCF designs allow for single-mode fiber cores with arbitrary core diameters [91]. However, in reality the core and mode field diameters are limited by the decreasing core NA with increasing core size. Thus, the to date largest commercial PCF structures with 70 or even 100  $\mu\text{m}$  core diameter have an NA of only about 0.02 [92]. Due to a high susceptibility to stress induced refractive index variations, they need to be embedded in millimeter thick glass rods, because any bending would lead to a massive deterioration of their waveguide properties (see, e.g., Ref. 93). If the embedding in glass rods is to be avoided – e.g., to be able to use a several meters long bendable fiber – the core NA is limited to about 0.03 [92]. In spite of these developments for  $\text{Yb}^{3+}$ -doped cores, for  $\text{Er}^{3+}$ -doped cores, there had up to now only been some efforts with small core photonic crystal fibers in the early stages of PCF development [94, 95].

Another recent development in near single-mode large mode area fibers are the so-called chirally coupled core (CCC) fibers, which rely on advanced step-index core technology [96, 97]. In these fibers, higher order modes are resonantly coupled out of the LMA core into a second core, which is chirally wound around the first one with a specific periodicity. For the large core diameter of 37  $\mu\text{m}$  reported in Ref. 54, also a nano-structured core has been used to achieve a very well defined index step, which was needed for (near) single-mode operation of the fiber. The CCC concept has been predicted to be also applicable to  $\text{Er}^{3+}$ -doped and  $\text{Er}^{3+}:\text{Yb}^{3+}$ -codoped fibers [96], so that it might be of interest for future experiments at 1.5  $\mu\text{m}$  wavelength.

Other types of fiber that are promising candidates for single-mode fibers with even larger mode areas are the so-called leakage channel fiber (LCF) and the closely alike large pitch photonic crystal fiber (LPF). In the LCF, the core waveguide is determined by the diameter and spacing of fluorine doped segments (with a refractive index lower than fused silica) surrounding the core area. Near single-mode LMA operation is reached through massively increased propagation losses for all fiber core modes except for the fundamental one. Leakage channel fibers have been demonstrated both in passive [22] and  $\text{Yb}^{3+}$ -doped [98] versions. These fibers are also very sensitive to bending so that, e.g., the  $\text{Yb}^{3+}$ -doped fiber from Ref. 98 had an impressive core diameter of 80  $\mu\text{m}$  but could only be bent down to a diameter of 76 cm. The recently reported large pitch photonic crystal fibers [90] rely on a concept that is very similar to the principle of leakage channel fibers. Near single-mode large pitch fibers with fundamental mode field diameters larger than 60  $\mu\text{m}$  have been demonstrated [99]. To reach such mode-field sizes, the core refractive index has to be carefully matched with that of the surrounding fused silica [90]. Recent large pitch fibers have also been embedded in glass rods due to the high susceptibility of their waveguide properties to external perturbations. While the mode-field diameters reported for fibers of these types are larger than for CCC fibers, the so far reported beam quality values are slightly worse. An  $M^2$  value of 1.05 has been reported in Ref. 54 for a CCC fiber, while, e.g., values of about 1.4 have been reported for the large pitch fibers of Ref. [99]. It is noteworthy that such  $M^2$  values can already point to significant higher order mode content with respect to the  $\text{TEM}_{00}$  mode [100].

It has been predicted that so-called gain-guided fibers [26, 101] can allow for single-mode operation at 1  $\mu\text{m}$  wavelength in cores with up to several hundred micrometer diameter. In gain-guided fibers, the core has a lower refractive index than the



cladding, so that all core modes experience large propagation losses. In the presence of gain the net loss can be overcome. As the fundamental mode experiences the smallest losses, it can be amplified, while all other modes are still antiguided, if an appropriate gain value is chosen. At 1  $\mu\text{m}$  wavelength, single-mode operation in core diameters up to 400  $\mu\text{m}$  has been demonstrated [102]. However, gain-guided fibers require a flat – i.e, not longitudinally depleted – pump light distribution along the fiber. Therefore, side-pumping instead of the typical end-pumping scheme needs to be used for power scaling of this concept [103]. This scheme is still highly experimental, but might lead to interesting possibilities, especially for pulsed applications with high peak intensities but relatively low requirements on cw power (see, e.g., Ref. 33).

Also in  $\text{Er}^{3+}:\text{Yb}^{3+}$ -codoped fibers an, at least micro-structured, core index averaging technique has also been successfully employed. This has been realized with the so-called multifilament-core (MFC) fibers [78, 104]. Here, a number of hexagonally aligned  $\text{Er}^{3+}:\text{Yb}^{3+}$ -codoped filaments with diameters on wavelength scale are used to guide the signal radiation. The individual filaments have V numbers smaller than unity. Therefore, the field distribution of radiation guided by an individual filament strongly leaks out of it. By choosing an appropriate spacing, strong coupling effects occur between the fields leaking out of each filament, which results in a common supermode spanning over the whole filamented fiber core. Only a small part of the radiation is actually guided inside of the high index filaments. Hence, a smaller effective core index – and also core NA – can be realized by embedding the filaments in a lower index host material. This technique has proven to be useful for making LMA cores with low NA, when high index core materials need to be utilized. Experiments on the beam quality obtainable with these fibers are presented in section 4.2 on pages 81 ff. This concept has also been demonstrated to be applicable at 1  $\mu\text{m}$  wavelength [105]. It is however noteworthy that there has been rather harsh criticism against this [106], which was based on the fact that the filament technology might not be able to lead to improvements with respect to the very mature step-index LMA technology of  $\text{Yb}^{3+}$ -doped fibers.

It is evident that  $\text{Yb}^{3+}$ -doped LMA fiber technology is to date far more advanced than that of the other active dopants. This is mostly due to more advanced material compositions and refractive index control for  $\text{Yb}^{3+}$ -doped fibers. The to date relatively small core sizes are especially of concern for  $\text{Yb}^{3+}$ -free  $\text{Er}^{3+}$ -doped fibers. Here, they lead to the necessity of accordingly small pump claddings due to the ap-

proximate scaling of the cladding pump absorption with  $r_{\text{core}}^2/r_{\text{clad}}^2$ . This results in high requirements on pump source brightness and often leads to output power constraints through limited launchable pump power. This has also been a major reason for initiating the development of an  $\text{Er}^{3+}$ -doped LMA PCF with a large 40  $\mu\text{m}$  diameter signal core for usage in the experiments of this work. This fiber employs a F-codoped nano-structured core alike those of  $\text{Yb}^{3+}$ -doped photonic crystal fibers. The experiments performed with this novel PCF are presented in section 5.4 on pages 105 ff.

#### 3.2.5 Beam Quality Degradation

An advantage compared to bulk solid state laser crystals is that fiber output beam profiles and their modal content are primarily determined by the refractive index properties of the core waveguide. However, for GWD laser sources, the degradation of beam quality – i.e., a decrease of the fractional  $\text{TEM}_{00}$  mode content – is equivalent to a loss of output power. Therefore, any possible mechanisms for beam quality degradation have to be taken into account carefully when developing fiber based GWD laser sources.

Power dependent beam quality degradation is also possible in fiber laser systems. Recently, for 80  $\mu\text{m}$  core diameter rod type PCF cores, output mode instabilities at about 100 W of output power per meter fiber length have been reported [99]. The instabilities occurred as a switching between fundamental and higher order modes. It has been proposed that this effect is induced by an interplay of modal interference and transverse hole burning effects [107]. According to Ref. 107 the described interplay creates inversion gratings along the fiber that lead to strong coupling and power transfer between the interfering modes. This effect could be slightly suppressed in the recently introduced large pitch fibers [90]. The achieved suppression is most probably due to increased losses for higher order modes through the so-called "optical sieve" effect [108]. The optical sieve effect is basically the same as the previously mentioned differential loss mechanism in leakage channel fibers that allows for very large near single-mode cores. Due to the importance of higher order mode losses, also the CCC fiber concept [96] is a promising candidate for high power, very large core fiber amplifiers with stable near diffraction limited beam quality. As the threshold for mode-switching effects reportedly scales with fiber length, they are probably



of greater importance for pulsed fiber amplifiers. High power cw systems typically employ slightly longer fiber lengths and smaller cores than pulsed systems. This is because – apart from stimulated Brillouin scattering – many nonlinear effects that play an important role for high peak power pulsed systems are far less detrimental in the cw case. Therefore, a trade-off in terms of nonlinear interaction length can often be made. This is especially the case at 1.5  $\mu\text{m}$  wavelength, where the lower optical amplification efficiency makes thermal issues and pump brightness more important than nonlinear effects. Thus, mode-switching will probably be a noteworthy, but not critical, issue for the design of GWD laser sources at 1.5  $\mu\text{m}$  wavelength.

The beam quality of fiber amplifiers can also be degraded by transverse hole-burning induced non-uniform inversion distributions [48, 109, 110]. This effect can also be suppressed by increasing losses for higher order modes. Also, it can be reduced by using pump wavelengths that result in lower inversion levels [48]. This can, e.g., be realized by use of the tandem-pumping scheme, when a fiber laser system is pumped by another one operating at only slightly shorter wavelength.

As discussed, beam degradation mechanisms also exist in optical fibers, in spite of their waveguide nature. However, by use of appropriate system and fiber design criteria, these effects can typically be shifted beyond other power scaling limits. Moreover, beam degradation effects in optical fibers are typically weak compared with the influence of thermal lensing or depolarization effects on bulk solid state lasers. Nevertheless, they might become an important limitation for fundamental mode output power scaling of kW-class cw fiber laser systems.

#### 3.2.6 Stimulated Brillouin Scattering

The effect of Stimulated Brillouin Scattering (SBS) is to date the main limitation for the further power scaling of  $\text{Yb}^{3+}$ -doped single frequency amplifiers with sub-MHz linewidth. The Brillouin scattering effect is the result of an interaction of laser photons with acoustic phonons [111–113]. In optical fibers, Brillouin scattered photons are scattered backward with respect to their propagation direction and shifted down in frequency by several GHz with a typical linewidth of some 10 MHz [113, 114]. The magnitude and linewidth of the spectral shift from the original photon frequency depend on several parameters. These are, e.g., the wavelength of the incident light and

both optical and acoustical dispersion relations inside of the specific fiber core material. Both magnitude and linewidth of the Brillouin shift can vary by some ten percent depending on dopant and operating wavelength.

Spontaneous Brillouin scattering is of no concern for single-frequency amplifiers. It results from the interaction of laser photons with thermally induced phonons that incidentally comply with the governing dispersion relations. However, the beating between the forward signal and backwards propagating scattered light leads to an increase of phonons with the correct propagation direction and matching Brillouin frequency through electrostriction [114]. When this process becomes sufficiently strong through rising incident and backscattered power, the spontaneous Brillouin scattering turns to stimulated Brillouin scattering (SBS). This means that the backscattered power grows nonlinearly with incident signal power. Besides the drop in output power in the desired direction, SBS usually leads to a massive increase in relative amplitude noise and detrimental self-pulsing effects. This means that reaching of the SBS threshold power imposes a limit to the maximum output power level of a given single-frequency fiber amplifier. When compared with Raman scattering, SBS is typically the dominant limiting process, if the laser linewidth is similar to or narrower than the Brillouin linewidth (see, e.g., Refs 20 and 114). While Raman scattering is more prominent in most other cases, SBS is therefore especially an issue for extremely narrow linewidth fibers amplifiers as they are required for GWDs.

The threshold optical input power for SBS roughly scales inversely with the effective mode field area and the (effective) length of the fiber [20, 114]. In order to account for the effective length of a fiber, every unit length is weighted by the amount of power propagating inside of it. Amplifiers with copropagating pump and signal radiation have a longer effective length than ones with a counterpropagating pumping scheme, because the main amplification occurs at the pump launch end of the fiber in both cases. Thus, in the copropagating pumping scheme the signal propagates with nearly full output power through almost the entire fiber length. This disadvantageous signal power distribution leads to a lower SBS threshold when compared with a counterpropagating pumping [115]. Recently, a more sophisticated copropagating pumping technique has been demonstrated that leads to similar SBS thresholds as a counterpropagating configuration [116]. In this, both a broadband signal around 1030 nm and a single-frequency signal at about 1065 nm are injected into a fiber amplifier with copropagating 976 nm pump radiation. If the fiber length is chosen appropri-

ately, first the 1030 nm signal is amplified and afterwards transfers its power to the single-frequency signal over a short distance at the fiber end. With optimized system parameters, a single-frequency all-fiber system with more than 200 W of output power at 1065 nm could be demonstrated with copropagating pumping by Zeringue et al. [117]. Especially in all-fiber setups, copropagating pumping is often favorable as it means a better protection of the pump sources against signal radiation.

Due to the high optical-to-optical efficiency and low pump brightness requirements of  $\text{Yb}^{3+}$ -doped optical fibers, SBS is the main limitation for the power scaling of single-frequency fiber amplifiers at 1  $\mu\text{m}$  wavelength. However, it is, e.g., possible to raise the SBS threshold by altering the Brillouin frequency shift along the fiber with a thermal gradient. More than 500 W of output power from near single-mode fibers could be demonstrated by two independent groups [52, 53]. In the experiments of Ref. 53, additionally a special fiber core with acoustic anti-guiding properties for acoustic modes (i.e. the stimulated phonons) was used to further increase the SBS threshold. It has been predicted theoretically that thermal gradients can raise the threshold for SBS by more than 3 dB [118]. In addition, even more than 7 dB of suppression could be demonstrated by a segmented temperature distribution with several temperature steps along the fiber [119]. For acoustic anti-guiding, theoretical fiber designs with almost 15 dB of SBS suppression have been presented [120]. Of course, also novel (near) single-mode fiber designs with larger mode area can also help to mitigate SBS. A single-frequency output power of 511 W at 1  $\mu\text{m}$  wavelength could be demonstrated with the recently introduced CCC fibers with 37  $\mu\text{m}$  core diameter [54].

Longer wavelengths of operation – in principle – also lead to the benefit of larger mode field diameters in (near) single-mode fibers as, e.g., the mode size scales with wavelength. This is reflected in the inverse scaling of the V number with signal wavelength. However, this effect can typically not be exploited to full extent as the achievable core NAs for  $\text{Er}^{3+}$ - and  $\text{Tm}^{3+}$ -doping are slightly higher than for  $\text{Yb}^{3+}$ -doped fibers. Another important difference to systems operating at 1  $\mu\text{m}$  wavelength is caused by the typically higher quantum defect of  $\text{Er}^{3+}$ - and  $\text{Tm}^{3+}$ -doped fiber amplifiers. Thus, stronger pump induced thermal gradients are introduced along the fiber. These lead to an increase of this intrinsic SBS suppression mechanism already at lower output powers than for  $\text{Yb}^{3+}$ -doped amplifiers. However, thermal gradients can of course also be induced by external heating (see, e.g., Ref. 115). A power record

of 608 W from a near-diffraction limited single-frequency amplifier could be realized with a conductively cooled 3 meter long  $\text{Tm}^{3+}$ -doped fiber amplifier by Goodno et al. [59]. The expected SBS threshold for this system was stated to be 750 W. This high threshold value could be achieved with a highly doped short piece of 20  $\mu\text{m}$  core LMA fiber together with strong thermal gradients and the favorable long operating wavelength of 2  $\mu\text{m}$ .

The SBS limited output power of a single-frequency amplifier can be roughly estimated as follows [60, 112]:

$$P_{\text{SBS}} = \frac{17 \cdot \pi \cdot r_{\text{core}}^2}{g_B \cdot L} \cdot \Gamma^2 \cdot \ln(G), \quad (3.13)$$

where  $\Gamma$  is the ratio of the respective radii of mode field and fiber core,  $G$  is the overall gain of the amplified signal,  $g_B$  is the peak Brillouin gain of the dominant acoustic mode [121] and  $L$  is the length of the fiber.

To date,  $\text{Er}^{3+}$ -doped LMA fiber amplifiers have rarely been limited by SBS. Amplifiers with codoped  $\text{Yb}^{3+}$ -ions tend to be limited by parasitic emission at 1  $\mu\text{m}$  and  $\text{Yb}^{3+}$ -free  $\text{Er}^{3+}$ -doped amplifiers are typically rather limited by available pump brightness or thermal effects. For a 5 m long piece of  $\text{Er}^{3+}:\text{Yb}^{3+}$ -codoped 25  $\mu\text{m}$  core LMA fiber an SBS threshold of 360 W has been measured with single-frequency ns pulses [122]. Due to the relatively low average power of only about 3 W, thermal gradient effects have most probably been negligible in these experiments. Therefore, an even about two times higher threshold could be expected for a comparable cw single-frequency amplifier.

### 3.2.7 Fiber End Facet Damage

The glass-air transition at the end facets of an optical fiber can tolerate the throughput of considerable optical power. However, at about 35  $\text{W}/\mu\text{m}^2$  the tolerable limit is reached in cw operation – even for an ideally clean and smooth fiber surface [123, 124]. This limit can be overcome by using fiber end-cap designs that lead to a beam expansion – and thus a reduction in optical power density – before the glass-air transition. Using such end-cap designs is often also useful in sub-kW systems. An example for this is the possibility to increase the tolerance regarding small dust particles

or imperfections on the fiber output facets. The threshold power for the damage of fiber facets without end-caps can be estimated as follows [60]:

$$P_{\text{end facet}} = \Gamma^2 \cdot \pi \cdot r_{\text{core}}^2 \cdot I_{\text{damage}}, \quad (3.14)$$

where  $\Gamma$  is the ratio of the respective diameters of mode field and fiber core and  $I_{\text{damage}}$  is the maximum tolerable radiation intensity of approximately  $35 \text{ W}/\mu\text{m}^2$  at the glass-air transition. When end-caps are used,  $P_{\text{end facet}}$  at the end-cap facet scales with the ratio of expanded and original mode field area. As the tolerable power density does typically not depend strongly on the laser wavelength, related problems occur more frequently for  $\text{Yb}^{3+}$ -doped than for  $\text{Er}^{3+}$ -doped systems. This is because signal power levels are far more critical than pump power levels due to the far higher resulting power densities.

### 3.2.8 Estimation of Power Scaling Limits at $1.5 \mu\text{m}$ Wavelength

In this section, the previously described power limits are combined to identify the power scaling limitation for specific values of fiber length and core diameter. The calculations are focused on 980 nm pumped  $\text{Yb}^{3+}$ -free  $\text{Er}^{3+}$ -doped single-frequency fiber amplifiers. In addition, also  $\text{Er}^{3+}:\text{Yb}^{3+}$ -codoped single-frequency systems are treated under the assumption of having overcome limitations imposed by parasitic emission at  $1 \mu\text{m}$  wavelength. The issue of this parasitic emission is then treated in more detail in section 3.3. Please note that Dawson et al. have also extended their initial work about power limitations of diffraction limited  $\text{Yb}^{3+}$ -doped fiber laser systems [60] in a later publication [123]. In Ref. 123 their formalism is, e.g., applied to  $\text{Tm}^{3+}$ -doped fibers and also to 1530 nm pumped  $\text{Yb}^{3+}$ -free  $\text{Er}^{3+}$ -doped fiber laser systems. However, 980 nm pumped  $\text{Yb}^{3+}$ -free  $\text{Er}^{3+}$ -doped and  $\text{Er}^{3+}:\text{Yb}^{3+}$ -codoped systems have not been included into their work.

The estimation of the power scaling limits of 980 nm pumped  $\text{Yb}^{3+}$ -free  $\text{Er}^{3+}$ -doped fiber amplifiers has been performed for two values (50 and  $1000 \text{ W}/(\text{m}^2 \cdot \text{K})$ ) of the heat transfer coefficient  $h$ . These, respectively, represent free convection air cooling at elevated temperatures and cooling techniques like free convection in water or immersion in thermally conductive paste. All other parameters used in the calculations are summarized in table 3.1.

Parameter	Symbol	Value	Unit
Rupture modulus (fused silica)	$R_m$	2460 [60]	W/m
Thermal conductivity (fused silica)	$k$	1.38 [60]	W/(m·K)
Fiber fuse ignition temperature	$T_f$	1300 [74]	K
Refractive index change with temp.	$dn/dT$	$11.8 \cdot 10^{-6}$ [60]	1/K
Brillouin gain coefficient	$g_B$	$5 \cdot 10^{-11}$ [60]	m/W
Fused silica surface damage intensity	$I_{\text{damage}}$	35 [123]	W/ $\mu\text{m}^2$
Max. pump brightness	$b_{\text{pump}}$	0.103 [31]	W/(Sr · $\mu\text{m}^2$ )
Core absorption at 980 nm	$\alpha_{\text{core}}$	20 [125]	dB/m
Amplifier pump absorption	$A$	15	dB
Amplifier gain	$G$	100	–
Ratio mode field/core diameter	$\Gamma$	0.8	–
Laser efficiency	$\eta_{\text{laser}}$	0.3	–
Heat generation efficiency	$\eta_{\text{heat}}$	0.7	–
Pump clad NA	$\text{NA}_{\text{clad}}$	0.46	–

**Table 3.1:** Parameters used in simulation of maximum output powers from 980 nm pumped  $\text{Yb}^{3+}$ -free  $\text{Er}^{3+}$ -doped fiber amplifiers. The simulation results are presented in Fig. 3.6.

The simulation results are presented in Fig. 3.6. First, calculations for both values of  $h$  were performed for an assumed SBS gain suppression of 3 dB (see Figs. 3.6(a) through 3.6(d)). This assumption of an intrinsic SBS suppression has been made due to the pronounced thermal gradient formation, which can be expected because of the significant quantum defect. Additionally, a calculation with an assumed SBS suppression of 10 dB was performed for  $h = 1000 \text{ W}/(\text{m}^2 \cdot \text{K})$  to show further power scaling prospects through the use of sophisticated SBS mitigation techniques (see Figs. 3.6(e) and 3.6(f)). All other simulation parameters are summarized in table 3.1.

At 1.5  $\mu\text{m}$  wavelength, core radii beyond 20  $\mu\text{m}$  seem to date not yet achievable, when diffraction limited beam quality is desired. However, it is interesting to look at a wide range of fiber lengths and core sizes to gain insight into the impact of possible future core size scaling. Therefore, the simulations were also performed for parameters beyond the range of current fiber technology.

In Figs. 3.6(a) and 3.6(b), it can be seen that without the application of fiber cooling techniques the fiber coating temperature easily rises beyond the long term tolerable limit of 80 °C. This leads either to a slow degradation of the coating or even directly results in massive thermal damage and consequent destruction of the optical fiber.



### 3.2 Design Criteria for High Power Fiber Amplifiers

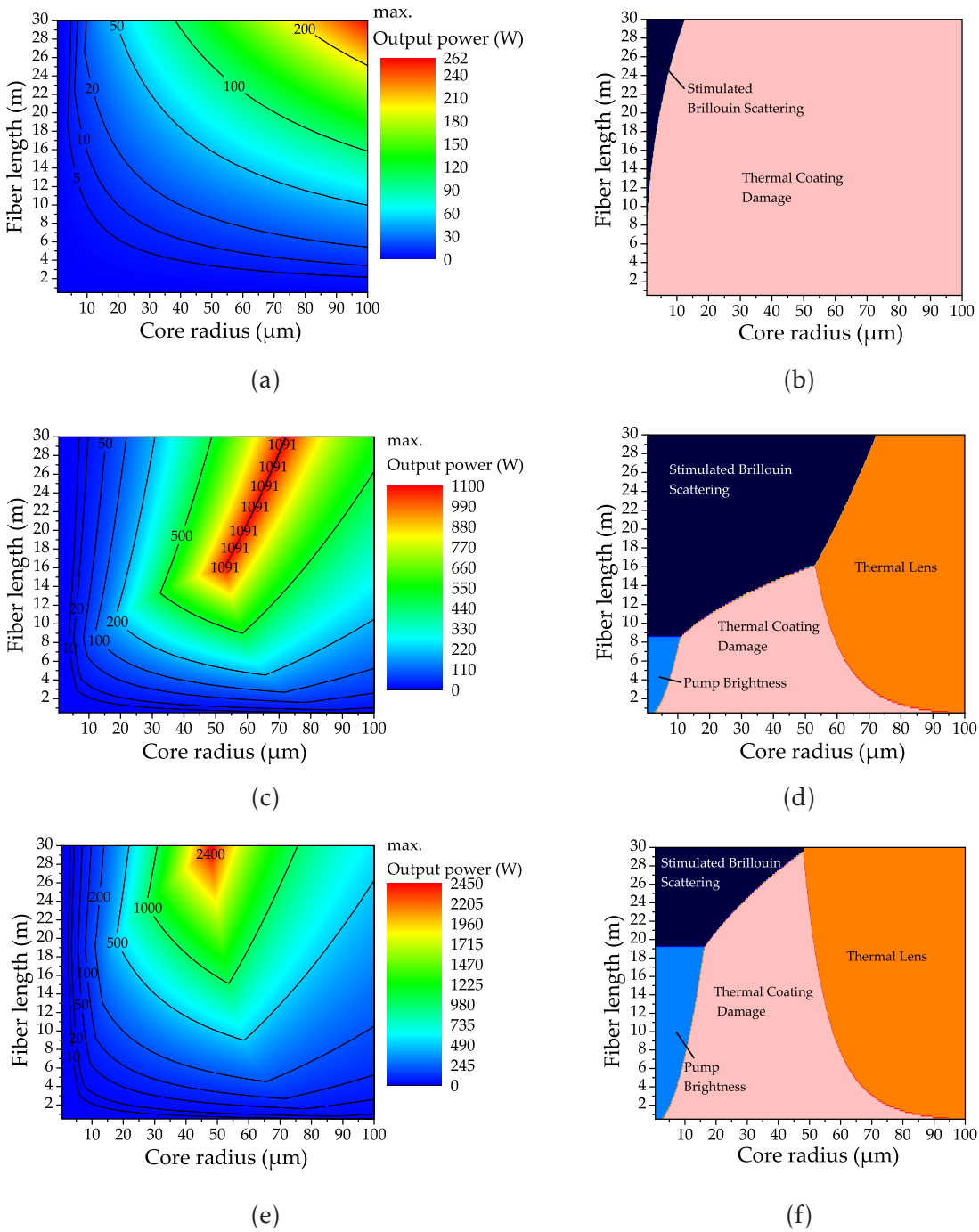


**Figure 3.6:** Calculated output power limits in dependence of fiber core diameter and length for 980 nm pumped  $\text{Yb}^{3+}$ -free  $\text{Er}^{3+}$ -doped fiber amplifiers. (a): Heat transfer coefficient  $h = 50 \text{ W}/(\text{m}^2 \cdot \text{K})$  and 3 dB suppression of SBS gain. (c):  $h = 1000 \text{ W}/(\text{m}^2 \cdot \text{K})$  and 3 dB SBS suppression. (e):  $h = 1000 \text{ W}/(\text{m}^2 \cdot \text{K})$  and 10 dB SBS suppression. (b), (d) and (f): Corresponding plots, identifying the limiting mechanism.

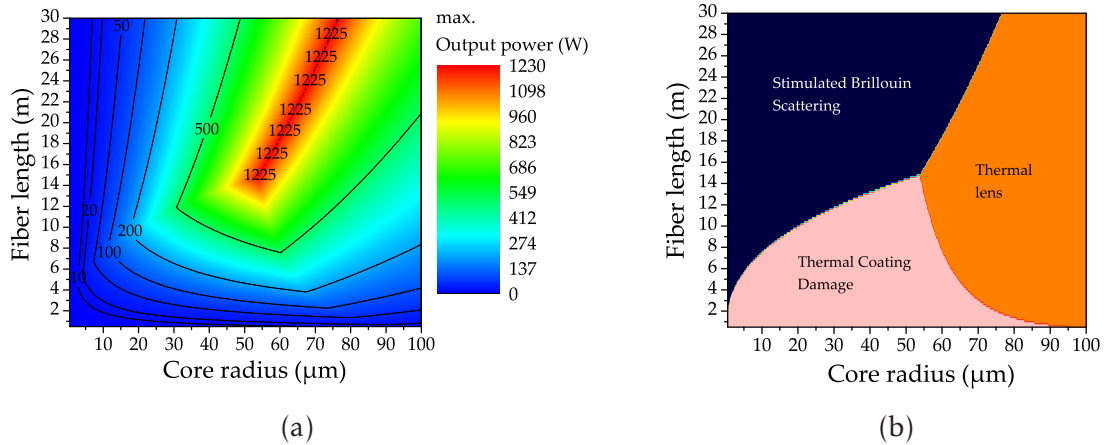


**Figure 3.7:** Calculated output power limits in dependence of fiber core diameter and length for 976 nm pumped  $\text{Er}^{3+}:\text{Yb}^{3+}$ -codoped fiber amplifiers emitting at 1.5  $\mu\text{m}$  wavelength. Parasitic emission at 1  $\mu\text{m}$  wavelength has been neglected. (a): Results for heat transfer coefficient  $h = 1000 \text{ W}/(\text{m}^2 \cdot \text{K})$  and 3 dB suppression of SBS gain. (b): Additional plot to identify the limiting mechanism. A peak core absorption of 360 dB/m and optical-to-optical efficiency of 35 % have been assumed, all other simulation parameters are the same as listed in table 3.1.

Only for small core diameters and long fiber lengths the SBS limited output power is lower than the limit set by the coating temperature. For a core radius of 10  $\mu\text{m}$  a maximum single-frequency output of only about 20 W is predicted. This is because power scaling by reducing the heat load per unit length cannot be continued at this point due to the decrease of the SBS threshold with increasing fiber length. Even with the extension of single-mode operation to cores with 20  $\mu\text{m}$  radius, no significant power scaling would be possible due to massive thermal effects.

The picture changes significantly when the heat flow out of the fiber is increased. A still relatively moderate value of  $h = 1000 \text{ W}/(\text{m}^2 \cdot \text{K})$  together with an unchanged SBS suppression of 3 dB results in the power limits displayed in Figs. 3.6(c) and 3.6(d). For small core sizes and short fibers – i.e. very small pump claddings due to the constant values of  $A$  and  $b_{\text{pump}}$  – the output power is limited below 20 W due to insufficient brightness of the pump radiation. For to date realistic core diameters, SBS limited output is reached for fiber lengths between 10 and 15 m. For very large core radii beyond 60  $\mu\text{m}$ , also thermal lensing might play a significant role in future power scaling. Such core radii are discussed to be reachable, e.g., with leakage channel or gain-guided fibers.

Also with a heat coefficient of  $h = 1000 \text{ W}/(\text{m}^2 \cdot \text{K})$ , thermal damage to the fiber coat-



ing is still the limiting factor for core radii beyond 10  $\mu\text{m}$  and relatively short fiber lengths of shorter than 10 meters. Of course, the influence of this effect could be further decreased by stronger cooling techniques. However, power scaling of diffraction limited  $\text{Yb}^{3+}$ -free  $\text{Er}^{3+}$ -doped fiber amplifiers currently seems only to be realistic with fiber lengths beyond 10 m. This is mainly due to the relatively low obtainable absorption values and decreases the immediate need for stronger cooling. The results presented in Fig. 3.6(c), suggest that, with 3 dB SBS suppression and  $h = 1000 \text{ W}/(\text{m}^2 \cdot \text{K})$ , output power levels of about 100 W could be extracted from fibers with 10  $\mu\text{m}$  core radius. When extending the core radius to 20  $\mu\text{m}$  the maximum output power reaches values of about 200 W.

Another interesting feature of the shown plots is the ridge of maximum power between the SBS and thermal lensing limited parameter ranges. The predicted maximum power of 1091 W cannot be increased by stronger fiber cooling [60]. However, it can be observed in Figs. 3.6(e) and 3.6(f) that an increase of the SBS suppression from 3 dB to 10 dB leads to an increase of this maximum power. By increase of the SBS suppression, the SBS limited parameter range is shifted to longer fiber lengths. With 10 dB SBS suppression, about 165 W of SBS limited output power are predicted for 10  $\mu\text{m}$  core radius. Moreover, maximum output powers even in excess of 600 W are calculated for cores with 20  $\mu\text{m}$  radius. It can be seen from Fig. 3.6(f) that the overall importance of the thermal damage limitation is increased with decreasing SBS. This naturally means that stronger cooling will become important, when other limiting effects are shifted to higher power levels.

In Fig. 3.7, results are presented for  $\text{Er}^{3+}:\text{Yb}^{3+}$ -codoped systems. A value of  $h = 1000 \text{ W}/(\text{m}^2 \cdot \text{K})$  and 3 dB of SBS suppression have been assumed. The  $\text{Yb}^{3+}$ -codoping is accounted for by an increase of the small signal core absorption to 360 dB/m and a slightly higher optical-to-optical efficiency of 35 % instead of 30 %. No significant changes are observable when comparing the results in Fig. 3.7 with the corresponding data in Figs. 3.6(c) and 3.6(d). This arises from the fact that in the presented calculations always brightness limited pumping is assumed, which implies small claddings because of the  $\text{Yb}^{3+}$ -codoping. Due to this, thermal problems with the coating material are the output power limiting mechanism up to fiber lengths of about 10 meters. At these lengths SBS is the main limiting mechanism independently from the  $\text{Yb}^{3+}$ -codoping. To benefit from the increase in core absorption, short fiber lengths of only a few meters and aggressive cooling techniques would need to be applied.

More than 400 W of output power are predicted to be reachable with a 2 m long fiber with 12.5  $\mu\text{m}$  core radius. However, one should also keep in mind that this would require cooling techniques capable of handling thermal loads of several hundred W/m. Moreover, near single-mode LMA fibers with core radii beyond 12.5  $\mu\text{m}$  have not yet been demonstrated, while a core radius of 20  $\mu\text{m}$  has been demonstrated with the  $\text{Yb}^{3+}$ -free  $\text{Er}^{3+}$ -doped PCF presented in section 5.4. Therefore, the access to power scaling through decreased thermal loads per unit length by decreased fiber nonlinearities seems to be accessible easier without  $\text{Yb}^{3+}$ -codoping. In conclusion, it can therefore be said that  $\text{Yb}^{3+}$ -free fibers are likely to become more and more attractive for high power single-frequency fiber amplifiers at 1.5  $\mu\text{m}$ . This is naturally also due to the several general drawbacks of  $\text{Yb}^{3+}$ -codoping, including the limited refractive index control of the highly phosphorous-codoped fiber cores and parasitic emission at 1  $\mu\text{m}$  wavelength, which is treated in more detail in the following section 3.3.

Also a promising alternative approach to power scaling of  $\text{Yb}^{3+}$ -free  $\text{Er}^{3+}$ -doped fiber laser systems exists. This is resonant (also called "intraband") diode pumping between 1480 and 1530 nm wavelength. It has the advantage of quantum defect values comparable to these of 915 to 976 nm pumped  $\text{Yb}^{3+}$  fiber lasers. In a core pumped single-mode amplifier a differential optical-to-optical efficiency of > 84 % could be demonstrated with 1480 nm pumping [126]. There has also been research on high power single-mode pump sources at 1480 nm. A Raman fiber laser with an output power of 81 W at this wavelength has been demonstrated recently [127]. This system was mainly developed for pumping  $\text{Er}^{3+}$ -doped higher order mode fiber amplifiers. In these, pump and signal radiation are injected into the  $\text{LP}_{01}$  fiber mode and then transferred to a specific higher order  $\text{LP}_{0n}$  mode via long period fiber Bragg gratings before starting the amplification process (see, e.g., Ref. 128). An advantage of this scheme is the increased mode area and reduced sensitivity to bending induced mode field distortions and intermodal coupling effects. Up to 5.8 W of output power from an amplifier operating in the  $\text{LP}_{0,10}$  mode have been demonstrated [129]. The concept of higher order mode amplifiers is interesting, but to date not applicable for GWD laser sources. This is because the currently used  $\text{LP}_{0n}$  modes have a significant central lobe in their transverse power distribution [130]. Moreover, the need for high power single-mode Raman laser pump sources significantly enhances the overall system complexity and imposes limits with respect to output power scalability.

Therefore, substantial output power levels might be easier to obtain with resonant

cladding pumping schemes. Here, the achievable efficiency values have up to now been slightly lower with a maximum reported value of 69 % [131]. Nevertheless, in Ref. 131 power scaling of an  $\text{Yb}^{3+}$ -free  $\text{Er}^{3+}$ -doped fiber laser to 88 W of output power at 1590 nm has been reported. Currently, this power scaling concept is also limited by available pump brightness. High power laser diodes at 1530 nm are not yet as sophisticated in technology as these operating around 976 nm. The brightness from commercial high power diode laser stacks is typically almost a factor of ten lower for 1530 nm sources. The results of Ref. 131 were obtained with custom made high power laser diodes. A restriction to commercially available pump sources would likely have meant a reduction of the maximum output power by several ten percent. It should also be noted that 1530 nm diode lasers have relatively low electrical-to-optical efficiency. Regarding amplifier overall electrical-to-optical efficiency, this even cancels out their advantage of a lower quantum defect when pumping  $\text{Yb}^{3+}$ -free  $\text{Er}^{3+}$ -doped fiber laser systems. Moreover, with respect to long-term reliability, more time may be needed until high power diode lasers at 1530 nm can fully compete with those at 976 nm. Nevertheless, with maturing 1530 nm diode technology, resonant pumping will probably become very attractive for future high power  $\text{Yb}^{3+}$ -free  $\text{Er}^{3+}$ -doped fiber laser systems.

It should be noted that all power limits presented in this section can only be regarded as rough estimates. However, the presented theoretical model is a valuable tool to identify probable output power limitations and reach better insight into fundamental design criteria. It is, e.g., evident that increased fiber lengths help to reduce the thermal load per unit length, as well as the requirements on pump brightness. However, they simultaneously lower the threshold power for SBS, which necessitates a compromise between these effects. The SBS threshold scales roughly with the inverse square root of the Brillouin gain  $g_B$ . This means that an increase in SBS suppression allows for accordingly longer fibers and thus higher output powers as, e.g., can be seen by comparison of Figs. 3.6(c) and 3.6(e). For the current generation of pump diodes, effects of thermal damage can almost generally be overcome by stronger cooling techniques. Additionally, it is possible to relax the requirements on fiber cooling by alternative fiber designs like air-clad fibers. These allow for the use of thermally more robust coating materials as their optical properties do not need to be considered. Finally, the effect of thermal lensing might also play a role in the limitation of fiber core sizes in the future. Strategies to overcome this effect will possibly be needed as leakage channel and gain guided fibers have been operated at least near

core sizes that might be prone to this effect.

### 3.3 Parasitic Emission from $\text{Er}^{3+}:\text{Yb}^{3+}$ -Codoped Fiber Amplifiers

After having been omitted in the previous section, the behavior and characteristics of parasitic emission at 1  $\mu\text{m}$  wavelength from  $\text{Er}^{3+}:\text{Yb}^{3+}$ -codoped fiber amplifiers will now be studied in detail. In section 3.3.1 the fundamental properties of  $\text{Er}^{3+}:\text{Yb}^{3+}$ -codoped fibers will be discussed. Numerical simulations of the behavior of parasitic emission at 1  $\mu\text{m}$  wavelength are presented and discussed in section 3.3.2.

#### 3.3.1 Introduction to $\text{Er}^{3+}:\text{Yb}^{3+}$ -Codoped Systems

The codoping with  $\text{Yb}^{3+}$ -ions is a method to increase the pump absorption of  $\text{Er}^{3+}$ -doped fibers [132, 133]. In bulk glass, this concept was successfully demonstrated already in 1965 [134]. A corresponding scheme of the most important ion excitation levels is shown in Fig. 3.8. In  $\text{Er}^{3+}:\text{Yb}^{3+}$ -codoped fibers, the  $\text{Yb}^{3+}$ -doping concentration is typically about an order of magnitude higher than that of the  $\text{Er}^{3+}$ -ions. Thus, the pump light is mainly absorbed by the  $\text{Yb}^{3+}$ -ions, which is also due to their significantly higher absorption cross section around 980 nm. The excitation energy is transferred to the  $\text{Er}^{3+}$ -ions in an efficient resonant transfer process. The here exploited resonance originates from the 980 nm absorption band of the  $\text{Er}^{3+}$ -ions. In order to make laser processes at 1.5  $\mu\text{m}$  efficient, the back transfer of energy to the  $\text{Yb}^{3+}$ -ions has to be depleted. This is usually done by strongly codoping the fiber with phosphorous, which leads to an increase of the first order Stokes Raman frequency shift [132, 135, 136]. In turn, a very fast depopulation of the  $\text{Er}^{3+}$ -ion  $^4\text{I}_{11/2}$ -level is induced. As only the energy from the  $\text{Er}^{3+}$ -ions in this excitation level can be transferred back to the  $\text{Yb}^{3+}$ -ions, this efficiently suppresses the energy backtransfer. A drawback of the codoping with phosphorous is that without further efforts in fiber design the typical core NA values of efficient fibers are about 0.2. This in turn leads to highly multi-mode waveguides for core diameters beyond 20  $\mu\text{m}$ . Also P-codoping typically leads to a relative index depression in the center of the fiber core ("dip formation") (see, e.g., page 36 and Ref. 78). This can lead to a further deterioration of the output beam profile, e.g., through distortion of the fundamental fiber mode [137]. On the other hand,  $\text{Yb}^{3+}$ -codoping has the advantage to lessen the detrimental

### 3.3 Parasitic Emission from $\text{Er}^{3+}:\text{Yb}^{3+}$ -Codoped Fiber Amplifiers

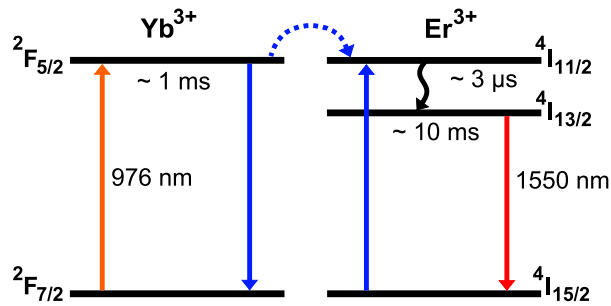


**Figure 3.8:** Schematic depiction of the level scheme of  $\text{Er}^{3+}:\text{Yb}^{3+}$ -codoped systems, showing the most important transitions and upper state lifetimes.

effect of ion clustering on the optical efficiency [138]. Fibers codoped with  $\text{Yb}^{3+}$ -ions typically have several percent higher optical-to-optical efficiency than  $\text{Yb}^{3+}$ -free  $\text{Er}^{3+}$ -doped fibers.

The codoping of  $\text{Er}^{3+}$ -doped fibers with  $\text{Yb}^{3+}$ -ions significantly reduces the requirements on pump brightness compared with  $\text{Yb}^{3+}$ -free fibers. This means that smaller core to cladding ratios can be used. Hence, larger pump claddings with several hundred micrometers in diameter become achievable without the need for unsuitable fiber lengths of several tens of meters. The possibility of using high power pump diodes with lower beam quality has enabled impressive power scaling at  $1.5 \mu\text{m}$  wavelength. Output power levels of 297 W for  $\text{Er}^{3+}:\text{Yb}^{3+}$ -codoped fiber lasers [139] as well as 151 W for single-frequency fiber amplifiers [140] could be demonstrated. However, the core parameters of the fiber utilized for the experiments of Ref. 140 do not suggest the applicability of this system as a laser source for GWD detectors. The fiber had a V number of  $> 12$  (core diameter:  $30 \mu\text{m}$ , core NA:  $> 0.2$ ) and could potentially guide almost 20 different higher order modes in the fiber core. The output power scaling of the systems presented in Refs. 139 and 140 has been limited by parasitic emission at  $1 \mu\text{m}$  wavelength. It led to an almost identical output power at  $1 \mu\text{m}$  and  $1.5 \mu\text{m}$  wavelength for the laser system. This went along with a decrease in differential optical-to-optical efficiency from 40 % at lower pump power to 19 % at full pump power. For the single-frequency amplifier system, it led to the – far more critical – emission of about 70 W of  $\text{Yb}^{3+}$ -ASE. This  $\text{Yb}^{3+}$ -ASE is a result of unsaturated small signal gain for  $1 \mu\text{m}$  radiation as the Yb pump rate is increased beyond the  $\text{Yb}^{3+}$ -to- $\text{Er}^{3+}$  transfer rate. At such massive  $\text{Yb}^{3+}$ -ASE power levels an amplifier is highly prone to detrimental self-lasing and -pulsing effects, which is due to the evident very high signal gain at  $1 \mu\text{m}$  wavelength.

Several approaches to suppress the emission of  $\text{Yb}^{3+}$ -ASE have been reported. In Ref. 141 (long period) fiber Bragg gratings (FBG) were used to filter out the  $\text{Yb}^{3+}$ -ion emission between a high power  $\text{Er}^{3+}:\text{Yb}^{3+}$ -codoped laser-amplifier system. For the presented setup, this all-fiber based solution was effective and elegant, but it did not address the gain at 1  $\mu\text{m}$  wavelength itself. Another approach is to use a counterpropagating pumping scheme together with a substantial amount of seed power to ensure an efficient energy extraction by the signal at 1.5  $\mu\text{m}$  [142]. This slightly lowers the gain for signals around 1.0  $\mu\text{m}$  by an increased depletion of the  $\text{Yb}^{3+}$ -inversion. However, as will be shown in the simulations of the following section, this has only minor influence on the gain at 1  $\mu\text{m}$  wavelength and, hence, the amount of emitted  $\text{Yb}^{3+}$ -ASE. Thus, the main drawback of this approach is the relatively low overall amplifier gain of about 10 dB until the onset of the  $\text{Yb}^{3+}$ -ASE. This in turn can lead to the need of carefully tailoring chains of several amplifiers for the case of high power and/or high gain applications (see, e.g. Ref. 143). Another potential issue of this approach is also the all-fiber implementation of the counterpropagating pumping scheme. As an example, standard tapered fiber bundle (TFB) couplers are not suitable for long-term operation as they have a low core-to-cladding isolation. Therefore, they typically transmit several percent of the amplified signal through every pump port of the coupler. This can decrease the lifetime of the pump diodes, unless additional optical isolators or dichroic mirrors are implemented to protect the pump sources. Another approach is to use photonic bandgap fibers that show only weak guidance for radiation around 1.0  $\mu\text{m}$  wavelength [144]. The main drawback of this approach has been the very low slope efficiency of the used fiber in the range of only a few percent. Moreover, increasing this efficiency would be very challenging, because the – for this purpose crucially important – codoping with phosphorus is to date incompatible with PCF structures. As mentioned before, this is because of the difficulty to control the refractive index of  $\text{Er}^{3+}:\text{Yb}^{3+}$ -codoped fibers with high phosphorous content. A novel scheme to extract the excess energy from the  $\text{Yb}^{3+}$ -ions has been developed within this thesis and is described in section 4.1. This was inspired by the high power laser demonstrated in Ref. 139, where a controlled simultaneous laser oscillation at 1.0  $\mu\text{m}$  rather than a suppression of such a laser oscillation was being utilized. More details on the power scaling of  $\text{Er}^{3+}:\text{Yb}^{3+}$ -codoped fiber amplifiers via an auxiliary signal at 1  $\mu\text{m}$  wavelength are presented on pages 67 ff.



Parameter	Value	Unit
$C_0$	$14.3 \cdot 10^{-50}$ [61]	$\text{m}^6/\text{s}$
$C_1$	$6.3 \cdot 10^{-50}$ [61]	$\text{m}^6/\text{s}$
$W_0$	$3.74 \cdot 10^{-24}$ [61]	$\text{m}^3/\text{s}$
Lifetime $\text{Er}^{3+} \ ^4\text{I}_{13/2}$ level	$9 \cdot 10^{-3}$ [61, 145, 146]	s
Lifetime $\text{Er}^{3+} \ ^4\text{I}_{11/2}$ level	$3 \cdot 10^{-6}$ [61, 145, 146]	s
Lifetime $\text{Yb}^{3+} \ ^2\text{F}_{5/2}$ level	$9 \cdot 10^{-4}$ [61, 145, 146]	s
Number density of $\text{Er}^{3+}$ -ions $N_{\text{Er}}$	$1 \cdot 10^{26}$ [142]	$1/\text{m}^3$
Number density of $\text{Yb}^{3+}$ -ions $N_{\text{Yb}}$	$6 \cdot 10^{26}$ [142]	$1/\text{m}^3$
Pump Wavelength	976	nm
Signal Wavelength	1556	nm
Background Loss	0.04	dB/m
Spacing of ASE channels	1.0	nm

**Table 3.2:** Parameters used in the numerical simulations of the parasitic emission at 1  $\mu\text{m}$  wavelength from  $\text{Er}^{3+}:\text{Yb}^{3+}$ -codoped fiber amplifiers. The fluorescence and nonradiative lifetimes of the excited ion states have been estimated from the data of several references. The  $\text{Er}^{3+}$  and  $\text{Yb}^{3+}$  number density values have been estimated from the discussion of optimum parameters in Ref. 142.

### 3.3.2 Numerical Simulations of Parasitic Emission

In the following, numerical simulations of  $\text{Er}^{3+}:\text{Yb}^{3+}$ -codoped LMA fiber amplifiers are presented. The calculations were performed with the commercial software *RP Fiber Power V2.0* (Version 2009-07-24 by Dr. Rüdiger Paschotta of RP Photonics Consulting GmbH)<sup>1</sup>. The goal mainly was a better understanding of the underlying mechanisms of parasitic emission, rather than a quantitative modeling of actual experimental results. Without substantial spectroscopic data of a specific fiber, quantitative modeling of  $\text{Er}^{3+}:\text{Yb}^{3+}$ -codoped fiber amplifiers is almost precluded. This is due to a typically large number of relatively uncertain fiber parameters like, e.g., the  $\text{Yb}^{3+}$ -to- $\text{Er}^{3+}$  transfer coefficient, the amount of non-transferring  $\text{Yb}^{3+}$ -ions [145] or even basic parameters like the  $\text{Yb}^{3+}$ - and  $\text{Er}^{3+}$ -doping concentrations. Nevertheless, the numerical results presented in this section are valuable for identifying the mechanisms leading to parasitic emission. Additionally, it is important to understand the influence of parasitic emission on the optical-to-optical efficiency of  $\text{Er}^{3+}:\text{Yb}^{3+}$ -codoped fiber amplifiers. As will be shown, it is possible to reduce the amount of emitted  $\text{Yb}^{3+}$ -ASE and maximize the amplification efficiency of the signal under certain premises.

<sup>1</sup>I would like to acknowledge that Dr. Rüdiger Paschotta provided the Laser Zentrum Hannover e.V. with a specially priced licence for the non-commercial usage of *RP Fiber Power V2.0*.

The underlying model is based on coupled rate equations. This means that the – steady state – population densities of the involved ion excitation levels and the corresponding photon flux are calculated. More details on comparable rate equation models can, e.g., be found in Refs. 34, 145 and 146. The used level scheme is depicted in Fig. 3.8. Parasitic upconversion effects have been neglected in the here presented calculations for two reasons. First, while these effects influence the absolute optical efficiency of  $\text{Er}^{3+}:\text{Yb}^{3+}$ -codoped systems, they have no direct connection to the onset of parasitic emission at 1  $\mu\text{m}$  wavelength and the associated roll-over in differential efficiency at 1.5  $\mu\text{m}$  wavelength. Second, the magnitude of these effects highly depends on the specific core composition and therefore varies from fiber to fiber (see, e.g., Refs. 147 and 148). Also ASE at 1.5  $\mu\text{m}$  wavelength has been neglected as it typically has insignificantly low power compared to the amplified signal. The used simulation parameters are listed in table 3.2. The absorption and emission cross sections, as well as the parameters  $C_0$ ,  $C_1$  and  $W_0$ , which are used in the calculation of  $K_{\text{Yb-Er}}$ , have been taken from Ref. 61. The  $\text{Yb}^{3+}$ -to- $\text{Er}^{3+}$  transfer coefficient is calculated as following [61]:

$$K_{\text{Yb-Er}} = \left( C_0 + C_1 \cdot e^{-\frac{N_{\text{Yb}}/N_{\text{Er}}}{8.4}} \right) \cdot N_{\text{Yb}} + W_0. \quad (3.15)$$

The transfer rate describes the change of the population density of the  ${}^4\text{I}_{11/2}$   $\text{Er}^{3+}$ -level per second at a point along the fiber. It is given by  $K_{\text{Yb-Er}}$  times the population densities of the  $\text{Er}^{3+}$  ground state level ( ${}^4\text{I}_{15/2}$ ) and the excited  $\text{Yb}^{3+}$  level ( ${}^2\text{F}_{5/2}$ ). The  $\text{Er}^{3+}$ -to- $\text{Yb}^{3+}$  backtransfer can typically be neglected. The doping concentrations  $N_{\text{Er}}$  and  $N_{\text{Yb}}$  are estimated from the values used in Ref. 142. In experiments, the relative and absolute values – and with them  $K_{\text{Yb-Er}}$  – can vary significantly for different fibers.

In the following simulations, the cladding sizes of the simulated fibers will be slightly larger than they are in reality, which has two main reasons. First, in the used software, the distribution of the pump radiation in the fiber cladding is not calculated by a true multi-mode propagation model. Instead, the cladding absorption is estimated by reducing the core absorption proportional to  $r_{\text{core}}^2/r_{\text{clad}}^2$ . The second reason are the relatively large assumed values of  $N_{\text{Er}}$  and  $N_{\text{Yb}}$ , which however lead to decent results in terms of the transfer parameter  $K_{\text{Yb-Er}}$ . Both facts lead to a slight overestimation of the pump absorption values [34, 149]. However, this does not impose a problem



for the qualitative simulations discussed in this section.

The simulated optical fiber has a core with 25  $\mu\text{m}$  diameter and a 600  $\mu\text{m}$  diameter pump cladding. The core NA is assumed to be 0.1 and the fiber length is 2 m. The amplifier is seeded by 100 mW at 1556 nm. Gaussian and top-hat transverse distributions have been used to model the propagation of signal and pump radiation, respectively. These mode shapes are used to model the overlap of the signal with the actively doped fiber core. The width of the signal mode-field is estimated by use of the well known Marcuse relation [20, 28]:

$$\frac{r_{\text{mode}}}{r_{\text{core}}} = 0.65 + 1.619 \cdot V^{-3/2} + 2.879 \cdot V^{-6}, \quad (3.16)$$

where  $r_{\text{mode}}$  and  $r_{\text{core}}$  are the respective radii of fundamental core mode and fiber core and the  $V$  number is calculated from eq. (3.2) using the previously given fiber parameters.

In Fig. 3.9, the optical output power of the signal, as well as forward and backward ASE at 1  $\mu\text{m}$  wavelength, are plotted versus launched pump power – both for co- (Fig. 3.9(a)) and counterpropagating (Fig. 3.9(b)) pump and signal radiation. It can be seen that the differential efficiency of the signal output is significantly reduced by the onset of parasitic emission from both fiber ends. The terms "forward" and "backward" ASE refer to radiation that is co- and counterpropagating to the signal, respectively. The  $Yb^{3+}$ -ASE emission from the pump launch end of the fiber rises already at lower pump power levels and more strongly than from the other fiber end. This behavior results in a relatively smooth roll-over of the optical-to-optical efficiency instead of a pronounced knee in the plotted signal output power. In the presented simulation data, the pump power is increased significantly beyond the limits of stable operation. However, calculating the output power levels for very large pump power reveals a threshold behavior for the emission of  $Yb^{3+}$ -ASE, as well as the linear dependence on pump power beyond this point. Aside from the obviously exchanged roles of forward and backward propagating  $Yb^{3+}$ -ASE, no significant difference can be observed between co- and counterpropagating pumping. After the roll-over in slope efficiency, the ASE in both directions has higher differential optical-to-optical efficiency than the signal. From the pump launch end of the fiber nearly 50 % percent of the pump power are reemitted as  $Yb^{3+}$ -ASE at a simulated launched pump power of 500 W. At the same point only about 95 W of signal power would be emitted. This underlines

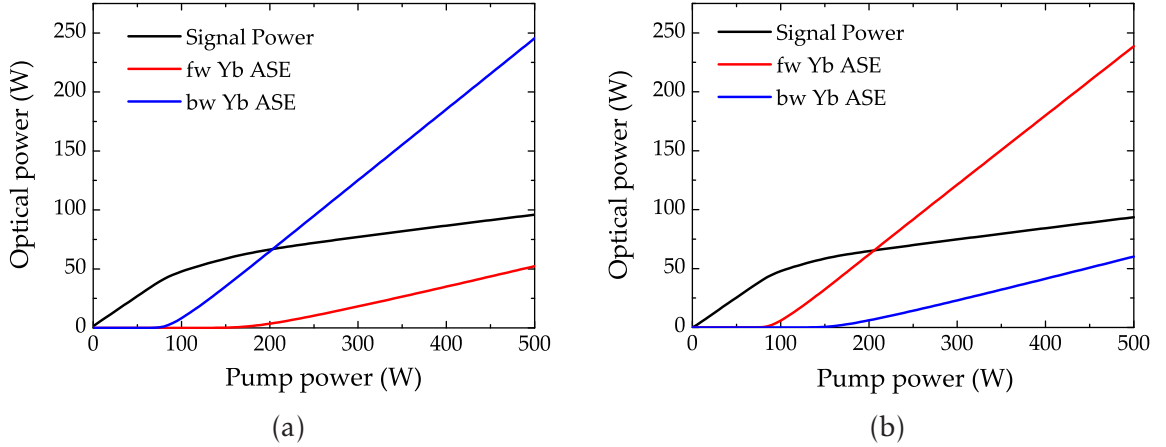


**Figure 3.9:** The output powers of 1.5  $\mu\text{m}$  signal, forward (fw) Yb-ASE and backward (bw) Yb-ASE are plotted versus launched pump power. The simulations have been performed both for (a) co- and (b) counterpropagating pump radiation.

the massive influence of strong  $\text{Yb}^{3+}$ -ASE emission on the amplification efficiency of the 1.5  $\mu\text{m}$  signal. Moreover,  $\text{Yb}^{3+}$ -ASE further restricts the maximum output power at 1.5  $\mu\text{m}$  through self-lasing and -pulsing effects. These are highly hazardous for the fiber end facets and other optical components along the beam path. Therefore, a better understanding of the origins and properties of the  $\text{Yb}^{3+}$ -emission is essential for finding routes to the power scaling of  $\text{Er}^{3+}:\text{Yb}^{3+}$ -codoped fiber amplifiers.

In Figs. 3.10(a), 3.10(c) and 3.10(e), the evolution along the fiber of pump and signal power, population of the excited  ${}^2\text{F}_{5/2}$   $\text{Yb}^{3+}$  level and forward and backward ASE power levels are presented. All calculations were performed for a copropagating pumping scheme at several pump power levels. In Figs. 3.10(b), 3.10(d) and 3.10(f) the same quantities are respectively shown for a counterpropagating pumping scheme.

In Figs. 3.10(a) and 3.10(b), it can be seen that the signal power exhibits relatively abrupt changes in the gain distribution along the fiber. This effect can be readily explained by the similar changes in differential pump absorption at the same positions along the fiber. These changes are in turn closely linked to the population of the excited  ${}^2\text{F}_{5/2}$   $\text{Yb}^{3+}$  level (Figs. 3.10(c) and 3.10(d)). This population density is directly connected to pump saturation effects and the emission of ASE at 1  $\mu\text{m}$  wavelength (Figs. 3.10(e) and 3.10(f)). When the population of the upper  $\text{Yb}^{3+}$ -level gets high enough to result in gain for spontaneously emitted photons at 1  $\mu\text{m}$  wavelength, the threshold for ASE emission is reached. This in turn depletes the upper  $\text{Yb}^{3+}$ -level

### 3.3 Parasitic Emission from $Er^{3+}:Yb^{3+}$ -Codoped Fiber Amplifiers

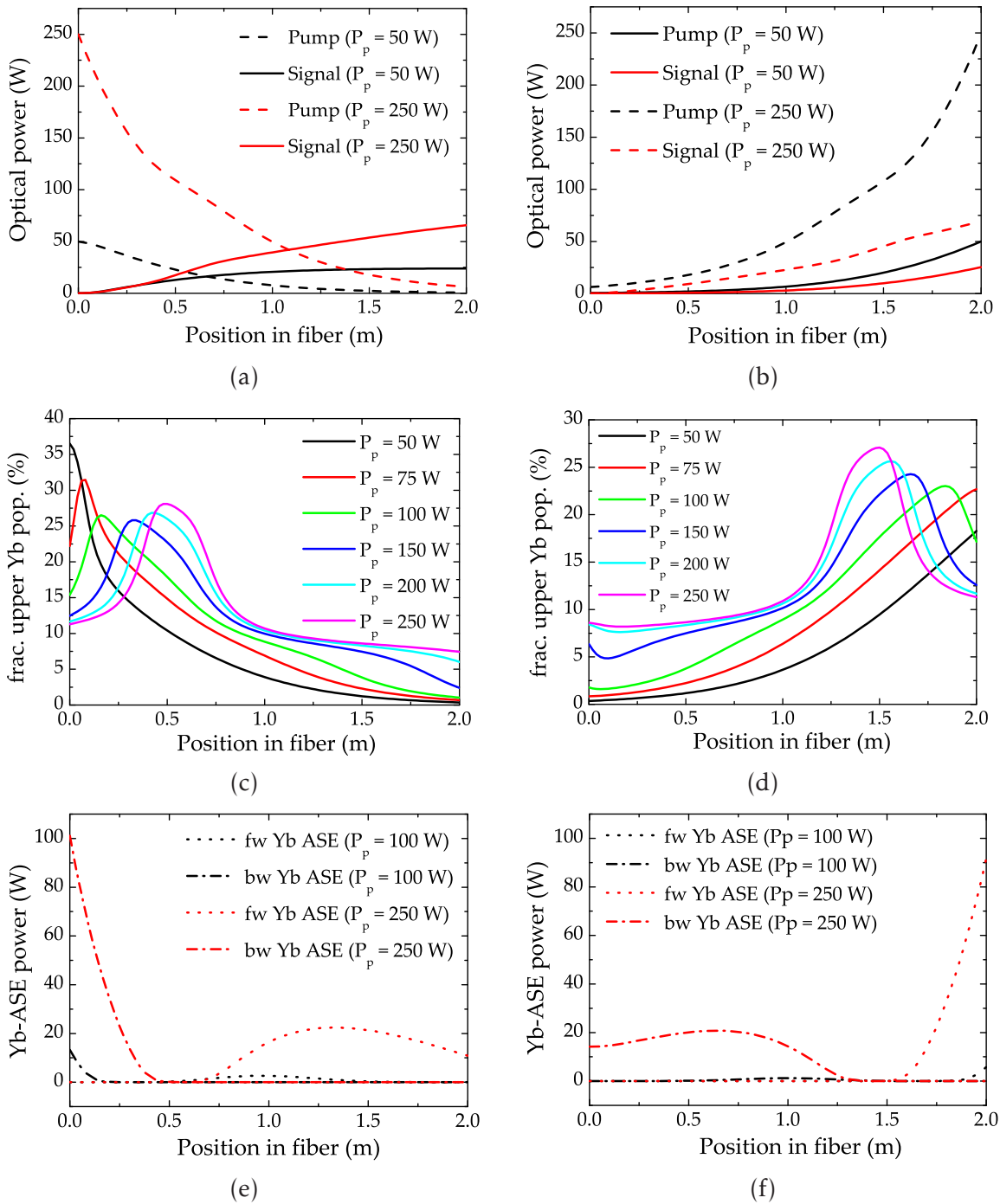


**Figure 3.10:** Evolution along the fiber of pump and signal power, population of the upper  $Yb^{3+}$ -level and forward and backward ASE power in co- (a,c,e) and counterpropagating (b,d,f) pumping configuration at different pump power levels.

population along its path of propagation and results in the observably stronger pump absorption in the regions of significant propagating ASE.

The emission of  $\text{Yb}^{3+}$ -ASE starts at the pump launch end of the fiber after the fractional population of the upper  $\text{Yb}^{3+}$ -level has been increased sufficiently. The increase of this population results from a shift of its steady state condition. This shift follows from the linear relationship between the upper  $\text{Yb}^{3+}$ -level population density and the  $\text{Yb}^{3+}$ -to- $\text{Er}^{3+}$  transfer rate. In other words, the  $\text{Yb}^{3+}$ -to- $\text{Er}^{3+}$  transfer rate follows an increase of the  $\text{Yb}^{3+}$  pump rate by growing with an increasing population of the upper  $\text{Yb}^{3+}$ -level. However, this increase not only leads to a growing transfer rate, but subsequently also to gain for emission at  $1 \mu\text{m}$ . Thus, the increase of the transfer rate through the growth of the  $\text{Yb}^{3+}$  pump rate directly leads to the emission of  $\text{Yb}^{3+}$ -ASE, as soon as the pump power is increased sufficiently. In the given case, this happens between 50 and 75 W of launched pump power for copropagating pump radiation and 75 and 100 W for counterpropagating pump radiation. Slightly less ASE is emitted for counterpropagating pump at the same input power levels. However, generally no major differences between the two pumping schemes can be observed with regard to emission of  $\text{Yb}^{3+}$ -ASE. The existing minor differences result from the slightly higher fractional population of the upper  $\text{Yb}^{3+}$ -level for the copropagating pumping scheme. These are reached because of the disadvantageous combination of low input signal power and high input pump power being injected into the same fiber end. It can be observed in Figs. 3.10(c) and 3.10(d) that the maximum of the fractional upper  $\text{Yb}^{3+}$ -level population moves towards the center of the fiber with increasing pump power. This peak marks the origin of the  $\text{Yb}^{3+}$ -ASE emitted in both forward and backward direction. Its shift with rising pump power is induced by the increasing steady state population of the upper  $\text{Yb}^{3+}$ -level. This in turn leads to an increase of fiber length over which the spontaneous  $\text{Yb}^{3+}$ -emission exhibits gain. As the  $\text{Yb}^{3+}$ -ASE leads to a depletion of the  $\text{Yb}^{3+}$  excitation, this leads to a spatial shift of  $\text{Yb}^{3+}$  excitation peak. As can be seen from Figs. 3.10(e) and 3.10(f) the ASE-emission is more intense from the pump launch end of the fiber. This follows from the higher pump photon flux – and thus higher gain – on this side of the fiber.

In the following, the consequences of the variation of several input and fiber parameters on the emission of  $\text{Yb}^{3+}$ -ASE are studied. In Fig. 3.11(a), signal, forward and backward ASE output power levels are plotted versus launched copropagating pump power for 100 mW (solid lines), 1 W (dashed lines) and 10 W (dotted lines) of seed

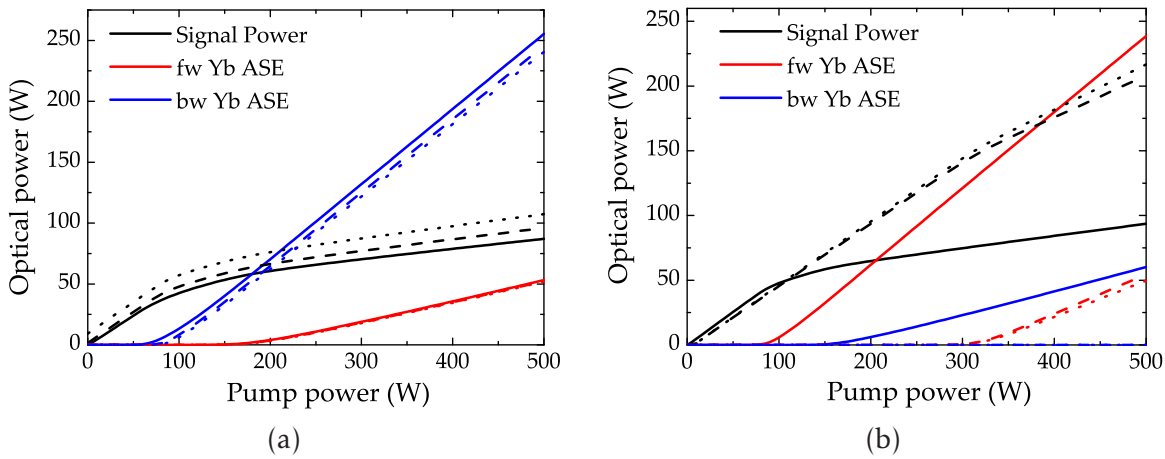


**Figure 3.11:** (a): Signal, forward and backward ASE output power versus launched copropagating pump power and 100 mW (solid lines), 1 W (dashed lines) and 10 W (dotted lines) of seed signal. (b): Signal, forward and backward ASE output power versus launched copropagating pump power for 976 nm pumping, 600 μm diameter cladding and 2 m long fiber (solid lines), 976 nm pumping, 1800 μm diameter cladding and 13 m long fiber (dashed lines) and 915 nm pumping, 600 μm diameter cladding and 13 m long fiber (dotted lines).

signal. It can be easily observed that the variation of seed power has only minor influence on the amplification behavior of both signal and ASE. The signal is only increased by the additional power at the fiber input. The threshold for the linear increase of emitted ASE power is not shifted to higher pump powers. However, its power at a given point is slightly reduced, which is probably due to the more efficient extraction of energy transferred to the  $Er^{3+}$ -ions. This is similar to the effect observed when comparing the  $Yb^{3+}$ -ASE emission for co- and counterpropagating pumping schemes in Fig. 3.9. In Fig. 3.11(b), the influence of a variation of pump absorption through changes in cladding diameter (increased by a factor of three) and pump wavelength (changed to 915 nm) is shown. The pump wavelength at 915 nm has been simulated by dividing the absorption cross section value at 976 nm by 10 and setting the emission cross section value to zero. For the lowered absorption cross section, the fiber length was increased until identical overall pump absorption was reached. For the case of the increased cladding size, the cladding diameter was chosen such that the necessary fiber length was the same as in the simulations with the lowered absorption cross section. The fiber length needed to be increased only to 13 m and not – by the intuitively expected factor of 10 – to 20 m as the influence of pump absorption saturation was decreased for the cases of lowered pump absorption values. A clear increase in threshold power for the  $Yb^{3+}$ -ASE as well as a weakened efficiency

roll-over for the signal can be observed. These result from the reduced ratio of pump photon and  $\text{Yb}^{3+}$ -ion densities leading to a lower pump rate for the  $\text{Yb}^{3+}$ -ions. This in turn also reduces the steady state  $\text{Yb}^{3+}$ -to- $\text{Er}^{3+}$  transfer rate. Hence, the population of the upper  $\text{Yb}^{3+}$ -ion level at a given power level is reduced and the threshold pump power value for the stimulated amplification of spontaneous emission at 1  $\mu\text{m}$  wavelength is increased. It is also noteworthy that changing the absorption per unit length by increasing the cladding size or altering the pump wavelength has almost the identical effect. This means that the nearly vanishing emission cross section at 915 nm does not play a significant role for the behavior of the  $\text{Yb}^{3+}$ -ASE. This behavior could also be expected as the vanishing emission cross section mainly increases the maximum reachable inversion of the  $\text{Yb}^{3+}$ -ions. This in turn has already not been limited by absorption saturation but by the onset of  $\text{Yb}^{3+}$ -ASE for 976 nm pump radiation, although here the zero-phonon line transitions were excited. Thus, a maximum excited state population of about 50 % could have been reached. In contrast, almost complete inversion is principally obtainable with 915 nm pumping [62].

When considering to mitigate ASE emission by the presented means, it should be kept in mind that a reduction of absorption also leads to the need for longer fibers. This in turn reduces the SBS threshold for single-frequency amplifiers. Therefore, advantages of  $\text{Er}^{3+}:\text{Yb}^{3+}$ -codoped fibers in comparison to  $\text{Yb}^{3+}$ -free  $\text{Er}^{3+}$ -doped systems in terms of necessary fiber lengths can quickly be canceled out. Of course, advantages with respect to relaxed pump brightness requirements remain unaffected. However, the current rapid increase in pump diode technology might reduce the importance of diode beam quality for the power scalability of  $\text{Yb}^{3+}$ -free  $\text{Er}^{3+}$ -doped fiber amplifiers in the near future. It is also noteworthy that reducing the core absorption of the fiber through altering the doping concentrations instead of fiber geometry or pump wavelength would not affect the average number of pump photons per  $\text{Yb}^{3+}$ -ion. Thus, inside of the fiber, basically the same processes as before would simply take place on accordingly altered length scales. Moreover, reducing the  $\text{Yb}^{3+}$ -density would even lead to a decrease of the  $\text{Yb}^{3+}$ -to- $\text{Er}^{3+}$  transfer parameter as higher doping densities lead to a more efficient transfer of excitation energy [61, 142]. Therefore, highest possible  $\text{Yb}^{3+}$ -ion concentrations are generally preferable in terms of amplifier efficiency.

For  $\text{Yb}^{3+}$ -ASE at wavelengths exhibiting significant reabsorption (e.g. 1030 nm), the efficiency roll-over through ASE at 1  $\mu\text{m}$  wavelength can also partly be avoided by another approach. This is, to increase the amplifier fiber length beyond the value



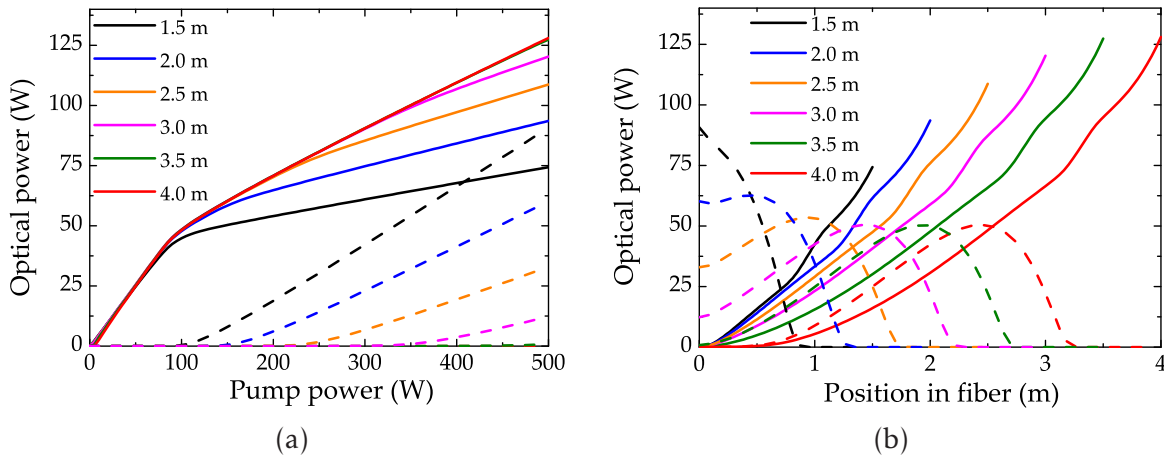


**Figure 3.12:** (a): Output signal (solid lines) and backward  $\text{Yb}^{3+}$ -ASE (dashed lines) power versus counterpropagating 976 nm pump power for various lengths of fiber with 25  $\mu\text{m}$  core and 600  $\mu\text{m}$  cladding size. (b): Corresponding evolution of signal and backward ASE power along the fiber with 500 W of counterpropagating pump power.

corresponding to 15 dB pump depletion, which typically gives rise to optimum amplifier efficiency in non-codoped fiber laser systems. The effect of an increase in fiber length is illustrated in Fig. 3.12 where the rising output power and decreased efficiency roll-over with increasing fiber length are shown. A pump light absorption of about 15 dB is reached for a fiber length of 2 meters. The origin of the positive effect of an increased fiber length on the amplification efficiency of the signal can be observed in Fig. 3.12(b). The backward emitted  $\text{Yb}^{3+}$ -ASE is reabsorbed after the pump light has been sufficiently depleted, so that the 1  $\mu\text{m}$  radiation is used to pump the 1.5  $\mu\text{m}$  signal. The same principle can also be used in amplifiers with copropagating pump radiation. It should however be noted that increasing the fiber length does not have influence on the – more powerful –  $\text{Yb}^{3+}$ -ASE emitted from the pump launch end of the fiber. Moreover, this technique cannot be used for all core-to-cladding ratios. Fibers with small core-to-cladding ratios – like all double-clad single-mode fibers – typically emit  $\text{Yb}^{3+}$ -ASE at wavelengths of 1060 nm and beyond. This leads to weaker reabsorption effects and, hence, also to decreased influences of extended fiber lengths on ASE at 1  $\mu\text{m}$  wavelength.

The described effects have also been demonstrated experimentally, which is presented in Fig. 3.13(a). Here, the output of two single-frequency amplifiers based on airclad LMA fibers (DC-250-25-ErYb from NKT Photonics) with 2.5 and 3 m length is compared. Both amplifiers were operated in a counterpropagating pump config-

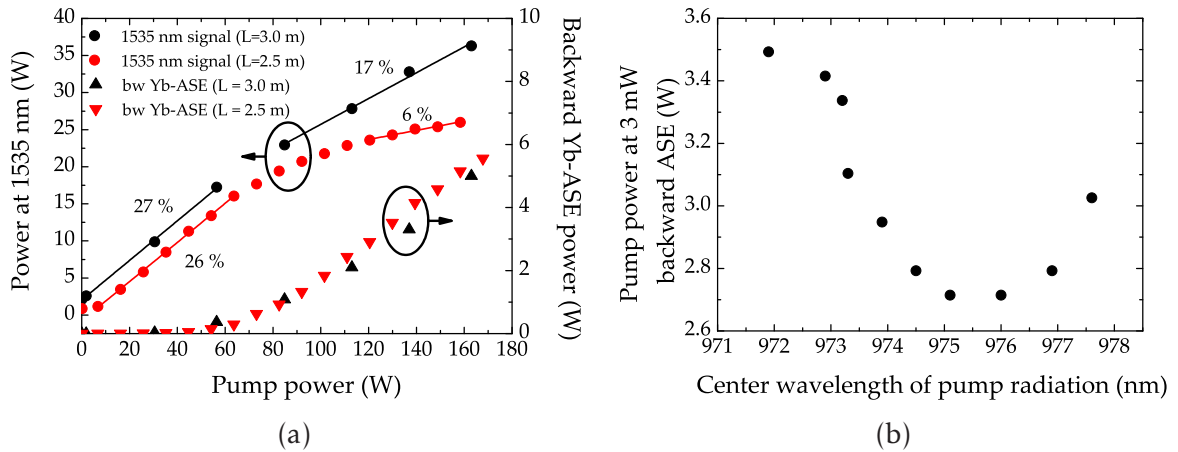


**Figure 3.13:** (a): Effect of fiber length increase from 2.5 m to 3 m in an  $\text{Er}^{3+}:\text{Yb}^{3+}$ -codoped air-clad LMA fiber with relatively large core-to-cladding ratio of about 1 : 10. (b): Demonstration of the spectral dependence of the threshold for  $\text{Yb}^{3+}$ -ASE from the fiber pump launch end. A pump diode laser with about 1 nm emission bandwidth was temperature tuned over the 976 nm absorption resonance of the  $\text{Yb}^{3+}$ -ions in a cladding pumped single-mode  $\text{Er}^{3+}:\text{Yb}^{3+}$ -codoped fiber.

uration. For further details about the fiber and the experimental setup see section 4.2.2 on pages 84 ff. By increasing the fiber length, the drop in optical efficiency after the onset of  $\text{Yb}^{3+}$ -emission could be significantly reduced. It dropped only to 17 % instead of 6 % from a nearly identical initial differential efficiency of about 26 %. Thus, at a pump power of about 160 W, a signal output power of 36 W instead of 26 W could be extracted from the amplifier. However, the reason of the only slight decrease of counterpropagating ASE power for the longer fiber is not fully clear. To be in full agreement with the above shown simulations this emission should be reduced for the longer fiber. Reasons for this discrepancy might be a different pump absorption distribution in the two different pieces of fiber or other effects not accounted for in the numerical model. Differences in the pump absorption distribution might, e.g., have arisen from doping concentration variations along the common preform of the two fiber pieces. Nevertheless, the above simulations suggest the correctness of the given explanation for the increase in differential optical efficiency for the longer piece of fiber.

In Fig. 3.13(b) also an experimental demonstration of the earlier onset of 1  $\mu\text{m}$  emission at a pump wavelength of 976 nm is presented. Here, the emission of counterpropagating ASE from a copropagatingly pumped double clad single-mode amplifier is shown for various central pump wavelengths. Thus, the  $\text{Yb}^{3+}$ -emission from the



### 3.3 Parasitic Emission from $Er^{3+}:Yb^{3+}$ -Codoped Fiber Amplifiers

pump launch end of the fiber is studied, so that eventual effects through different overall pump absorption do not play a role in this case. The 1  $\mu\text{m}$  wavelength emission solely depends on the pump power and wavelength in this case. The experiments were performed with a pump diode laser of type *BMU10A\_975\_01\_R* from *Oclaro Inc.* with a spectral full width at half maximum (FWHM) linewidth of about 1 nm. The center emission wavelength of this diode laser was temperature tuned around the  $Yb^{3+}$  absorption maximum at 976 nm. The threshold for ASE emission at 1  $\mu\text{m}$  wavelength was determined by measuring the pump power needed to obtain 3 mW of counterpropagating ASE power. It can be clearly observed that this threshold was decreased by almost 30 % when tuning the pump diode laser from 972 to 975 nm. This clearly supports the above obtained numerical results.

In conclusion, the simulation data presented in this section shows that parasitic  $Yb^{3+}$ -emission cannot be fully suppressed but influenced by specific design parameters of an  $Er^{3+}:Yb^{3+}$ -codoped fiber-based laser amplifier. It has been shown that the onset of parasitic emission is linked to the values of the  $Yb^{3+}$  pump rate and the connected  $Yb^{3+}$ -to- $Er^{3+}$  transfer rate. The input signal power and the choice between a co- and a counterpropagating pumping scheme have only minor influence on the parasitic  $Yb^{3+}$ -emission. However, if the  $Yb^{3+}$ -emission is in the spectral range of 1030 nm, an optimized fiber length can be used to partly reabsorb  $Yb^{3+}$ -ASE emitted from the fiber facet opposite of the pump launch end. Thus, higher amplification efficiency for the signal at 1.5  $\mu\text{m}$  wavelength can be reached. In order to increase the threshold for the emission of  $Yb^{3+}$ -ASE either larger pump claddings or a pump wavelength with correspondingly lower absorption cross sections can be used. This reduces the average number of absorbed pump photons per  $Yb^{3+}$ -ion and thus leads to a decrease of the  $Yb^{3+}$ -pump rate at a given point of the fiber. In order to further suppress  $Yb^{3+}$ -ASE, also several spectral filtering techniques can be used, which have been discussed briefly in the beginning of this section. It is also possible to inhibit parasitic ASE by extracting excess energy from the  $Yb^{3+}$ -ions with an auxiliary seed signal at 1  $\mu\text{m}$  wavelength as is described in more detail in the following section.



## 4 Experiments with $\text{Er}^{3+}:\text{Yb}^{3+}$ -Codoped Fibers

In the following chapters, experimental results that have contributed to the progress of the power scaling of single-frequency fiber amplifiers at 1.5  $\mu\text{m}$  wavelength are discussed. This chapter deals with the power scaling of  $\text{Er}^{3+}:\text{Yb}^{3+}$ -codoped fiber amplifiers. Experimental results obtained with  $\text{Yb}^{3+}$ -free  $\text{Er}^{3+}$ -doped LMA fibers are presented in chapter 5.

For the experiments presented in this thesis, different  $\text{Er}^{3+}:\text{Yb}^{3+}$ -codoped fibers have been used in several configurations. First, a novel scheme for the power scaling of  $\text{Er}^{3+}:\text{Yb}^{3+}$ -codoped single-mode fiber amplifiers by controlling the emission at 1.0  $\mu\text{m}$  wavelength is analyzed and discussed. In section 4.2 experiments with a novel type of  $\text{Er}^{3+}:\text{Yb}^{3+}$ -codoped LMA fiber are presented. The fractional  $\text{TEM}_{00}$  content of these so-called multifilament core (MFC) fibers was measured and compared to values obtained with commercial step index LMA fibers.

### 4.1 Experiments with Auxiliary Seed Signal at 1.0 $\mu\text{m}$ Wavelength

In years passed, output power levels in excess of 100 W have been reached with  $\text{Er}^{3+}:\text{Yb}^{3+}$ -codoped continuous wave fiber amplifiers. The highest output power from a single-frequency MOPA was reported by Jeong et al. in 2005 [140]. This work also impressively showed the onset of massive parasitic ASE emission around 1.0  $\mu\text{m}$  wavelength at high pump power levels. As mentioned before, significant ASE power levels typically imply a highly unstable and potentially hazardous mode of operation. Thus, the achievement of long-term stable operation of high power  $\text{Er}^{3+}:\text{Yb}^{3+}$ -codoped fiber amplifiers requires careful suppression of the gain for signals around 1  $\mu\text{m}$  wavelength.

As previously discussed in section 3.3, there have been several approaches to suppress parasitic emission at 1  $\mu\text{m}$  wavelength. However, all of these approaches relied on mere suppression of the  $\text{Yb}^{3+}$ -emission without addressing its origin. Thus, only

the threshold for parasitic emission at 1.0  $\mu\text{m}$  wavelength was increased without solving the fundamental problem of high small signal gain values in the  $\text{Yb}^{3+}$ -band. In 2007, Jeong et al. [139] showed that an  $\text{Er}^{3+}:\text{Yb}^{3+}$ -codoped fiber laser could be scaled to higher power levels around 1.5  $\mu\text{m}$  wavelength, when a controlled simultaneous laser oscillation at 1.0  $\mu\text{m}$  was supported instead of suppressed. This stable laser operation led to an efficient energy extraction from the  $\text{Yb}^{3+}$ -ions and prevented uncontrolled self-pulsing. Due to the stable laser oscillation, also the gain at 1.0  $\mu\text{m}$  and the  $\text{Yb}^{3+}$ -inversion were set to fixed values. For the work of this thesis, it was thus interesting to investigate the transfer of this scheme to single-pass single-frequency fiber amplifiers. The important difference is that the  $\text{Yb}^{3+}$ -inversion and thus the amplifier gain at 1  $\mu\text{m}$  are not clamped to a fixed specific value in such a system.

The following results are especially interesting as the codoping with  $\text{Yb}^{3+}$ -ions is currently the only way to realize truly single-mode  $\text{Er}^{3+}$ -doped double-clad fibers, while also allowing for fiber lengths with suitable SBS threshold values. These fibers typically have respective core and cladding diameters of about 7  $\mu\text{m}$  and 125  $\mu\text{m}$ . The core diameter cannot be increased because of the requirement for true single-mode waveguide properties, i.e., a V number of smaller than 2.405. The cladding diameter is in principle more flexible but commercial single-mode fibers are typically made with the industry standard cladding diameter of 125  $\mu\text{m}$ , because this diameter allows for the usage of most commercial pump couplers and other fiber based components without the need for customization. Without an increase in core absorption through  $\text{Yb}^{3+}$ -codoping the core to cladding ratio of these fibers would not allow for fiber lengths suitable for single-frequency fiber amplifiers. In the following, power scaling experiments performed with  $\text{Er}^{3+}:\text{Yb}^{3+}$ -codoped double-clad single-mode fiber amplifiers are presented and discussed. The performance of amplifiers simultaneously seeded around 1.5  $\mu\text{m}$  and 1.0  $\mu\text{m}$  is compared to that of conventional amplifiers without an auxiliary seed signal.

##### 4.1.1 Output Power Scaling with Auxiliary Seed Signal at 1064 nm

The setup of the experiments with an auxiliary seed signal at 1064 nm is shown in Fig. 4.1. The system was a double-clad single-mode  $\text{Er}^{3+}:\text{Yb}^{3+}$ -codoped single-frequency fiber amplifier. A commercial fiber-coupled single-frequency single-mode distributed feedback (DFB) diode (Type EM253-080-069 from EM4 Inc.) was used

#### 4.1 Experiments with Auxiliary Seed Signal at 1.0 $\mu\text{m}$ Wavelength

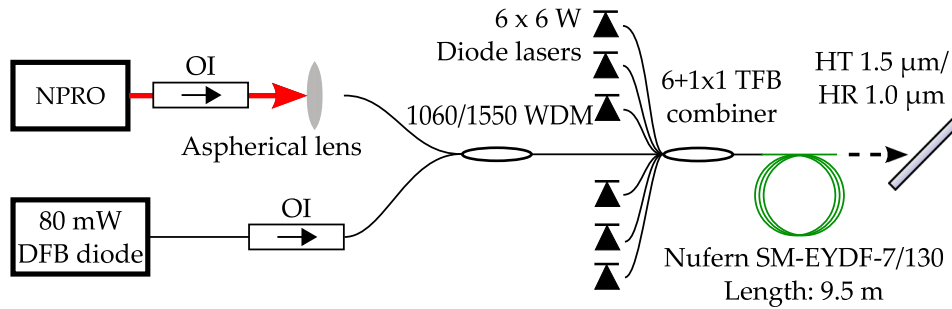


**Figure 4.1:** Setup of the experiments with the auxiliary seed signal at 1064 nm. NPRO: Non-Planar Ring Oscillator, OI: Optical Isolator, TFB: Tapered Fiber Bundle, WDM: Wavelength Division Multiplexer.

as seed source around 1.5  $\mu\text{m}$  wavelength. It emitted up to 80 mW of optical power at 1556 nm with a linewidth of  $< 10$  MHz. The linewidth was mainly determined by the noise characteristics of the utilized laser diode current driver. The auxiliary seed source at 1064 nm was a single-frequency Nd:YAG non-planar ring oscillator (Type Mephisto from Innolight GmbH) with a linewidth of  $< 1$  kHz. This narrow laser linewidth was not necessary for the intended use of the laser. However, the device was used due to its ability to provide up to 2 W of output power and also because of its availability at the time of the experiments. The two signal sources were protected against backreflections by a fiber-coupled and a free-space optical isolator, respectively.

The two signals were combined in a commercial 1060/1550 nm wavelength division multiplexer (WDM) coupler (Type FFW-8C32B2510 from Sifam Fibre Optics Limited) and then passed through a tapered fiber bundle (TFB) coupler (Type TFB-550611B70 from Sifam). The TFB coupler had a signal feedthrough and six ports for launching multi-mode pump radiation and combined the single-mode signal and multi-mode pump radiation in a double-clad output fiber. Six single-emitter laser diodes coupled to multi-mode fibers (Type SP-976-303 from Sheavmann, Inc.) were used as pump sources. Each of these diodes emitted up to 6 W of radiation at 976 nm out of delivery fibers with 105  $\mu\text{m}$  core diameter and NA of 0.15. The double-clad output fiber of the TFB coupler was spliced to the active fiber. This was a 9.5 m long piece of SM-EY-7/130 fiber from Nufern with a core NA of 0.17 and respective core and cladding diameters of 7 and 130  $\mu\text{m}$ . A measurement showed that about 50 mW of the input seed power at 1.5  $\mu\text{m}$  wavelength actually reached the active fiber. All free fiber ends were either angle-cleaved or terminated by angle-polished fiber con-

#### 4 Experiments with $Er^{3+}:Yb^{3+}$ -Codoped Fibers

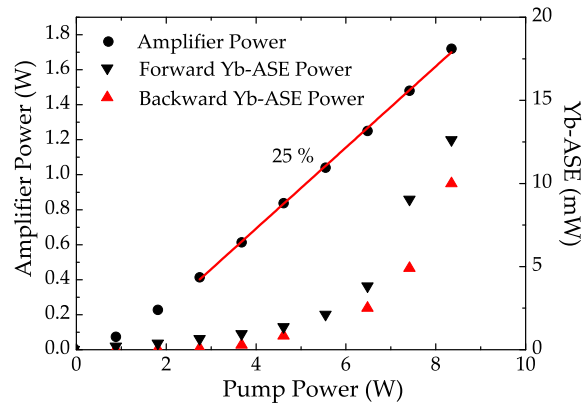


**Figure 4.2:** Emitted pump power plotted against signal power at  $1.5 \mu\text{m}$  wavelength in W (left) and  $Yb^{3+}$ -ASE power in mW (right) for no auxiliary seed signal at  $1064 \text{ nm}$ .

nectors to suppress backreflections.

First, the amplifier output characteristics without an input signal at  $1064 \text{ nm}$  are presented. Here, the differential optical-to-optical efficiency of the signal amplification at  $1.5 \mu\text{m}$  wavelength was 25 % with a maximum output power of  $1.72 \text{ W}$  (see Fig. 4.2). The power scaling was limited by the onset of parasitic emission at  $1.0 \mu\text{m}$  wavelength. This can be seen from the rise of  $Yb^{3+}$ -ASE power in Fig. 4.2 at high pump power levels and also from the corresponding developing maximum in the  $Yb^{3+}$ -ASE spectra shown in Fig. 4.3(b). The differential optical-to-optical efficiency was measured with respect to emitted pump power. This means that losses at splice connections and the TFB coupler were included into the calculated efficiency values. Behind the TFB coupler losses of about 10 % were measured. In addition, it is realistic to assume losses of 5 to 10 % at the splice connection of the TFB output and the active fiber. The chosen operating point of this amplifier was a relatively conservative one. It is likely that slightly higher output power levels could have been extracted from this system. However, one should keep in mind that this would have led to an increased storage of excess energy into the  $Yb^{3+}$ -ions. Consequently, also the probability and potential effect of occurring instabilities would have been increased. Unstable spurious lasing at  $1.0 \mu\text{m}$  wavelength would be likely to occur in such a state of operation, which could easily have led to the destruction of one or even several fiber end facets. On the other hand it was observable that the shape and characteristics of the spectra around  $1.5 \mu\text{m}$  (see Fig. 4.3(a)) were almost identical at all applied pump power levels. Unless stated otherwise, the resolution bandwidth of the optical spectrum analyzer (OSA) was set to  $0.5 \text{ nm}$  in all measurements of this

#### 4.1 Experiments with Auxiliary Seed Signal at 1.0 $\mu\text{m}$ Wavelength

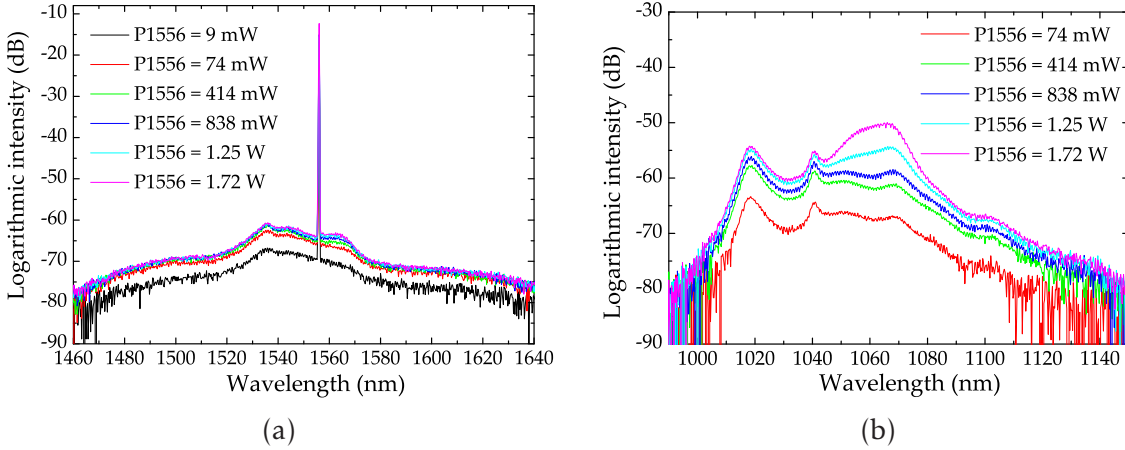


**Figure 4.3:** Signal spectra at 1.5  $\mu\text{m}$  wavelength (a) and Yb<sup>3+</sup>-ASE spectra (b) on logarithmic scale without any additional seed signal at 1064 nm. The resolution bandwidth of the OSA was set to 0.5 nm.

work. The most important fact regarding the spectra in Fig. 4.3(a) is that no significant changes were observable at power levels where the differential efficiency of the signal at 1.0  $\mu\text{m}$  started to increase and the shapes of the spectra around 1.0  $\mu\text{m}$  were altered. These facts already suggested that successfully extracting the excessive energy from the Yb<sup>3+</sup>-ions without unreasonable depletion of the signal at 1.5  $\mu\text{m}$  was indeed feasible.

When the non-planar ring oscillator (NPRO) was set to an output power of 60 mW, the optical spectra in the two emission bands changed to the ones shown in Fig. 4.4. The amplified signal at 1064 nm showed stable operation and a peak-to-peak ASE-suppression of > 40 dB. The peak-to-peak ASE-suppression at 1.5  $\mu\text{m}$  wavelength was even slightly larger and reached values of > 50 dB. The background ASE in Fig. 4.4(a) is not as observable as it is in Fig. 4.3(a). This is because a larger dynamic range was necessary to raise the ASE signals above the noise floor of the OSA. However, coupling more light into the OSA would have meant to risk damage to the device in case of unexpected pulsing behavior of the amplifier. This safety measure thus slightly complicates a direct comparison of the shape of the spectra at 1.5  $\mu\text{m}$  with and without the auxiliary signal. Nevertheless, it is clearly observable that in both cases a stable amplification process was achieved. However, the safely reachable output power levels were significantly higher when the auxiliary signal at 1.0  $\mu\text{m}$  wavelength was utilized. Thus, a clear increase in amplifier output power along with a significant decreased risk of amplifier instabilities could be reached with this novel amplifier



#### 4 Experiments with $Er^{3+}:Yb^{3+}$ -Codoped Fibers

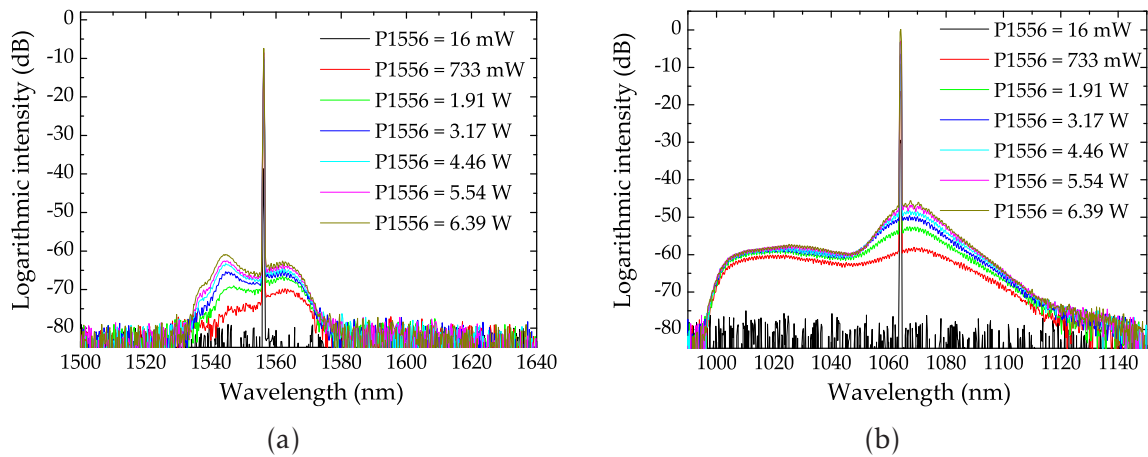


**Figure 4.4:** Spectra at (a) 1.5  $\mu\text{m}$  and (b) 1.0  $\mu\text{m}$  wavelength for 60 mW of auxiliary seed signal input power at 1064 nm. The resolution bandwidth of the OSA was set to 0.5 nm.

scheme.

The differential optical-to-optical efficiency of the 1.5  $\mu\text{m}$  signal remained at the value of 25 % up to pump power levels of about 25 W. At higher pump power it showed a slight roll-over to a value of 20 %. The output power versus launched pump power at 1.5  $\mu\text{m}$  is plotted in Fig. 4.5(a). The maximum obtained output power of 8.7 W was limited by the amount of available pump power instead of the onset of instabilities. In Fig. 4.5(b) the output power at 1.0  $\mu\text{m}$  wavelength is plotted against launched pump power. The optical-to-optical efficiency of below 10 % shows that the energy transfer between the  $Yb^{3+}$ - and  $Er^{3+}$ -ions was almost unaffected by the auxiliary 1064 nm signal. For a significant detrimental influence of the 1064 nm signal, a higher optical efficiency for the amplification at 1.0  $\mu\text{m}$  – and in turn a lowered efficiency at 1.5  $\mu\text{m}$  – would have been expected.

The low efficiency of the amplification at 1064 nm was probably caused by two effects. First, the heavy phosphorus co-doping of the utilized fiber, which led to an efficient depletion of the backtransfer of excitation energy from the  $Er^{3+}$ - to the  $Yb^{3+}$ -ions. Second, it was most probably supported by the non-zero absorption cross-section at 1064 nm of  $Yb^{3+}$ -ions in P-codoped glass [150]. It has even been reported on the pumping of  $Er^{3+}:Yb^{3+}$ -codoped fiber amplifiers at this wavelength [151]. The 976 nm pump light depletion at the end of the active fiber therefore allows for the reabsorption of the 1064 nm signal and an associated additional conversion of 1.0  $\mu\text{m}$  to 1.5  $\mu\text{m}$  radiation. It is noteworthy that this effect requires for pump and auxiliary



#### 4.1 Experiments with Auxiliary Seed Signal at 1.0 $\mu\text{m}$ Wavelength

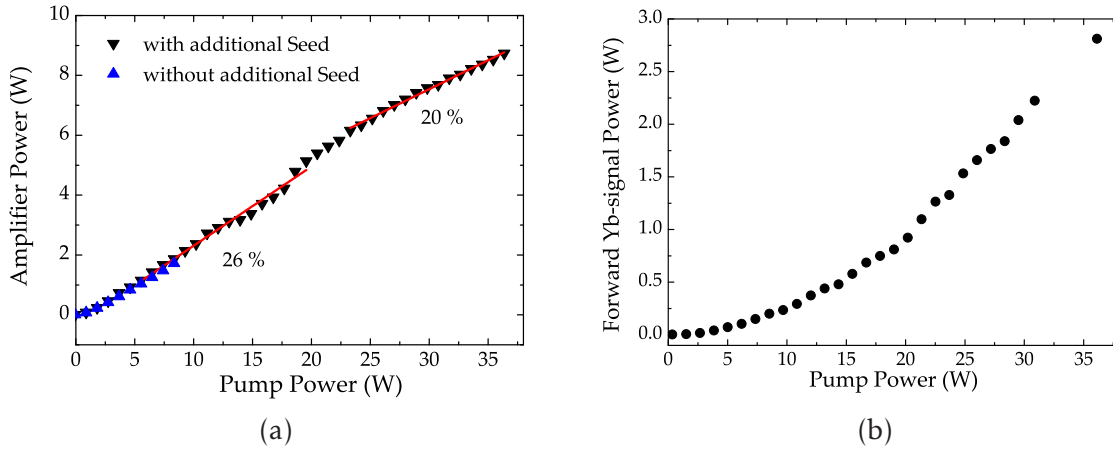


**Figure 4.5:** (a): Emitted pump power plotted against signal power at (a) 1.5  $\mu\text{m}$  and (b) 1.0  $\mu\text{m}$  wavelength for 60 mW auxiliary seed signal at 1064 nm input power.

seed radiation to be launched in the same direction. However, it should in principle be independent from the propagation direction of the signal at 1.5  $\mu\text{m}$  wavelength.

To further investigate the effect of the reabsorbed auxiliary seed signal, the influence of a change of its input power was examined. The input power levels of 1.5  $\mu\text{m}$  seed and 976 nm pump power were held constant, when the power of the auxiliary seed signal was changed. The feasibility of core pumping the amplifier with a 1064 nm signal is shown in Fig. 4.6(a). Here the 1556 nm signal – in absence of 976 nm pump radiation – is either amplified or at least less attenuated inside of the fiber as the 1064 nm signal power is increased. With increasing pump power at 976 nm the effect of a variation of the 1064 nm signal power changes. While for low diode pump power levels the 1064 nm radiation behaves like a pump signal, it partly becomes a competing seed signal with increasing diode pump power. This becomes manifest in the slight roll-over of the differential optical-to-optical efficiency of 1.5  $\mu\text{m}$  versus 1.0  $\mu\text{m}$  signal power near the maximum output power of the NPRO in Figs. 4.6(b) through 4.6(d). However, these results also pronounce once more the robustness of the amplification efficiency of the 1.5  $\mu\text{m}$  signal, even in the presence of a substantially stronger 1.0  $\mu\text{m}$  signal.

The fluctuations in output power, which are most pronounced in Figs. 4.6(b) and 4.6(d) can be explained by changes of the temperature of the active fiber. These temperature variations probably led to corresponding changes of the  $\text{Yb}^{3+}$  absorption cross-sections [142]. This means that tuning of the pump power led to a slow

#### 4 Experiments with $Er^{3+}:Yb^{3+}$ -Codoped Fibers

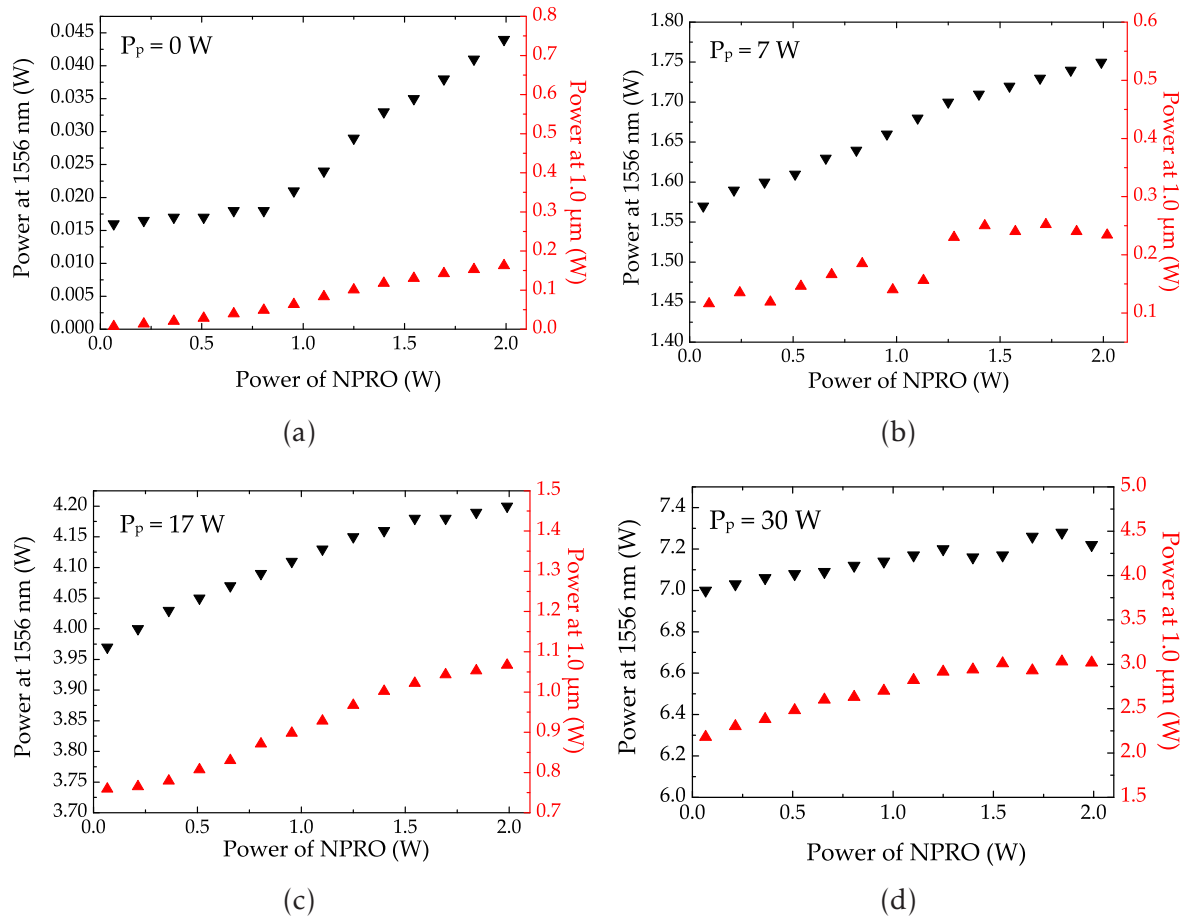


**Figure 4.6:** Emitted signal power at 1.0  $\mu\text{m}$  plotted against output power at 1.5  $\mu\text{m}$  (left; black) and at 1.0  $\mu\text{m}$  (right; red) for 80 mW seed power at 1.5  $\mu\text{m}$  and (a) 0 W, (b) 7 W, (c) 17 W and (d) 30 W of emitted pump power at 976 nm.

#### 4.1 Experiments with Auxiliary Seed Signal at 1.0 $\mu\text{m}$ Wavelength

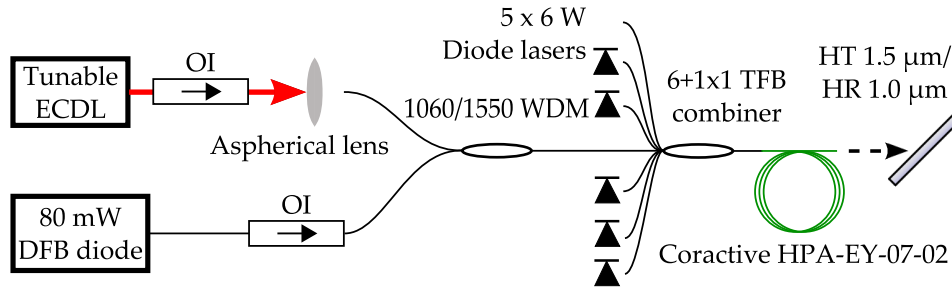


**Figure 4.7:** Experimental setup of the  $\text{Er}^{3+}:\text{Yb}^{3+}$ -codoped fiber amplifier auxiliary seeded by an ECDL. OI: Optical isolator; ECDL: External cavity diode laser; DFB-diode: Distributed feedback diode; WDM: Wavelength division multiplexer; TFB: Tapered fiber bundle; HR: High reflection; HT: High transmission

drift and relatively high uncertainty of the measured output power due to the large quantum defect of the laser system. This effect could in principle be suppressed by the utilization of temperature stabilization schemes for the active fiber. However, no changes to the applicability and underlying physics of the introduced operating scheme of  $\text{Er}^{3+}:\text{Yb}^{3+}$ -co-doped amplifiers were to be expected in this case.

##### 4.1.2 Influence of Auxiliary Seed Signal Wavelength Tuning

The experiments described in the previous section mainly focussed on the output power scaling of  $\text{Er}^{3+}:\text{Yb}^{3+}$ -codoped fiber amplifiers by using an auxiliary seed signal at 1  $\mu\text{m}$  wavelength. Following this, Han et al. [152] presented theoretical work, coming to the conclusion that the performance of  $\text{Er}^{3+}:\text{Yb}^{3+}$ -codoped fiber amplifiers with auxiliary 1  $\mu\text{m}$  wavelength seed should largely depend on the choice of wavelength in the  $\text{Yb}^{3+}$ -band. This is supposed to be due to the differing impact of reabsorption processes. Experiments that were performed to verify these theoretical predictions are presented in the following. In contrast to the experiments of the previous section, the focus now lay on effects related to tuning of the auxiliary seed wavelength rather than mere output power scaling at 1.5  $\mu\text{m}$  wavelength. As auxiliary seed source a tunable narrow-linewidth external cavity diode laser (ECDL) was employed.

The experiments were again performed with a cladding-pumped single-frequency amplifier with 7  $\mu\text{m}$  diameter truly single-mode fiber core. The only changes to the setup were the use of the ECDL as auxiliary seed source and the replacement of the active fiber due to a previously occurred damage. The setup is presented in Fig. 4.7.

#### 4 Experiments with $\text{Er}^{3+}:\text{Yb}^{3+}$ -Codoped Fibers

The tunable single-frequency signal of the ECDL had a linewidth of below 1 MHz and was tuned between 1055 and 1075 nm. The ECDL provided output power levels of about 55 mW between 1055 and 1070 nm and 47 mW at 1075 nm measured directly in front of the free-space-to-fiber coupling – i.e., behind the optical isolator. The combined losses of WDM coupler, optical isolators and – for the 1  $\mu\text{m}$  signal – free-space coupling resulted in respective transmission values of 58 % and 40% behind the WDM coupler for the 1.5  $\mu\text{m}$  and 1.0  $\mu\text{m}$  signals. An  $\text{Er}^{3+}:\text{Yb}^{3+}$ -codoped 7  $\mu\text{m}$  core and 125  $\mu\text{m}$  cladding single-mode fiber of type *HPA-EY-07-02* from *CorActive High-Tech Inc.* now served as active fiber. The specified cladding absorption at 915 nm was 0.7 dB/m and the pump power was provided by five fiber-coupled single-emitter diodes. Again, each of them delivered up to 6 W of output power at 976 nm out of multi-mode-fibers with 105  $\mu\text{m}$  core and a NA of 0.15. The emission of the two wavelength bands at 1.0  $\mu\text{m}$  and 1.5  $\mu\text{m}$  was separated by a dichroic mirror behind the active fiber. To study the effects of reabsorption of the  $\text{Yb}^{3+}$ -signal, an initial fiber length of 7.2 m was chosen. This led to an absorption of about 20 dB for the pump radiation at 976 nm. To further investigate the influence of reabsorption effects on the amplifier performance in a second series of measurements the fiber length was increased to 8.4 m by fusion splicing. Here, the application of high-index liquid to the splice connection ensured that almost no cladding guided pump light was able to enter the additional piece of fiber. To examine the influence of the auxiliary seed wavelength on the performance of the amplifier, the ECDL was tuned in 5 nm steps from 1055 nm to 1075 nm. The long wavelength limit was set by the tuning range of the ECDL, while the short wavelength limit was set by the amplification bandwidth of the utilized active fiber.

For the shorter fiber length of 7.2 m, the output power levels at 1.5  $\mu\text{m}$  and 1  $\mu\text{m}$  wavelength are shown in Fig. 4.8(a). The  $\text{Yb}^{3+}$ -emission began to rise at pump power levels above 5 W independently from the wavelength of the auxiliary seed. Before the onset of the  $\text{Yb}^{3+}$ -emission, the differential optical-to-optical efficiency of the 1556 nm amplification was nearly 20 % for all auxiliary seed wavelengths. However, the amplification efficiency at 1.0  $\mu\text{m}$  and the strength and exact position of the roll-over for the efficiency of the 1.5  $\mu\text{m}$  already show a significant dependence on the wavelength of the auxiliary seed signal. The roll-over of the 1.5  $\mu\text{m}$  amplification efficiency was very pronounced for the 1070 nm signal – as the differential efficiency dropped down to 4.6 % – while it became weaker for shorter auxiliary signal wavelengths. For the 1055 nm signal the differential efficiency only dropped to 12.8 %.

#### 4.1 Experiments with Auxiliary Seed Signal at 1.0 $\mu\text{m}$ Wavelength

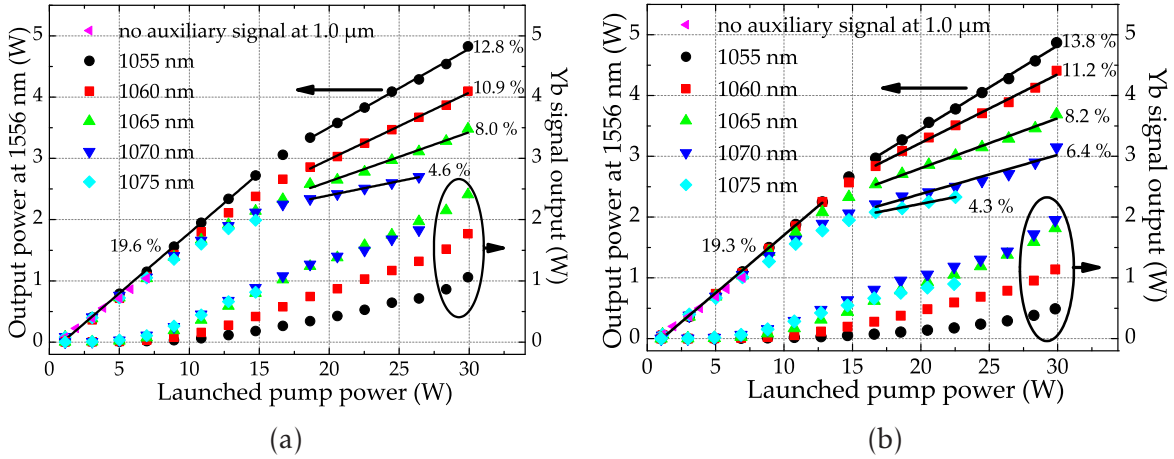


**Figure 4.8:** (a): Output power at 1.5  $\mu\text{m}$  (left scale) and 1.0  $\mu\text{m}$  (right scale) versus pump power at 976 nm for the different auxiliary seed wavelengths for active fiber lengths of (a) 7.2 m and (b) 8.4 m.

In the spectral range from 1075 to 1055 nm the absorption cross-section of the  $\text{Yb}^{3+}$ -ions increases for shorter wavelengths. Thus, the experimental data clearly supported the theoretical prediction of Han et al. [152]. They had underlined that efficient reabsorption of the auxiliary signal at 1.0  $\mu\text{m}$  allows for the conversion of 1.0  $\mu\text{m}$  to 1.5  $\mu\text{m}$ . The amplification efficiency of auxiliary signals at 1070 and 1075 nm decreased at high pump power levels, which ultimately even resulted in parasitic laser processes at shorter wavelengths. A possible explanation is that the net gain of the active fiber was shifted to shorter wavelengths with increasing pump power, which can have happened out of two main reasons. First, it could have been caused by thermal influences on the cross-sections of the  $\text{Yb}^{3+}$ -ions. Second, it could have happened due to the fact that – in contrast to a laser oscillator – the inversion level in and along a fiber amplifier is not fixed in case of pump power variations. The shift of the net gain is the reason why the amplifier was not operated at full pump power for wavelengths longer than 1065 nm. A decrease in amplification efficiency for the  $\text{Yb}^{3+}$ -signal would have implied the risk of the onset of  $\text{Yb}^{3+}$ -ASE and hence amplifier instabilities.

Also the short wavelength limit for the auxiliary seed signal was determined by the shifting net gain of the amplifier. The importance of this effect may also have been increased by the phosphosilicate host material with a possibly relatively narrow amplification bandwidth [153]. For an auxiliary seed signal at 1055 nm only insignificant amplification and hence longer wavelength ASE was observed at low pump powers.

#### 4 Experiments with $Er^{3+}:Yb^{3+}$ -Codoped Fibers

With increasing pump power the gain was sufficiently shifted to amplify the 1055 nm signal and inhibit the excessive generation of ASE. For auxiliary signals with wavelengths shorter than 1055 nm, the pump power necessary to induce a sufficient gain shift was higher than the power level at which the amplifier could be operated safely without a stably amplified auxiliary signal at 1  $\mu\text{m}$ . Therefore, the shortest auxiliary wavelength used in the experiments was 1055 nm, as the use of shorter wavelengths would have meant to risk damage to the amplifier system during turn-up of the pump power.

For the increased fiber length of 8.4 m, the output powers at 1.5  $\mu\text{m}$  and 1.0  $\mu\text{m}$  wavelength versus pump power are shown in Fig. 4.8(b). The amplification efficiency of the 1556 nm signal was increased for all auxiliary signals. However, the actual change in output power is most pronounced for the auxiliary signals with 1060 and 1065 nm wavelength. Comparison of Figs. 4.8(a) and 4.8(b) reveals that the increase in reabsorption of the  $Yb^{3+}$ -signal is stronger for the wavelengths between 1055 and 1065 nm than for the longer wavelengths. This explains the relatively weak influence of the fiber length on the output power at 1.5  $\mu\text{m}$  wavelength for auxiliary signals with 1070 and 1075 nm wavelength. In this spectral range, the optimum fiber length would still have been far longer. For the signals at 1060 nm and 1065 nm wavelength, the increase in reabsorption of the  $Yb^{3+}$ -signal led to a clearly observable increase also in absolute output power at 1556 nm. Thus, the predicted positive effects of increased reabsorption at 1.0  $\mu\text{m}$  were demonstrated for these wavelengths. For the 1055 nm auxiliary signal, the absolute output power at 1556 nm remained nearly unaffected at maximum pump power, as the roll-over in differential efficiency is also less pronounced, but takes place at slightly lower pump power levels. It can be observed for both wavelength bands that at maximum pump power all data points in Fig. 4.8 lie above their respective linear fit. The origin of this upward discrepancy is not fully clear, but seems to be solely depending on the pump power as it occurs simultaneously at both signal wavelengths. Therefore, it might be linked to a change to a more equally distributed pump light absorption behavior. This could have occurred as the emission spectra of the pump diodes were shifted slightly beyond the main  $Yb^{3+}$  absorption peak at 976 nm when being operated at full power.

In Fig. 4.9, the output spectra at 1.0  $\mu\text{m}$  wavelength for the 8.4 m long active fiber are shown together with the backward emitted  $Yb^{3+}$ -ASE without auxiliary seeding at an accordingly reduced pump power level. Again, the results are in good agreement

#### 4.1 Experiments with Auxiliary Seed Signal at 1.0 $\mu\text{m}$ Wavelength

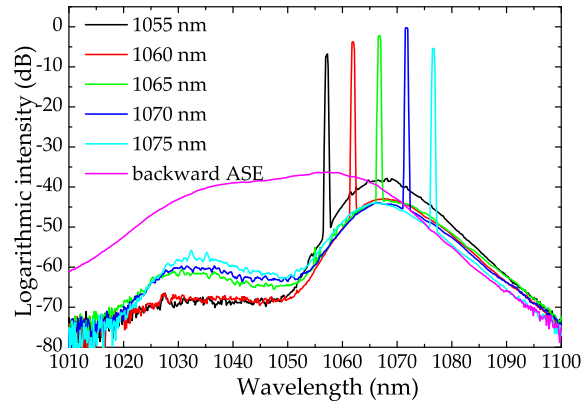


**Figure 4.9:** Representative output spectra of the auxiliary signal recorded at pump power levels of about 25 W for the 8.4 m long active fiber. The backward ASE spectrum was recorded at 7.5 W of pump power and is displayed for comparison and not to scale. The resolution bandwidth was set to 0.5 nm.

with the predictions of Ref. 152. The best performance of the system was reached, when the auxiliary seed was tuned to 1055 nm. This almost coincides with the maximum of the backward emitted  $\text{Yb}^{3+}$ -ASE as predicted by Han et al. [152]. Please note that the ASE maximum at a pump power level of 25 W would probably have been at a slightly shorter wavelength. However, at this high power level the position of the maximum could not be determined, because the auxiliary seed signal was mandatory for stable amplifier operation. A method to determine the optimal auxiliary seed wavelength for  $\text{Er}^{3+}:\text{Yb}^{3+}$ -codoped fiber amplifiers has been reported in a second publication by Han et al. in Ref. 154. Also this refined theoretical work leads to the conclusion that the spectral maximum of the  $\text{Yb}^{3+}$ -ASE emitted from the pump launch end of a fiber amplifier without any 1.0  $\mu\text{m}$  seed signal is a good indicator for its optimum auxiliary seed wavelength.

##### 4.1.3 Summary of Experiments with Auxiliary Seed Signal

In the experiments presented in this section, a new scheme to stabilize  $\text{Er}^{3+}:\text{Yb}^{3+}$ -codoped fiber amplifiers against parasitic emission at 1.0  $\mu\text{m}$  wavelength could be demonstrated. This was achieved with commercially available optical components and the use of an auxiliary seed signal at 1064 nm wavelength. An increase of single-frequency single-mode output power from below 2 W to 8.7 W at 1556 nm with an ASE suppression of  $> 50$  dB could be achieved by use of an auxiliary 1064 nm seed



signal. The fraction of the 1556 nm signal that reached the active fiber was only about 50 mW. Thus, a stable amplification of  $> 22$  dB was demonstrated, which is – especially in a co-directional pumping scheme – a very high value for a large signal  $\text{Er}^{3+}:\text{Yb}^{3+}$ -codoped fiber amplifier.

In further experiments, the influence of different auxiliary seed wavelengths was investigated for the first time. The results showed good agreement with the theoretical predictions of Han et al. in Ref. 152. Shorter auxiliary seed wavelengths and increased reabsorption clearly increase the efficiency of the 1.5  $\mu\text{m}$  signal. It could also be observed that the optimum auxiliary seed wavelength roughly coincided with the maximum of the backward  $\text{Yb}^{3+}$ -ASE of the system when seeded only at 1.5  $\mu\text{m}$ , which was also theoretically predicted. Due to the increased reabsorption for shorter wavelength auxiliary seed signals such amplifier systems can also be realized with only slightly increased fiber lengths compared to conventional amplifiers.

Additionally, the relatively weak influence of a power variation of the auxiliary seed signal at 1064 nm wavelength indicated an intrinsic robustness to auxiliary signal input power variations. This should guarantee for a broad range of applicable input powers and power densities in an amplifier of the described kind. Therefore, similar behavior of high power LMA fiber amplifiers can be expected, as long as also the pump absorption coefficient is similar [152]. Thus, the demonstrated scheme shows good prospects to allow for high power  $\text{Er}^{3+}:\text{Yb}^{3+}$ -codoped fiber amplifiers without the  $\text{Yb}^{3+}$ -ASE induced instabilities.



## 4.2 Study of Mode Content from Multifilament and Step-Index Fiber Cores

It is challenging to develop  $\text{Er}^{3+}:\text{Yb}^{3+}$ -codoped LMA fibers with low core NA values. In conventional step-index designs, the necessary codoping with phosphorus raises the core NA to about 0.2. This leads to multi-mode fiber cores for core diameters larger than about  $7\ \mu\text{m}$ . Thus, several approaches to realize  $\text{Er}^{3+}:\text{Yb}^{3+}$ -codoped low NA fibers have been made, as was previously discussed in section 3.2.4. The most conventional approach to decrease the core NA despite the high index of refraction of the core material is to surround the fiber core with a Ge-doped refractive index pedestal. This leads to a decrease of the index difference between the fiber core and its environment and allows for a reduction of the core NA to values of about 0.1. Feasible values for the refractive index step are limited by inhomogeneities in the core-pedestal boundary and the finite refractive index flatness of the fiber core. For core diameters larger than  $20\ \mu\text{m}$ , the NA values achievable with pedestal designs allow only for the fabrication of few mode fibers with V numbers still larger than 5. Such values naturally lead to the need of further investigations concerning the actual mode composition of the fiber output. This is especially the case, if not only low  $M^2$ -values, but predominant  $\text{TEM}_{00}$  operation is required.

A different approach to realize  $\text{Er}^{3+}:\text{Yb}^{3+}$ -codoped LMA fibers with excellent output beam quality and simultaneously larger mode areas are multifilament core (MFC) fibers. Here, the core region consists of many small  $\text{Er}^{3+}:\text{Yb}^{3+}$ -codoped filaments. In earlier described multi-core fibers (MCFs) [155] an arrangement of isometric and equally-spaced single-mode cores with weak intercore coupling was used. This allowed for the formation of different supermodes [156]. In contrast to multi-core designs multifilament core fibers aim for strong coupling between the smaller sized individual filaments. This results in the propagation of only one supermode when adequate values are chosen for diameter and spacing of the filaments. Active as well as passive MFC fibers have been demonstrated, which allowed transversely single-mode output with nearly Gaussian-shaped intensity mode profiles [105, 157]. The main advantage of this new fiber type is the low effective core numerical aperture despite the above mentioned necessary strong codoping with phosphorus. The effectively low NA results from refractive index averaging effects caused by the sub-wavelength dimensions of the filaments in the transverse fiber profile. Important

properties of the MFC fibers can be explained using an equivalent step index based on the theory of the fundamental space filling mode [104].

In the following, the measurement and comparison of fractional  $TEM_{00}$  content in the output beams of pedestal design and MFC fiber based amplifiers are described. The major motivation for this was that laser sources for the current interferometric GWD concepts require the highest possible relative  $TEM_{00}$  mode content. However, knowledge about the  $TEM_{00}$  content is also of relevance for many more applications, especially, when narrow laser linewidths are required. This is because higher order modes can lead to uncontrollable pointing instabilities and peak power fluctuations in the output beam of a fiber laser system [100]. Therefore,  $M^2$ -measurements are very often not fully adequate for a sufficient characterization of the output beam of a (fiber) laser system.

Regarding the special waveguide properties of the MFC fibers, it is not obvious that a single guided supermode will also result in a near fundamental mode output with respect to TEM modes. These uncertainties could also not fully be ruled out by Refs. 105 and 157 as the  $M^2$ -measurements therein only give limited information about the mode content. Even  $M^2$ -values of  $< 1.1$  still allow for the fraction of higher order mode beam content to be as high as 30 % [100]. The experiments presented in the following were thus focussed on a comparison of the  $TEM_{00}$  mode content in large mode area MFC- and pedestal-design fibers. The measurements were performed with a non-confocal scanning ring cavity. The fibers were used in single-frequency amplifier configuration. The non-confocal scanning ring cavity technique was first introduced by Willke et al. in Ref. 1 and afterwards utilized and refined in several subsequent experiments [158, 159]. In the experiments performed for this thesis, this technique was for the first time applied in the wavelength region of  $1.5 \mu\text{m}$ . In addition, it was also used for the first time for the measurement of the fractional  $TEM_{00}$  content of the output of MFC and pedestal design fibers.

There have also been reports on an alternative method of fiber mode content evaluation, the so called  $S^2$ -imaging. This technique has also been applied in the vicinity of  $1.5 \mu\text{m}$ , giving access to information about the eigenmodes of an  $Er^{3+}$ -doped fiber with  $70 \mu\text{m}$  core diameter [160]. However, especially for the development and characterization of GWD laser sources the non-confocal scanning ring cavity technique has two major advantages with respect to  $S^2$ -imaging. First, the scanning ring cavity technique measures the beam content in free-space TEM modes instead of the fiber

eigenmodes. Thus, the mode of interest for GWD applications is directly accessed. Therefore, the  $TEM_{00}$  content measurements are not subject to uncertainties related to eventual – and especially in phosphorus-doped fibers very common – fiber-mode distortions. These can for example be the result of deviations from an ideal step-index profile and can potentially decrease the overlap of the fundamental fiber mode with the  $TEM_{00}$  mode. Such deviations can, e.g., originate from a center dip formation or index oscillations in the transverse refractive index profile. The  $S^2$ -imaging technique is also able to reconstruct the shape of the fiber eigenmodes to some extent, but the mode scanning technique is intrinsically less sensitive to the described effects by using a fixed set of modes. Agreeably, these facts do not impose a drawback on the vast majority of applications. However, the described issues can be noteworthy for systems with very high requirements on mode purity with respect to free-space modes. Second, the mode scanning technique cannot only be used to determine the  $TEM_{00}$  mode content of a laser beam, but is also readily applicable to clean it from higher order modes by locking the cavity to the transmission of the  $TEM_{00}$  mode as already demonstrated in by Willke et al. in Ref. 1. Thus, high power laser beams with extremely high  $TEM_{00}$  mode purity can be reliably produced and injected into interferometric gravitational wave detectors.

### 4.2.1 Mode Cleaning Cavity Setup

The schematic of the used triangular scanning ring cavity is shown in Fig. 4.10. The measurement principle exploited that the scanning cavity was non-confocal. Thus, its different transverse eigenmodes – which are by design the TEM modes – had non-degenerate eigenfrequencies. In addition, the cavity had a finesse of about 285 at 1535 nm. This led to a narrow transmission bandwidth of about 2.5 MHz that – if a single-frequency beam was analyzed – allowed only for distinct transverse modes to be transmitted through the cavity with its free spectral range of 714 MHz. Since this transmission band could be tuned by changing the length of the resonator, a single-frequency input beam could be decomposed into TEM modes by injecting a ramp signal to the piezoelectric transducer shown in Fig. 4.10. Afterwards a time-resolved analysis of the signal transmitted through the cavity was carried out. It should be noted that all beam content that was at a given time not transmitted through the cavity was rejected from it and therefore sent into the reflection path depicted in

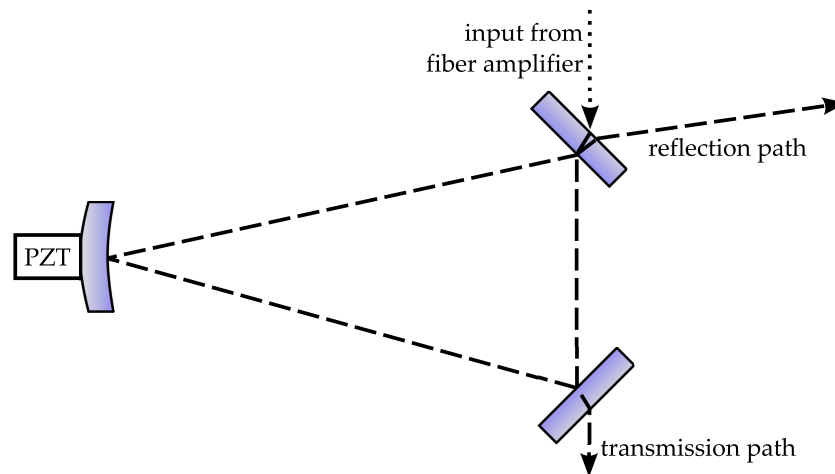


**Figure 4.10:** Schematic depiction of the triangular non-confocal mode scanning cavity that was used for the TEM mode content analysis. PZT: Piezoelectric transducer.

Fig. 4.10. A detailed description of this measurement technique and the associated analyzing algorithm can be found in Ref. 159.

#### 4.2.2 Fiber Amplifier Setup

All of the examined fibers were used in the single-frequency amplifier configuration depicted in Fig. 4.11. This configuration was chosen for two main reasons. First, the performed measurements could only be made with single-frequency beams. Second, the intention was to test the fibers under operating conditions. Thus, the beam composition of the amplifier output beams was measured at several watts of power instead of performing the measurement on a single-mode beam being simply transmitted through a short piece of unpumped fiber. This approach thus also accounted for the possible influence of excess gain for higher order modes (see e.g. Ref. 48).

The seed source of the amplifier was a single-frequency DFB-diode (manufactured by EM4 Inc.) with a maximum output power of 80 mW at 1535 nm wavelength. The linewidth of about 10 MHz was again limited by noise of the driving current. Therefore, the spectral linewidth of the measured peaks in the mode scanning signals was mainly determined by the seed source. As cavity and diode linewidth were in the same order of magnitude, eventual effects of the amplification process on the signal linewidth could not be fully resolved in the presented experiments.

The input signal was amplified to 1.5 W in an all-fiber preamplifier based on a

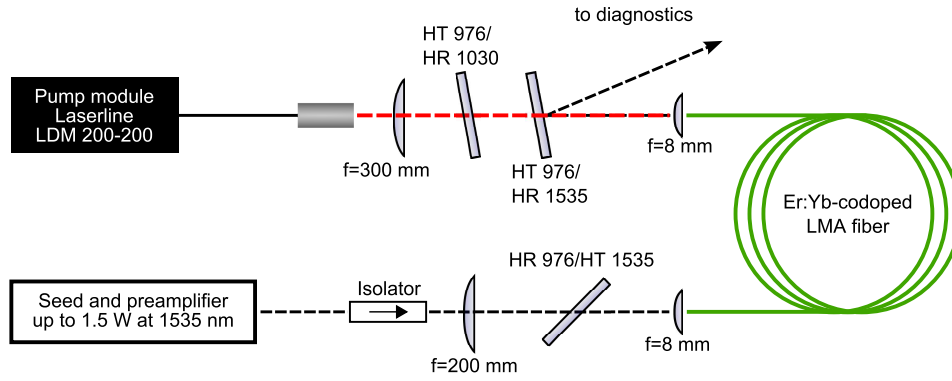


**Figure 4.11:** Schematic depiction of the experimental setup of the fiber amplifiers that were analyzed with the non-confocal scanning ring cavity.

7  $\mu\text{m}$  core  $\text{Er}^{3+}:\text{Yb}^{3+}$ -codoped single-mode double-clad fiber. The output beam of the preamplifier was collimated with an aspherical lens and then passed through a Faraday isolator for protection against backreflections. The beam was mode-matched to the respective signal core of the utilized LMA fibers with a spherical  $f = 200$  mm lens and a  $f = 8$  mm aspherical lens, collimated again at the fiber exit and separated from the pump light by a dichroic mirror (high transmission for 976 nm, high reflection for 1535 nm). The mode content measurements were performed after reflection from the dichroic mirror, a power adjustment to the scanning cavity via waveplates and polarizers – as the scanning cavity needed a linearly polarized input beam at a power level between 80 and 90 mW – and after mode-matching to the mode scanning cavity with the help of two spherical lenses.

The LMA fiber amplifiers were pumped in a counter-propagating scheme with a diode laser module (Laserline LDM 200-200 by Laserline GmbH) that delivered up to 200 W at 976 nm. The pump light was delivered through a 200  $\mu\text{m}$  fiber with a NA of 0.22, collimated in a commercial high power fiber collimator and coupled into the active fibers by a spherical  $f = 300$  mm lens and an aspherical lens with a focal length of 8 mm.

Mode content measurements were performed on the output beams of three different active fibers, one with pedestal design and two of MFC type. Details about the specific fibers are listed in Table 4.1. The pedestal design fiber was a commercial product. Its core parameters resulted in a V number of 5.2 at 1535 nm wavelength. Both of the investigated MFC fibers were manufactured by the Institute of Photonic Technology (IPHT) Jena. Their common initial preform was prepared by MCVD (Modi-

#### 4 Experiments with $Er^{3+}:Yb^{3+}$ -Codoped Fibers

Fiber No.	Core diameter	Core type	Manufacturer	Fiber ID
1	23 $\mu\text{m}$	pedestal	NKT Photonics	DC-250-25-ErYb,Ge-PM
2	31/28 $\mu\text{m}$	MFC	IPHT Jena	620sKK2
3	41/38 $\mu\text{m}$	MFC	IPHT Jena	620sKK3

**Table 4.1:** Properties of the fibers that were analyzed regarding their fractional  $TEM_{00}$  output beam content.

fied Chemical Vapor Deposition) and solution doping in a fluorine-doped silica tube. The fluorine-doped silica had an index difference of  $\Delta n = -1 \cdot 10^{-3}$  relative to fused silica. For the fabrication of the fiber preform, a stack of 37 Er:Yb-codoped rods was jacketed with a silica tube and milled to form the double-D shaped cladding around the filamented core (see Fig. 4.12) [157]. This final preform was drawn to fibers with cladding diameters of 250/210  $\mu\text{m}$  and 330/270  $\mu\text{m}$ , respectively. Here, the larger number is the diameter of the round fiber part while the smaller number indicates the flat-to-flat distance of the double-D shaped fiber. The fibers were then coated with silicone rubber, which led to a cladding NA of 0.35. In the final fibers, the filaments had diameters of 1.8  $\mu\text{m}$  and 2.4  $\mu\text{m}$  and a center-to-center distance of 5.1  $\mu\text{m}$  and 6.7  $\mu\text{m}$ , respectively. This resulted in hexagonal cores with diameters of 31/28  $\mu\text{m}$  (fiber No. 2) and 41/38  $\mu\text{m}$  (fiber No. 3). The core diameters of the hexagonal MFC fiber cores are given in the form of tip-to-tip/face-to-face distance to fully account for their non-circular shape. Hence, "31/28  $\mu\text{m}$  core" denotes a tip-to-tip diameter of 31  $\mu\text{m}$  and a face-to-face diameter of 28  $\mu\text{m}$  of the hexagonal core. A schematic depiction of the transverse profile of the fiber with 31/28  $\mu\text{m}$  core is shown in Fig. 4.12(a). The following presentation of the results is mainly focused on fibers No. 1 and No. 2. Fiber No. 3 reached efficiency values comparable to the smaller MFC fiber – as expected as they were made from the same perform – but produced a clearly multi-mode output.

#### 4.2.3 Numerical Simulations of Fiber Mode Contents

In addition to the experiments also numerical calculations of the fiber core waveguide properties were performed. Eigenmodes of the examined fibers were calculated with the widely known beam propagation method [161] by use of the commercial software BeamProp (developed and distributed by RSoft Design Group, Inc.). According to the simulation data, fiber No. 1 was capable of guiding four modes, namely  $LP_{01}$ ,  $LP_{11}$ ,

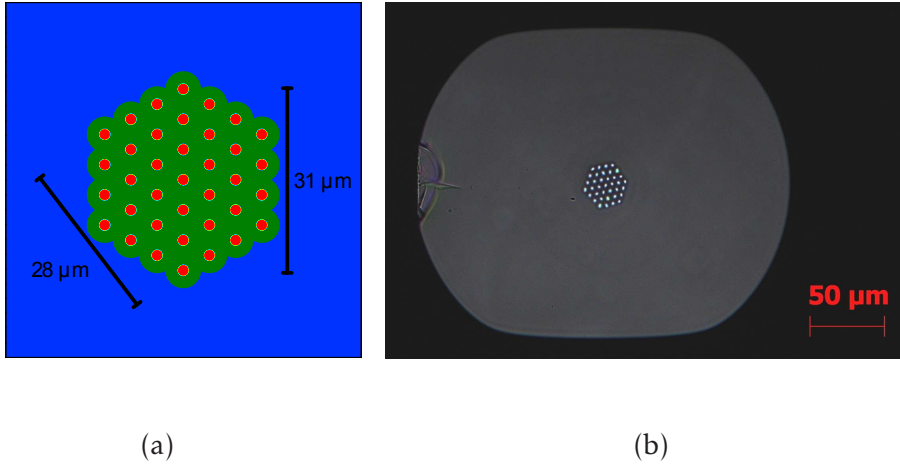


**Figure 4.12:** (a): Schematic depiction of the transverse profile of MFC fiber core with 31/28 μm diameter. The filaments are shown in red, fluorine doped silica in green and undoped silica in blue. (b): Corresponding photograph of cleaved end facet.

$LP_{21}$  and  $LP_{02}$ . In these simulations, only the index step from core to pedestal was taken into account and an ideal step-index profile was assumed. In addition to the core diameter and the numerical aperture, bending of the fiber with a diameter of about 20 cm was included into the simulations. The same diameter was applied in the experiments. It was the smallest value that could be reached without applying strong force to the fiber and risking its damage. With respect to its  $1/e^2$ -diameter, the intensity profile of the  $LP_{01}$ -mode had a simulated mode area of 290 μm<sup>2</sup> and 19.2 μm diameter.

For fiber No. 2 the simulations were performed using an index difference of 0.012 between the filaments and the surrounding fluorine-doped silica. The F-doped silica had an index reduced by 0.001 compared with the silica cladding. The values for the index differences were deduced by the IPHT Jena from measurements on the fiber preform. Only one mode was retrieved during these simulations. The intensity profile of this mode is shown in Fig. 4.13. The profile clearly shows structures related to the filament topology of the fiber core. Because of these deviations from conventional fiber mode shapes, the mode field area was not defined by the  $1/e^2$ -diameter with respect to intensity. Instead, the more general relation (see, e.g., [162])

$$A_{\text{eff}} = \frac{\left( \int |E|^2 dA \right)^2}{\int |E|^4 dA} = \frac{\left( \int I dA \right)^2}{\int I^2 dA} \quad (4.1)$$



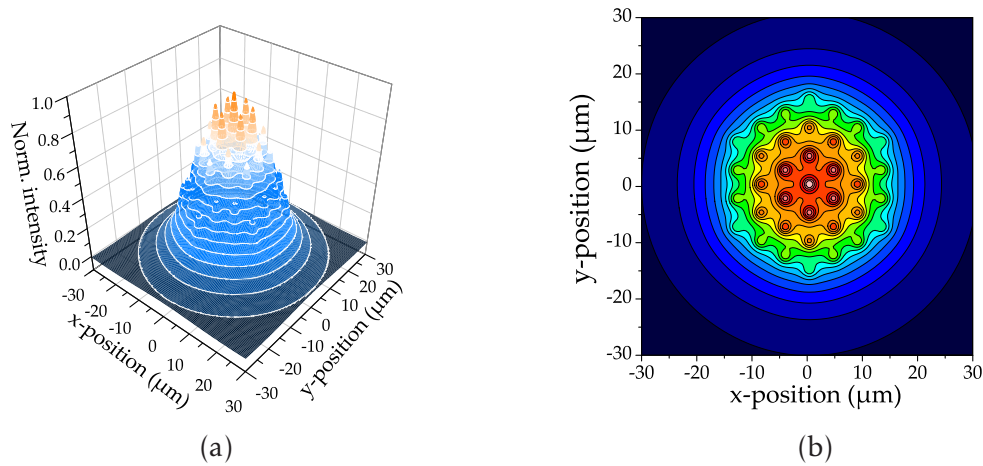


**Figure 4.13:** (a): 3D-plot of calculated fiber mode field profile of the 31/28  $\mu\text{m}$  MFC fiber. (b) Contour plot of calculated fiber mode field profile of the 31/28  $\mu\text{m}$  MFC fiber.

was used to determine the size of the mode field area. For a Gaussian shaped intensity distribution with a radial  $e^{-r^2/r_{\text{mode}}^2}$ -dependence, the result of eq. (4.1) equals  $\pi \cdot r_{\text{mode}}^2$ . By applying this formula to the calculated mode field, its area was estimated to be about  $720 \mu\text{m}^2$ . This is about 2.5 times larger than for the previously treated pedestal design fiber. A Gaussian shaped fiber mode of equivalent mode area would have a  $1/e^2$ -diameter of  $30.3 \mu\text{m}$ . The numerical overlap integral between the calculated fundamental MFC mode and the Gaussian mode with equivalent mode area resulted in a value of 92 %. It is noteworthy that the calculated overlap with a Gaussian mode with a diameter of slightly above  $20 \mu\text{m}$  was even higher and reached values greater than 99 %. Thus, a very high overlap with the fundamental Gaussian mode could be expected in the experiments. Nevertheless, due to the filamented structure of the fiber core it seemed also possible that the fundamental mode of the MFC-fiber consisted – as a supermode – of several modes with not fully degenerate propagation constants. However, the performed simulations did not reveal any hints to a substructure of the obtained fiber mode. Moreover, weakly non-degenerate modes would not impose an immediate drawback for GWD applications. The reason for this is that in a MOPA configuration no additional spectral components can be generated in case of the occurrence of different modal propagation constants. Varying phase shifts between these potential sub-modes would only lead to slight changes of the output beam profile. Thus only weak influences on the long term stability of the mode profile and consequently also on the fractional  $\text{TEM}_{00}$  content would potentially be observable.



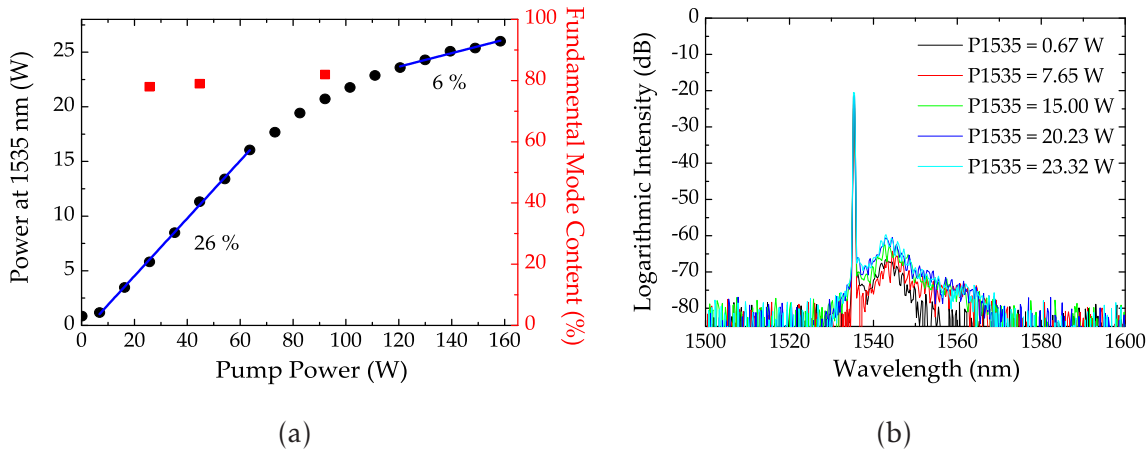


**Figure 4.14:** (a): Signal output power at 1535 nm of fiber No. 1 (black circles; left scale) and measured  $TEM_{00}$  mode content (red squares; right scale) versus emitted pump power at 976 nm. (b) Output spectra obtained with amplifier built with fiber No. 1 around 1535 nm at various output power levels.

#### 4.2.4 Experiments

In the following, the amplifier performance and measured  $TEM_{00}$  mode content values obtained for the pedestal-design fiber are presented. The amplifier output power at 1535 nm versus emitted pump power at 976 nm is plotted on the left scale in Fig. 4.14(a). The active fiber was a 2.5 m long piece of fiber No. 1, which corresponded to about 15 dB of pump light absorption at 976 nm wavelength. The output spectra are shown in Fig. 4.14(b). They indicate stable amplifier output and show a peak-to-peak ASE suppression of about 40 dB at 23.3 W of output power. The resolution bandwidth was set to 0.5 nm. A roll-over in differential optical-to-optical efficiency can be observed around 90 W of emitted pump power. This occurred due to an insufficient energy transfer from the  $Yb^{3+}$ -ions to the  $Er^{3+}$ -ions at these relatively high pump power levels (see section 3.3.2 on pages 55 ff.).

As shown on the right scale in Fig. 4.14(a), the fractional  $TEM_{00}$  content was measured to be above 80 % at all power levels. The highest value of 82 % was obtained at an output power of 20 W. No mode content values were recorded at higher power levels, because these measurements required stable operation for at least several minutes that could not be guaranteed at high  $Yb^{3+}$ -ASE power levels. The corresponding transmission signal of a complete sweep through the free spectral range of the scanning cavity is shown in Fig. 4.15. The  $TEM_{00}$  content was determined from this

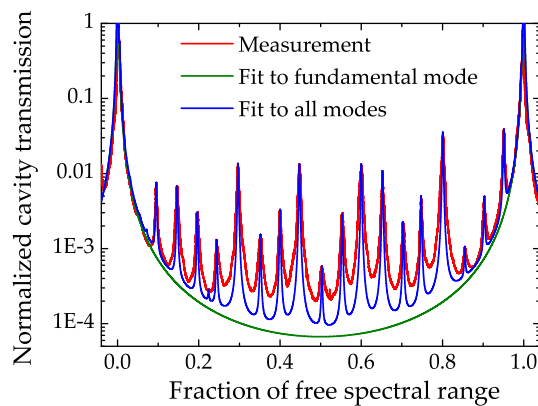


**Figure 4.15:** Mode scanning signals on logarithmic scale of fiber No. 1 at 20 W output power with a result of 82 %  $TEM_{00}$  mode content.

signal by comparing a perfect  $TEM_{00}$  fit (dashed green line in Fig. 4.15) and a complete modal fit (dotted blue line) of the measured signal (solid red line). Each peak in the mode scanning signal represents a distinct transverse mode. However, it is very important to note that the number of observed modes gives only very limited information about the actual beam quality, as also the magnitudes of the individual modes have to be taken into account. Furthermore, there is no immediate connection between the number of guided fiber core modes and the number of detected free-space TEM modes. Even for predominant  $TEM_{00}$  beam content, the mode scanning signal will – especially on a logarithmic scale – still show many small peaks. This is, e.g., due to unavoidable residual mode mismatching between the  $TEM_{00}$  content of the analyzed beam and the fundamental mode of the mode scanning cavity. Any mismatched part of the input beam was thus decomposed into the set of cavity higher order modes.

The slight improvement in beam quality with rising output power, which can be observed in Fig. 4.14(a), differs from previous reports on  $TEM_{00}$  content measurements on an  $Yb^{3+}$ -doped photonic crystal fiber amplifier reported by Hildebrandt et al. in Ref. 9. However, this difference might be readily explained by the fact that the measurements of this thesis were performed on the output of an all-glass signal waveguide fiber. While this showed even larger internal heat generation (due to the lower optical-to-optical efficiency), the fiber itself was most probably far less sensitive to thermal stress induced effects than the photonic crystal fiber of Ref. 9.

Despite the relatively large  $V$  number of above 5, the commercial pedestal design

## 4.2 Study of Mode Content from Multifilament and Step-Index Fiber Cores

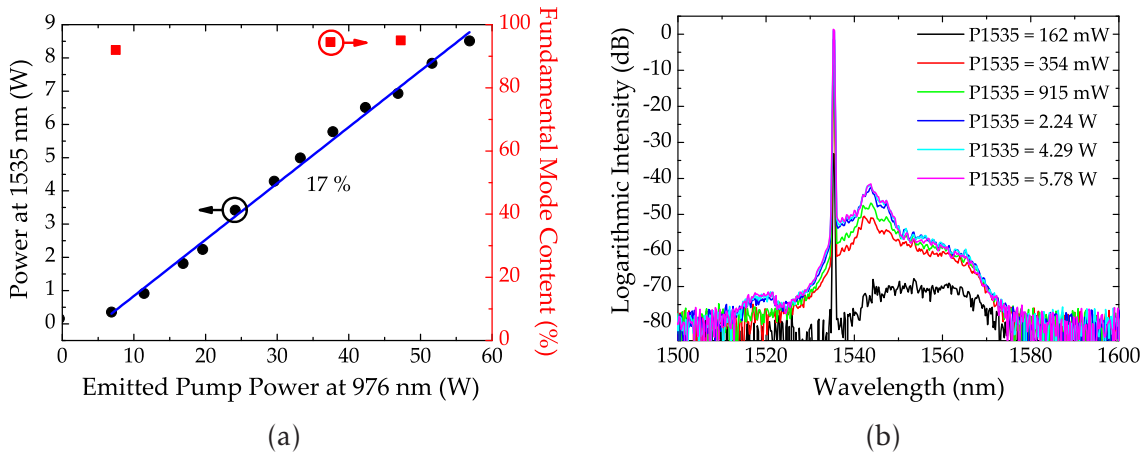


**Figure 4.16:** (a): Output power of the 31/28  $\mu\text{m}$  MFC fiber (circles) and measured fractional  $TEM_{00}$  content (squares) versus emitted pump power at 976 nm. (b) Output spectra obtained with amplifier built with 31/28  $\mu\text{m}$  MFC fiber around 1535 nm at various output power levels. The output spectra at the highest output power is missing due to thermal failure of the fiber at this power level.

fiber delivered output beams with more than 80 % of measured fractional  $TEM_{00}$  content. However, the fiber also showed behavior known from fibers capable of guiding more than one transverse mode. For example, the output beam profile (monitored with a phosphor coated silicon chip camera) was very sensitive to external forces applied to the fiber or changes in the alignment of the single-mode input beam.

A clear reduction of the influence of external forces was observed when switching to fiber No. 2. Here, it was also possible to excite at least a type of  $LP_{11}$  mode by changing the alignment at the input of the fiber. However, once the fundamental fiber mode was excited cleanly, there were only negligible distortions of the beam profile observed when applying external stress. Output power at 1535 nm and fractional  $TEM_{00}$  beam content versus emitted pump power at 976 nm are plotted in Fig. 4.16(a). The used fiber length was 3.8 m, which led to a pump absorption of slightly below 15 dB. The average differential optical-to-optical efficiency with respect to emitted pump light was 17 %. The maximum extracted power of 8.5 W was limited by thermal failure of the silicone rubber fiber coating. Please note that the differential efficiency with respect to emitted pump power also includes other losses than the quantum defect of the fiber. These originate, e.g., from the pump light coupling to the fiber and the transmission of non-absorbed pump light, so that the efficiency with respect to absorbed pump light was several percent higher. As shown

in Fig. 4.16(b), the amplifier operated with a peak-to-peak ASE suppression of about 40 dB measured with a resolution bandwidth of 0.5 nm. The emission of  $Yb^{3+}$ -ASE was negligible at all applied pump power levels, but would surely have increased at higher pump power levels, given that thermal damage of the fiber could have been prevented.

The transmission signal through the mode scanning cavity at about 7 W of output power at 1535 nm is shown in Fig. 4.17(a). As also included into Fig. 4.16(a), the measured  $TEM_{00}$  mode content exceeded 90 % at low output power levels and at high power levels even reached 95 %. These values are in good agreement with the earlier calculated theoretical limit of the overlap between the fundamental mode of the MFC fiber and a Gaussian mode of equivalent size. Thus, the fiber was not truly single-mode – as it was susceptible to input beam alignment – but was able to preserve the beam quality of a correctly aligned single-mode input beam exceptionally well. Furthermore, this even held for simultaneous significant amplification. These results are also in good agreement with work published by Le Gouët et al. [163], who investigated the mode content of a comparable MFC fiber by use of the  $S^2$  technique.

The fiber behavior changed when the larger MFC fiber instead of the smaller version was used. It could be observed that the larger core was supporting too many transverse modes to predominantly amplify the fundamental one. This is in agreement with the theoretical treatment of MFC fibers of Ref. 104. Many more and significantly stronger higher order modes were observed for this larger MFC fiber, which is illustrated in an exemplary mode scanning signal shown in Fig. 4.17(b). A higher order mode content of 35 % was measured. However, it should be noted that the beam pointing and higher order mode content were very sensitive to movement of the fiber. This means that the figure of 35 % should better be thought of as an indicator of the higher order mode content produced by this fiber rather than a truly fixed value. Due to the described problems, the fiber was not operated at higher power levels than 400 mW. Further experiments did not seem promising as the beam profile clearly consisted of many transverse modes. These were even easily observable when simply being examined with a detector card for infrared radiation.

Nevertheless, due to the performance of fiber No. 2, the concept of multifilament core fibers has proven to have many advantages in comparison with conventional step-index fiber technology. This is especially the case when a predominant part of  $TEM_{00}$  content is needed as for example for GWD applications. Multifilament core fiber

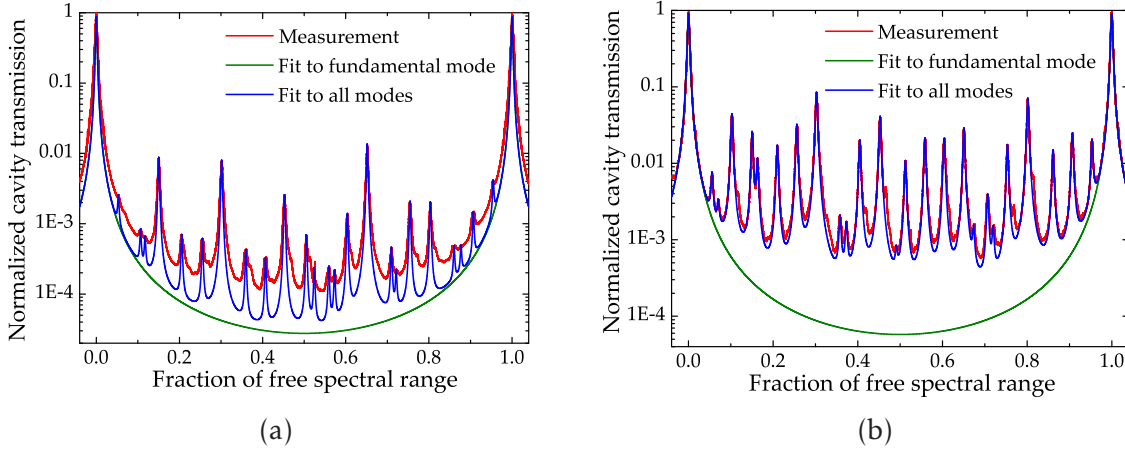


**Figure 4.17:** (a): Mode scanning signal on logarithmic scale of 31/28  $\mu\text{m}$  core MFC fiber at 7 W output power with a result of 95 %  $\text{TEM}_{00}$  mode content. (b) Corresponding signals for the 41/38  $\mu\text{m}$  core MFC fiber at 400 mW output power with a result of 65 %  $\text{TEM}_{00}$  mode content.

technology allows for fibers with high efficiency and simultaneously very low core numerical apertures, even when fiber dopants are involved which typically inhibit these properties.

#### 4.2.5 Summary of Mode Content Measurements

In the experiments presented in this section, the non-confocal scanning ring cavity technique was used to analyze the fractional  $\text{TEM}_{00}$  content of the output beams of single-frequency fiber amplifiers. The amplifiers were based on  $\text{Er}^{3+}:\text{Yb}^{3+}$ -codoped fibers with pedestal or multifilament core design and were operated at 1535 nm. At output power levels of several watts, a commercial step-index pedestal-design fiber with 23  $\mu\text{m}$  core diameter showed a fractional  $\text{TEM}_{00}$  content exceeding 80 % and mode field areas of about 300  $\mu\text{m}^2$ . These values were surpassed by a recently developed multifilament core fiber with a hexagonal core size of 31/28  $\mu\text{m}$ . This fiber delivered output beams amplified to multiple watts of power and a  $\text{TEM}_{00}$  content of up to 95 %. Simultaneously, it had a significantly larger calculated mode field area of about 720  $\mu\text{m}^2$ . In addition to this, MFC fibers also have interesting characteristics with regard to stimulated Brillouin scattering. Due to the different spatially distributed fiber dopants, the fibers typically have two distinct Brillouin gain peaks in the frequency domain. For an  $\text{Er}^{3+}:\text{Yb}^{3+}$ -codoped MFC fiber very similar to the

one used in this work, an SBS suppression of up to 4 dB with respect to conventional single-mode fibers has been demonstrated by Canat et al. [164].

It should be noted that the power handling capability of the presented MFC fibers could most probably be increased relatively easily. One way would be to increase the size of the pump cladding for a reduction of pump absorption – and therefore also heat generation – per unit length. Another way would be to apply cooling techniques to the fibers. A possible technique will be shown in the following sections for  $Yb^{3+}$ -free  $Er^{3+}$ -doped fibers. Yet, several issues remain for the development of future MFC fibers. The composition of the fiber core may need to be optimized to increase the amplification efficiency and to make strictly single-mode MFC fibers with possibly even larger mode field areas. Also, the possibility to splice MFC fibers to each other or to conventional step-index fibers remains to be thoroughly investigated. However, MFC fibers have good prospects for future use in combination with or as an alternative for step-index design fibers in many applications. The demonstrated predominant  $TEM_{00}$  content from a fiber core with very large mode field area makes this fiber type also appear to be a potential candidate for GWD systems at 1.5  $\mu\text{m}$  wavelength. This is also because of the potential of using this novel fiber type in the auxiliary seeded amplifier scheme that was introduced in the previous section. However, the most direct way to avoid parasitic emission at 1.0  $\mu\text{m}$  wavelength is to omit the  $Yb^{3+}$ -codoping. Therefore, power scaling experiments performed with  $Yb^{3+}$ -free  $Er^{3+}$ -doped fibers will be the topic of the following chapter.

## 5 Experiments with Yb<sup>3+</sup>-free Er<sup>3+</sup>-doped fibers

After the presentation and analysis of novel concepts for high power Er<sup>3+</sup>:Yb<sup>3+</sup>-codoped fiber amplifiers in the previous sections, experiments performed with Yb<sup>3+</sup>-free Er<sup>3+</sup>-doped fibers will be presented in the following. One of the drawbacks of these fibers is their very low pump absorption per unit length. When similar fiber core to cladding ratios are used, the absorption per unit length of these fibers is about two orders of magnitude lower than for Yb<sup>3+</sup>- and Tm<sup>3+</sup>-doping. Therefore, small pump claddings and high brightness pump diodes have to be used to achieve fiber lengths suitable for single-frequency amplification. Otherwise, the need for an increase of the pump absorption by codoping with Yb<sup>3+</sup>-ions would become unavoidable.

However, especially the recent major increase in output power of high brightness pump diodes has strongly contributed to interest in high power cladding pumped Yb<sup>3+</sup>-free – and hence also Yb<sup>3+</sup>-ASE-free – Er<sup>3+</sup>-doped fiber laser systems. Similar to Yb<sup>3+</sup>-doped fibers, this kind of system can be pumped around 980 nm wavelength. Also resonant pumping into the laser level manifold is possible with wavelengths between 1480 and 1530 nm. Previously, the highest reported output power levels of near diffraction limited Yb<sup>3+</sup>-free Er<sup>3+</sup>-doped fiber amplifiers were 3.5 W for 980 nm pumping [165] and 10.4 W for resonant pumping around 1530 nm [166]. With a highly multi-mode 100 μm core fiber with a NA of 0.10, a 980 nm pumped pulsed fiber amplifier with more than 50 W of average power has been reported [167]. Also a resonantly pumped near diffraction limited Yb<sup>3+</sup>-free Er<sup>3+</sup>-doped fiber laser with a record output power of 88 W has been reported [168]. Resonant pumping is attractive due to the demonstrated optical-to-optical efficiency values of more than 50 % resulting from the low quantum defect of this pumping scheme. However, it has the drawback of limited available pump power from high brightness pump diodes. This constitutes an even larger problem in case of the restriction to commercially available diodes. Moreover, the limitations in diode output power at 1530 nm wavelength originate from a low electrical-to-optical efficiency. As a consequence, 980 nm



and 1530 nm pumping lead to almost identical electrical-to-optical efficiency values with respect to the overall fiber amplifier system. Also the principally reachable absolute amplifier output power is almost the same, which is because of the availability of far more powerful and higher brightness diodes at 980 nm wavelength. Moreover, diode laser technology at 980 nm is far more sophisticated and reliable, which gives an additional advantage with respect to long term operation of amplifier systems. This motivated my power scaling experiments with  $\text{Yb}^{3+}$ -free  $\text{Er}^{3+}$ -doped single-frequency amplifiers. The goal of these experiments was to achieve output power levels of multiple 10 W with a high power pump source operating around 976 nm.

This chapter is organized as follows: First, thermal simulations are presented that allowed to evaluate the expected radial heat distribution inside of the fibers under different cooling conditions. Experiments performed with a commercial  $\text{Er}^{3+}$ -doped double-clad multi-mode fiber with 40  $\mu\text{m}$  core and 140  $\mu\text{m}$  cladding diameter are presented and treated with the thermal model. The fiber was coated with a conventional fluorinated low index polymer for pump light guidance. This specific fiber was chosen, because it was ideal for testing the tolerances of  $\text{Yb}^{3+}$ -free  $\text{Er}^{3+}$ -doped fibers with respect to thermal loads. Due to its higher absorption per unit length, this multi-mode fiber was especially suited for this task, because it allowed for more severe thermal conditions than to be expected for its also commercially available near single-mode counterpart. Experiments performed with this near single-mode double-clad fiber with 20  $\mu\text{m}$  core and 125  $\mu\text{m}$  cladding diameter are then presented after the description of the thermal load experiments. Working with the near single-mode fiber was interesting with regard to the potential development of even completely fiber-based high power sources for GWD applications. Finally, experiments performed with a newly developed  $\text{Er}^{3+}$ -doped photonic crystal fiber are presented. With this fiber the highest output power levels and simultaneously best beam quality were achieved. Thus, also here very promising results with regard to GWD laser source development were achieved.

### 5.1 Transverse Temperature Distribution

Simulations of the transverse temperature distribution inside of the active fibers were performed to evaluate the feasibility to reach high power operation despite the large



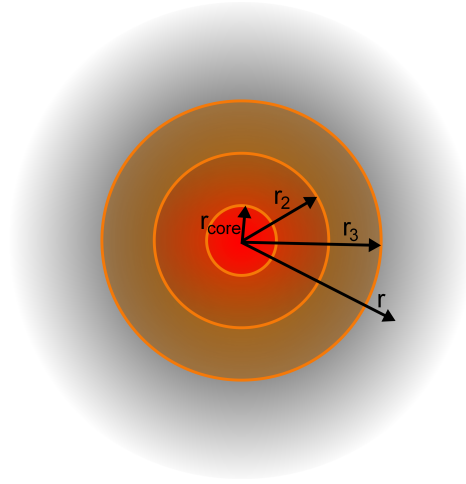


**Figure 5.1:** Depiction of different layers used for the simulation of transverse temperature distribution inside of the  $\text{Er}^{3+}$ -doped active fibers.

quantum defect of 980 nm pumped  $\text{Er}^{3+}$ -doped fibers. In the following, the simulation model is introduced and applied to the case of a double-clad fiber with 40  $\mu\text{m}$  core and 140  $\mu\text{m}$  cladding diameter. The calculations were performed with a model similar to that presented by Lapointe et al. in Ref. 41. In these models, the temperature distribution has the following form:

$$T(r) = T_{\text{center}} - \frac{q_0 \cdot r_{\text{core}}^2}{4\lambda_1} - \frac{q_0 \cdot r_{\text{core}}^2}{2\lambda_2} \cdot \ln\left(\frac{r_2}{r_{\text{core}}}\right) - \frac{q_0 \cdot r_{\text{core}}^2}{2\lambda_3} \cdot \ln\left(\frac{r_3}{r_2}\right) - \dots \quad (5.1)$$

$$\dots - \frac{q_0 \cdot r_{\text{core}}^2}{2\lambda_{n-1}} \cdot \ln\left(\frac{r_{n-1}}{r_{n-2}}\right) - \frac{q_0 \cdot r_{\text{core}}^2}{2\lambda_n} \cdot \ln\left(\frac{r}{r_{n-1}}\right),$$

where  $T(r)$  is the temperature inside of the fiber at the radial position  $r$ ,  $T_{\text{center}}$  is the temperature in the center of the fiber core,  $q_0$  is the thermal load per unit volume inside of the fiber core,  $r_{\text{core}}$  is the radius of the fiber core,  $r_n$  is the radius of the  $n$ -th material layer such as, e.g., cladding and coating and  $\lambda_n$  is the thermal conductivity of the respective layers. From this expression,  $T_{\text{center}}$  and hence the complete temperature distribution can be calculated when using a known surface or environmental temperature as boundary condition. An illustration of the different layers inside of the fiber is given in Fig. 5.1.

For the fiber with 40  $\mu\text{m}$  core and 140  $\mu\text{m}$  cladding diameter, the transverse temperature distribution was calculated at the pump end for 300 W of coupled pump power at 976 nm. For the calculation of  $q_0$ , an exponential pump light depletion

was assumed. The calculations were performed for cooling by free convection and thermal radiation and also for conductive cooling with thermally conductive paste and an aluminum heat sink. In the simulations heat generation from 70 % of the absorbed power and a pump absorption of 1.2 dB/m were assumed. The pump absorption value was deduced from the pump light transmission in the experiments described later on. The fiber was modelled with a respective core, cladding and coating diameter of 40  $\mu\text{m}$ , 140  $\mu\text{m}$  and 250  $\mu\text{m}$ . Core and cladding were modelled with the thermal conductivity of fused silica ( $\lambda = 1.37 \text{ W}/(\text{m} \cdot \text{K})$ ), while for the coating a typical value for the thermal conductivity of polymers of only  $0.2 \text{ W}/(\text{m} \cdot \text{K})$  was assumed. In the conduction cooling scheme, the coating is followed by a 200  $\mu\text{m}$  layer of thermal conductance paste ( $\lambda = 3.0 \text{ W}/(\text{m} \cdot \text{K})$ ) and a 2 cm thick aluminum plate ( $\lambda = 235.0 \text{ W}/(\text{m} \cdot \text{K})$ ). It is however noteworthy that the temperature is largely independent from the thickness of the thermal conductance paste layer. The main contribution to the thermal resistance originated from the fiber coating and the fiber cooling results became decent as soon as this layer was assumed to be smoothly contacted with thermally conductive paste. It was assumed that an ambient temperature of 20  $^{\circ}\text{C}$  was reached inside of the aluminum plate at a transverse distance of 2 cm.

To model the cooling with free convection and thermal radiation the fiber was assumed to behave like a horizontal cylinder. An equation for the heat flow can then be derived by use of common textbooks (see, e.g., Ref. 169):

$$Q_l = \left( \left[ \frac{3.93}{D/\text{mm}} \left( \frac{\Delta T}{\text{K}} \right) + \frac{7.67}{\sqrt{D/\text{mm}}} \left( \frac{\Delta T}{\text{K}} \right)^{\frac{7}{6}} + 1.57 \left( \frac{\Delta T}{\text{K}} \right)^{\frac{4}{3}} \right] \frac{\text{W}}{\text{m}^2} + \sigma \varepsilon (T_f^4 - T_a^4) \right) \cdot \pi D. \quad (5.2)$$

The term in squared brackets represents free convection cooling in air and the second term represents cooling effects through thermal radiation. In the presented case free convection is the dominant cooling mechanism. In the equation  $Q_l$  is the heat deposition per meter fiber,  $D$  is the fiber diameter,  $\Delta T$  is the temperature difference between the fiber surface temperature  $T_f$  and ambient temperature  $T_a$ ,  $\sigma$  is the Stefan-Boltzmann constant and  $\varepsilon = 0.92$  [41] is the value assumed for the emissivity of the fiber. The values of  $Q_l$  and  $q_0$  are related by  $q_0 = Q_l/(\pi \cdot r_{\text{core}}^2)$ . Thus – for a given  $Q_l$  or  $q_0$  – the fiber surface temperature  $T_f$  can be determined by numerically solving eq. (5.2) for  $\Delta T$ . It is noteworthy that this calculation only leads to an estimated result with an error of possibly several ten percent as, e.g., the convection properties of air change with temperature. However, also this estimate is helpful to evaluate,

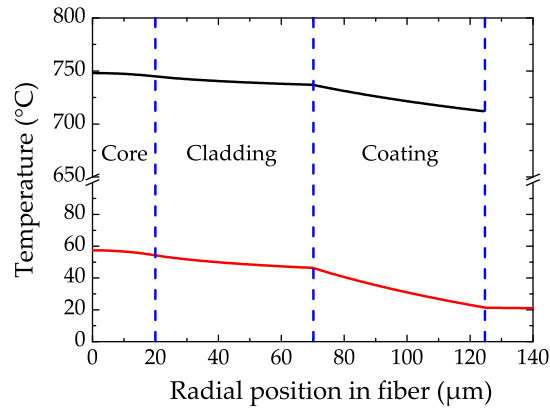


**Figure 5.2:** Simulation results of the transverse temperature profile at the pump end of the  $\text{Er}^{3+}$ -doped active fiber with 40  $\mu\text{m}$  core diameter. The pump power launched into the fiber is assumed to be 300 W with a wavelength of 976 nm. The calculations were performed for cooling with free convection and thermal radiation (black line) and a thermally conductive heat sink (red line).

whether operation without further cooling techniques is realistic or not.

It can, for example, be seen from Fig. 5.2 that it was not realistic to operate the fiber with the previously given parameters without any additional cooling. The temperature of fluorinated low index polymer coatings should typically not exceed 120 °C even in short term operation. However, in the presented case the coating temperature would rise to several hundred °C under the condition of free convection cooling. Thus, additional cooling of the entire pump end of the fiber without intermediate uncooled pieces needed to be ensured in the experiments. Furthermore, it should be noted that the resulting fiber temperature does not depend strongly on the core size and the overall fiber diameter, but mainly on the pump absorption per unit length. This means that tolerances of the 40/140  $\mu\text{m}$  fiber regarding heat generation can also be expected to apply for other fibers with different core and cladding sizes. Solely, the heat generation per unit length should be similar or smaller than in the presented case.

## 5.2 Power Scaling and Thermal Loading Experiments

As the thermal simulations led to the conclusion that at least a passive cooling scheme was necessary for high power operation, the heat sink depicted in Fig. 5.3 was developed. The active fiber was placed in a V-groove, which spiralled around the alu-

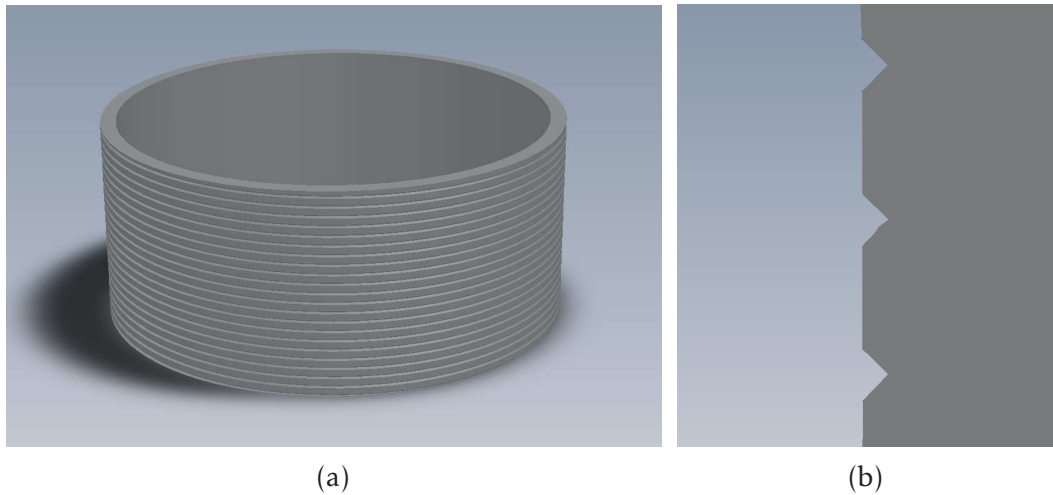


**Figure 5.3:** (a): Drawing of the utilized fiber heat sink. Its outer diameter was 30 cm. (b): Detailed view of heat sink profile. The V-groove had a depth of 1 mm and a width of 2 mm.

minum body and had a respective width and depth of 2 mm and 1 mm. The thermal contact was ensured by the application of thermal conductance paste on heat sink and fiber. The fact that the fiber was fully surrounded by the paste but only partly by the aluminum did not impose a problem. This was due to the previously mentioned large tolerance regarding the layer thickness of the paste. In the calculations even millimeter thick layers could be applied without raising the fiber temperature by more than a few °C at full pump power.

The initial power scaling experiments were performed with the 40/140  $\mu\text{m}$  fiber out of two reasons. First, to relax potential problems with the free space coupling of the pump light, thus increasing the accessible pump power range for the power scaling experiments. Second, because of the additional advantage of a 2.6 times higher specified pump absorption per unit length compared with an also available 20/125  $\mu\text{m}$  fiber. Thus, the thermal properties and the fiber cooling scheme could be investigated under tightened conditions of increased heat generation. The experimental setup of the fiber amplifier is shown in Fig. 5.4. The seed signal at 1570 nm was provided by a fiber-coupled single-frequency DFB-Diode with a linewidth of about 10 MHz limited by the used current source. It was preamplified from 80 mW to about 800 mW (measured behind the following free-space isolator) in a completely single-mode fiber-based preamplifier.

The used active LMA fiber was an angle-cleaved 7.5 m piece of *Er60-40/140* from *nLIGHT Corporation* with a core NA of 0.09. This resulted in a relatively high  $V$

## 5.2 Power Scaling and Thermal Loading Experiments

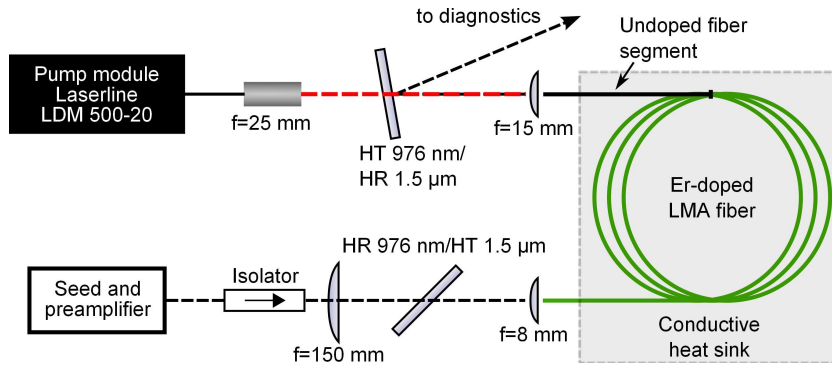


**Figure 5.4:** Experimental setup of the high power  $\text{Yb}^{3+}$ -free  $\text{Er}^{3+}$ -doped fiber amplifiers. Seed and signal radiation at 1570 nm are indicated in black, pump radiation at 976 nm is indicated in red. HR: high reflection, HT: high transmission.

number of 7.2. The fiber cladding with a diameter of only 140  $\mu\text{m}$  led to a large core-to-cladding ratio. Therefore, the cladding could probably not shield the core against external perturbations and micro-bending effects so that strong transverse mode-coupling was very likely to occur [81]. Thus, single-mode operation by preferential excitation of the fundamental mode was not likely to be sustainable along the relatively long active fiber.

Due to the results of the thermal simulations, a 75 cm piece of matching undoped fiber was fusion spliced to the pump end of the active fiber. This splice connection was recoated with UV-curable low index coating material to preserve the waveguide properties for the pump radiation. The active fiber was then put onto the conductive heat sink in order to achieve proper cooling for the part of the active fiber that encountered the largest amount of heat generation. The pump power was launched in a counterpropagating scheme and was provided by a fiber coupled diode laser module (Laserline LDM 500-20). This delivered up to 500 W at 976 nm out of a pump fiber with 200  $\mu\text{m}$  core diameter and NA of 0.22. The pump light was delivered through a commercial high power collimator with a focal length of 25 mm and free-space coupled by an aspherical lens with  $f = 15$  mm to the passive fiber pigtail. This pump launch end of the fiber was placed into a water-cooled V-groove. In transmission tests through the matching passive fiber, the pump launching efficiency was determined to be about 60 %. The pump depletion in the active fiber was measured to be about 9 dB during amplifier operation. Thus, about 90 % of the launched pump power was absorbed.

The output power versus estimated absorbed pump power is plotted in Fig. 5.5(a).

## 5 Experiments with $\text{Yb}^{3+}$ -free $\text{Er}^{3+}$ -doped fibers

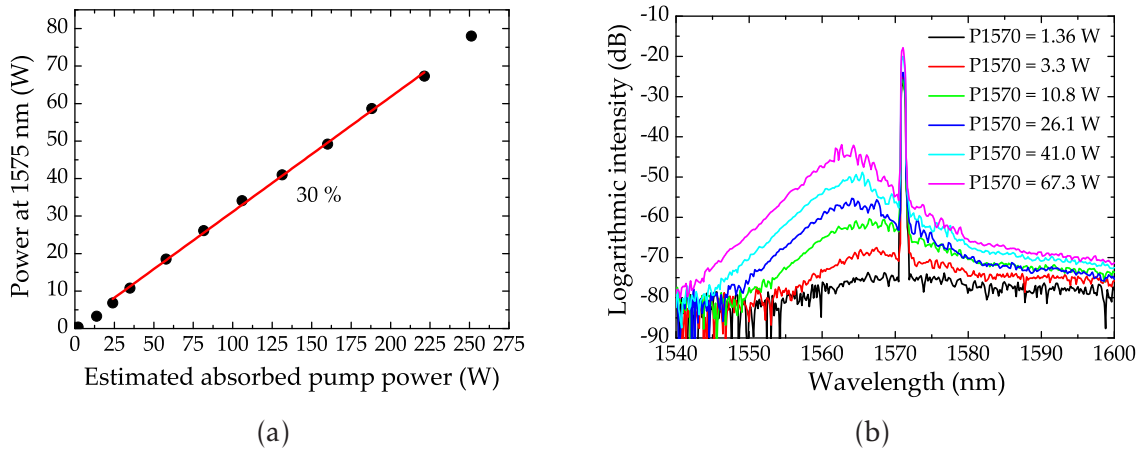


**Figure 5.5:** (a): Signal power at 1570 nm plotted versus estimated absorbed pump power at 976 nm. The last data point is excluded from the differential efficiency calculation as parasitic laser processes occurred at this output power. (b): Spectra of the amplified signal at various output powers. The resolution bandwidth of the spectrometer was set to 0.5 nm.

The differential optical-to-optical efficiency of the amplifier with respect to estimated absorbed pump power was about 30 %. At an absorbed pump power of about 250 W and a corresponding signal output power of 78 W parasitic laser processes occurred at 1560 nm, which limited the power scaling of the amplifier.

The output spectra at various output power levels are shown in Fig. 5.5(b). It can be seen that the chosen signal wavelength did not coincide with the spectral maximum of the ASE, which limited the suppression of the latter. Thus, further power scaling could most probably have been achieved by changing the seed wavelength to 1560 nm, which was not available for the here presented experiments. This assumption is supported by the fact that no thermal or optical damage occurred to any of the components throughout the here presented experiments. The additional structure observable on the ASE part of the spectra originated from highly suppressed spectral side lobes of the used DFB-diode, which were also amplified in the active fiber. The two spikes close to 1560 nm on the spectrum recorded at 67.3 W of output power might also already be a slight indication of the onset of parasitic laser processes. However, the differential efficiency of the system was not yet influenced at this point, which was in contrast to an increase in efficiency observed at 78 W of output power.

The  $M^2$  parameter of the amplifier output was measured to be about 8 at power levels of 3 W and 10 W, which was due to the previously discussed implications of the large core size. The data points of the  $M^2$  measurement are plotted in Fig. 5.6. Mea-

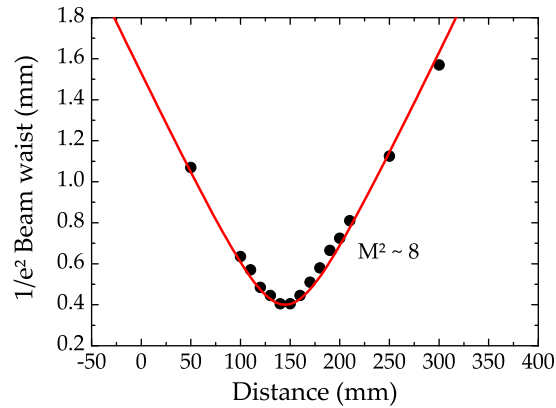


**Figure 5.6:** Data of beam waist measurement for determination of  $M^2$  parameter of the output beam from the multi-mode  $\text{Er}^{3+}$ -doped fiber with 40  $\mu\text{m}$  core diameter.

measurements of the  $M^2$  parameter were not performed at higher output power levels, as the risk of fiber damage by a slow thermal degradation of the fiber coating could not be fully ruled out despite the applied cooling technique. It is noteworthy that with core pumping of fibers with similar dimensions almost diffraction limited output has been demonstrated [170]. Thus, an increase in output beam quality could also be expected for the used fiber when, e.g., applying mode selective pumping techniques instead of high power cladding pumping. Mode selective core pumping would also have the additional advantage of shorter possible fiber lengths – if the corresponding increase in heat generation could be tolerated. This could reduce the amount of higher order mode excitation through transverse mode coupling effects. However, it would of course massively increase the complexity and cost for suitable high power pump sources.

The intention of the experiments of this section was to verify the concept of the passive fiber heat sink. Also the power scalability of  $\text{Yb}^{3+}$ -free  $\text{Er}^{3+}$ -doped fibers with 980 nm pumping had not been shown before. Therefore, it was also important to, e.g., rule out potential problems related to nonlinearly increasing upconversion effects [171]. However, the beam quality from the used multi-mode fiber was far from diffraction limited as can be seen from the relatively large  $M^2$  parameter. Therefore, experiments performed with a fiber which allowed for near diffraction limited beam quality through a smaller core diameter are presented in the following section.



### 5.3 Conventional Near Single-Mode Fiber

After the successful power scaling and thermal load experiments of the last section, the experiments of this section were performed with a near single-mode fiber with 20  $\mu\text{m}$  core diameter and a core NA of 0.09 (Er60-20/125 from nLIGHT Corporation). The seed signal at 1570 nm was again provided by the preamplified single-frequency DFB-Diode. The active LMA fiber was 15 meters long to reach an at least decent pump absorption of above 75 % and angle-cleaved to suppress backreflections. The fiber parameters resulted in a moderate V number of 3.6 and allowed for near-single mode operation despite the long fiber length. The cooling scheme – again including a piece of matching passive fiber – and pump launch configuration were the same as in the previous experiments. Also for this fiber thermal simulations were performed. These were carried out with the specified pump absorption value of about 0.75 dB/m at 980 nm. It should be noted that the experimental absorption was probably lower than this, because the fiber had a circular refractive index pedestal around the fiber core. This led to an amount of unabsorbed pump light that could not be safely determined without cutting back – and thus destroying – the active fiber. The calculated thermal load was therefore probably slightly higher than the practical one, which however adds a safety margin to the calculated temperature distribution. The results for a coupled pump power level of 300 W are shown in Fig. 5.7. The simulated coating temperatures were well below 80°C, which is considered as a limit for standard double-clad polymer coatings in long-term operation [41].

The obtained output power of the main amplifier is plotted versus estimated absorbed pump power in Fig. 5.8(a). At an absorbed pump power of about 250 W a maximum output power of 54 W was reached. The limit was set by the amount of available pump power. The pump coupling efficiency was limited to slightly above 50 % due to the relatively small pump cladding of the active fiber. In Fig. 5.8(b), the output spectrum at full pump power is shown. A peak-to-peak ASE suppression of > 40 dB was measured. Regarding beam quality, measurements with the scanning non-confocal ring cavity were performed in order to determine the  $\text{TEM}_{00}$  mode content of the amplifier output. The beam profile and a mode scanning signal at high power are shown in Fig. 5.9. The beam profile looked like that of a near Gaussian beam. However, it already showed some distortions that indicated the influence of higher order modes. A fractional fundamental mode content of  $\geq 75$  % was mea-



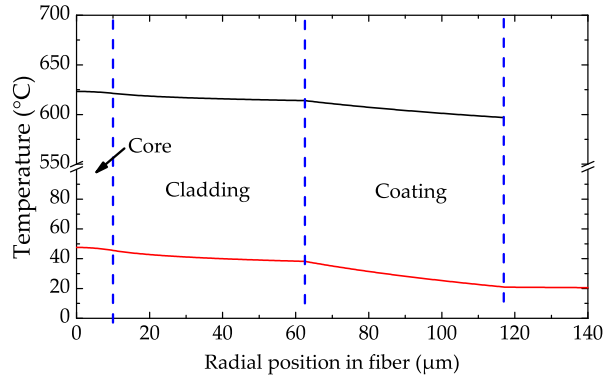


**Figure 5.7:** Simulation results of the transverse temperature profile at the pump end of the  $\text{Er}^{3+}$ -doped active fiber with 20  $\mu\text{m}$  core diameter. The pump power launched into the fiber is assumed to be 300 W with a wavelength of 976 nm. The calculations were performed for cooling with free convection and thermal radiation (black line) and a thermally conductive heat sink (red line).

sured with the mode scanning cavity. This value corresponds to  $M^2$  values close to unity. However, for GWD applications further optimization steps in fiber design and manufacturing would probably be necessary. This together with the already quite small core diameter of 20  $\mu\text{m}$  raised the question, if step index designs were the best way of realizing  $\text{Yb}^{3+}$ -free  $\text{Er}^{3+}$ -doped LMA fibers. In the following experiments performed with the first  $\text{Er}$ -doped photonic crystal LMA fiber – that was developed for the experimental work of this thesis – will be presented.

## 5.4 Photonic Crystal Fiber

Power scaling experiments with  $\text{Yb}^{3+}$ -free  $\text{Er}^{3+}$ -doped double-clad fibers with step index cores and standard fluorinated polymer low index coatings have been presented in the previous sections. The fibers have been a near single-mode fiber with 20  $\mu\text{m}$  core diameter and a multi-mode fiber with 40  $\mu\text{m}$  core diameter, respectively. A considerably lower fiber core NA is needed, when striving to achieve single-mode properties while maintaining a large 40  $\mu\text{m}$  core size and continuing the use of cladding pumping. This could be achieved with the – to the best of my knowledge – first  $\text{Er}^{3+}$ -doped LMA photonic crystal fiber. This fiber was manufactured by *NKT Photonics A/S* and had a core diameter of 40  $\mu\text{m}$  and a core NA of  $< 0.04$ . A picture of a cleaved end facet of this fiber is shown in Fig. 5.10(a). The fundamental mode

5 Experiments with  $\text{Yb}^{3+}$ -free  $\text{Er}^{3+}$ -doped fibers

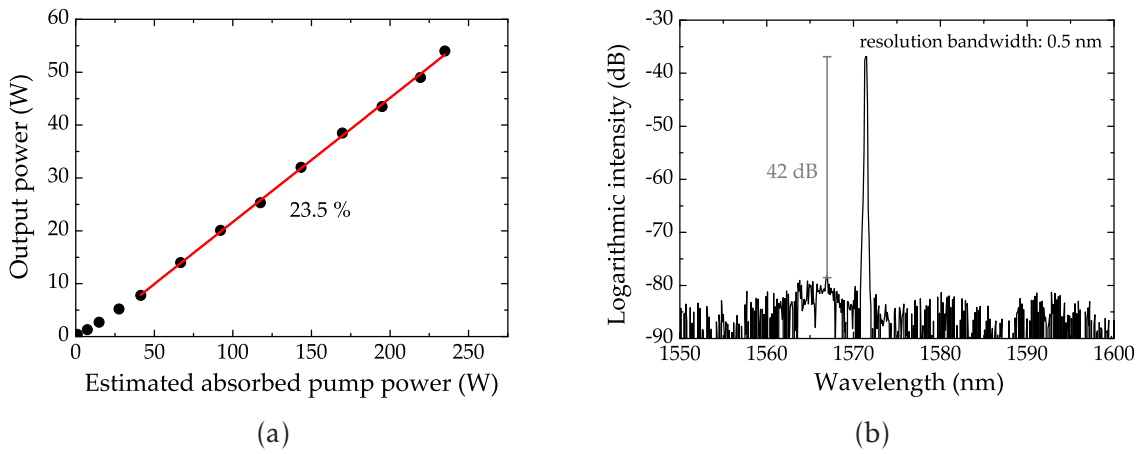


**Figure 5.8:** (a): Signal output power at 1570 nm versus estimated absorbed pump power at 980 nm of single-frequency MOPA based on the  $\text{Er}^{3+}$ -doped LMA fiber with 20  $\mu\text{m}$  core diameter. (b): Output spectrum recorded at maximum output power of 54 W.

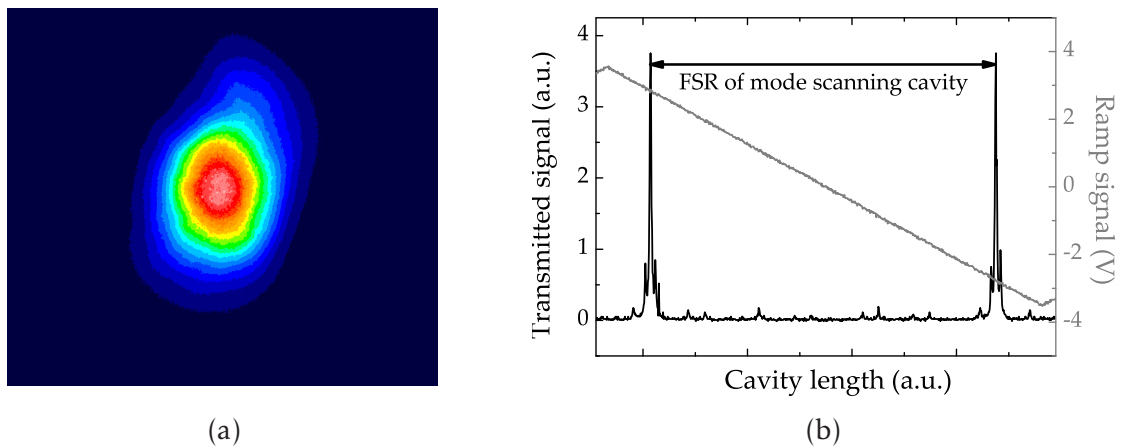


**Figure 5.9:** Beam profile (a) and transmitted mode scan signal (b) of output beam of the single-frequency MOPA based on the  $\text{Er}^{3+}$ -doped LMA fiber with 20  $\mu\text{m}$  core diameter at high output power.

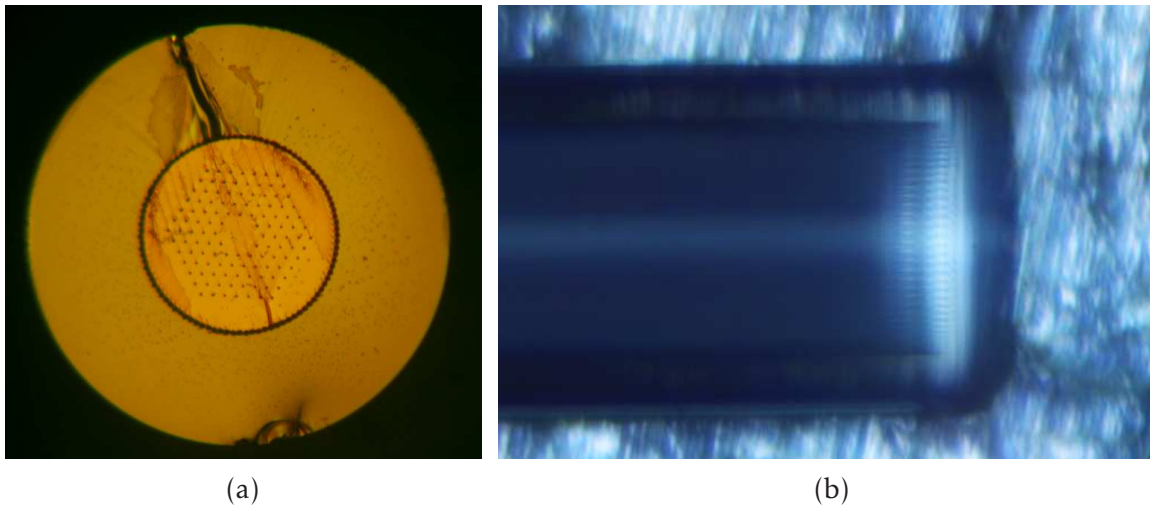


**Figure 5.10:** (a): End facet of non-collapsed cleaved Er-doped PCF. (b): Side view of collapsed and cleaved Er-doped PCF.

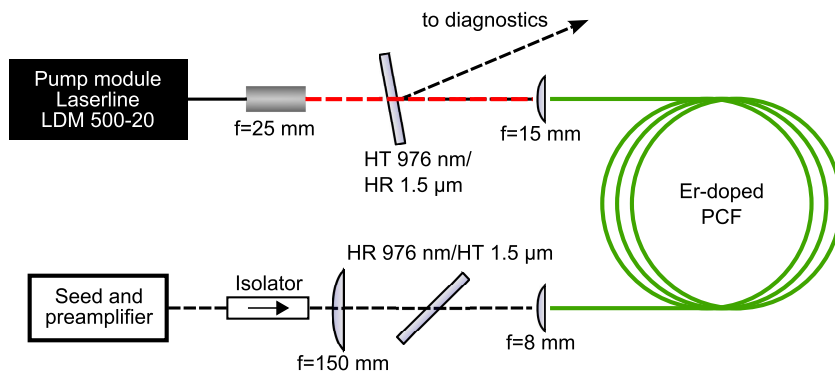


**Figure 5.11:** Depiction of the experimental setup. HT: High transmission, HR: High reflection.

field diameter was  $31 \mu\text{m}$  with a corresponding mode field area of about  $750 \mu\text{m}^2$  at  $1550 \text{ nm}$ . The fiber had an air cladding with  $170 \mu\text{m}$  diameter and NA of  $> 0.55$ . This resulted in a cladding absorption of  $0.6 \text{ dB/m}$  at  $980 \text{ nm}$ . The fiber coating consisted of a single layer of thermally robust high temperature acrylate as the use of low refractive index polymer was unnecessary due to the air-cladding. According to the fiber manufacturer, this high temperature coating could tolerate temperatures in excess of  $200 \text{ }^\circ\text{C}$ .

A  $19 \text{ m}$  long piece of this fiber was used in a single-frequency MOPA setup, which is depicted in Fig. 5.11. The fiber ends were angle cleaved after the air hole structure had been collapsed with a fusion splicer to seal the fiber ends. A photograph of the

## 5 Experiments with $\text{Yb}^{3+}$ -free $\text{Er}^{3+}$ -doped fibers

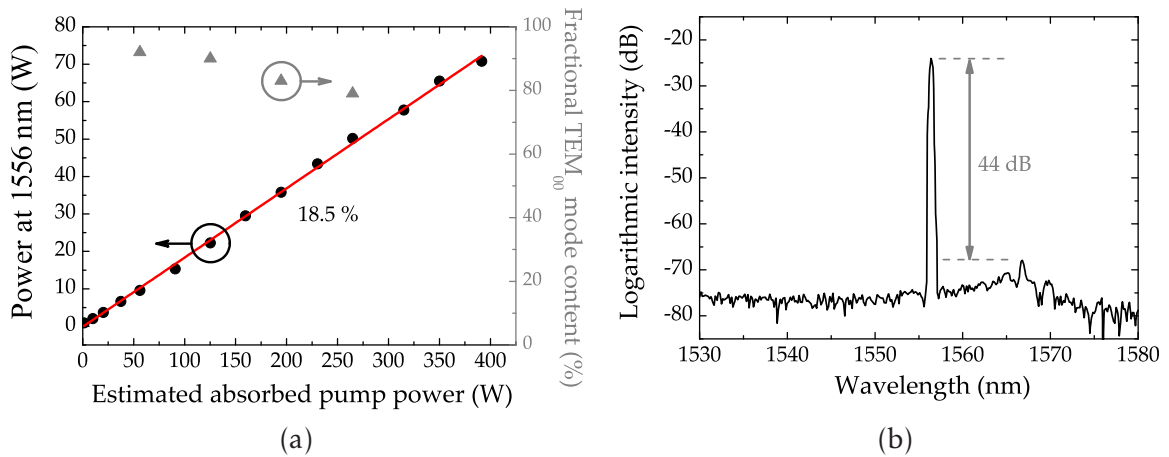


**Figure 5.12:** (a): Output power at 1556 nm (left scale) of amplifier based on  $\text{Er}^{3+}$ -doped photonic crystal fiber and corresponding fractional  $\text{TEM}_{00}$  content (right scale) versus estimated absorbed pump power around 980 nm. (b): Output spectrum at full output power of 70.8 W. The resolution bandwidth of the spectrum analyzer was set to 0.5 nm.

prepared fiber end can be seen in Fig. 5.10(b). As seed source a commercial preamplified single-frequency fiber oscillator from *NP Photonics, Inc.* was used, which emitted 2 W of output power with kHz linewidth at 1556 nm. The pump source was again the diode laser module from *Laserline GmbH* that emitted up to 500 W around 980 nm out of a fiber with 200  $\mu\text{m}$  core diameter and NA of 0.22. This time the pump end of the active fiber itself had to be placed in the water cooled metal V-groove as no matching passive fiber existed. High power splice connections are to date not feasible for this kind of fibers. Behind the water cooled V-groove the fiber remained uncooled. However, as the fiber was coated with high temperature acrylate, this did not impose an immediate problem. The seed signal was mode-matched to the fundamental mode of the PCF by a spherical lens with  $f=150$  mm and a  $f=8$  mm aspherical lens. Pump and signal were again launched in a counterpropagating scheme and after amplification the signal was separated from the pump radiation by a set of dichroic mirrors.

The amplifier output power versus estimated absorbed pump power is shown in Fig. 5.12(a). The differential optical-to-optical efficiency with regard to estimated absorbed pump power was 18.5 %. At full pump power a maximum signal output power of 70.8 W could be extracted from the amplifier. Throughout the experiments, no thermal damage occurred to the fiber, so that the power scaling was solely limited by the amount of available pump power. The signal spectrum at full output power is presented in Fig. 5.12(b). The peak-to-peak ASE suppression was measured to be

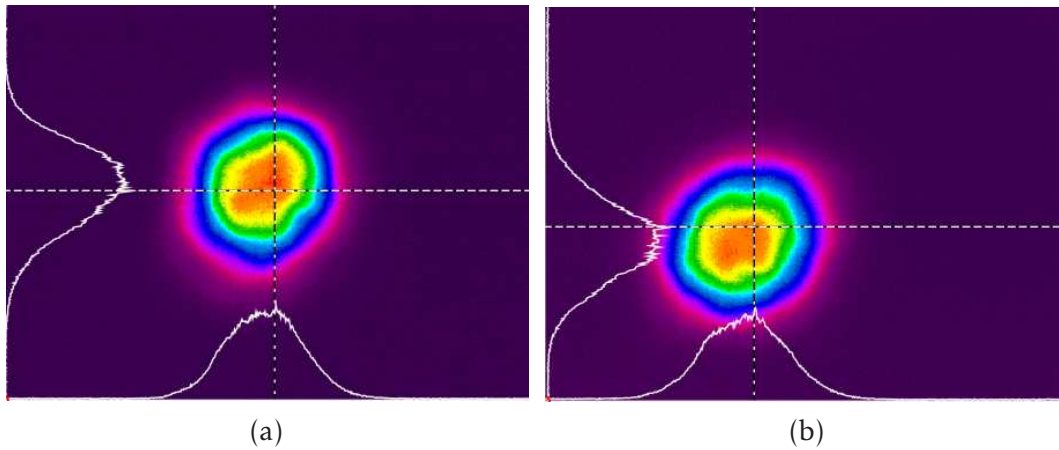


**Figure 5.13:** Transverse output beam profiles of collimated signal output from  $\text{Er}^{3+}$ -doped PCF, recorded with a phosphor coated silicon chip camera at 10 W (left) and full output power of 70.8 W (right).

44 dB with a resolution bandwidth of 0.5 nm. Beam profiles of the collimated output beam recorded with a phosphor coated silicon chip camera are shown in Fig. 5.13 for 10 W (left) and 70.8 W (right) of output power. No pronounced higher order modes – i.e. no additional peaks in the transverse beam profile – have been observed throughout the experiments.

However, for GWD applications the most important figure of merit regarding beam quality is the fractional  $\text{TEM}_{00}$  content. Therefore, also for this fiber, measurements of the modal content with the non-confocal scanning ring cavity were performed. The relative  $\text{TEM}_{00}$  content was measured in reflection of the cavity. This means that the drop of the reflected optical power occurring at the times when the fundamental mode was transmitted through the cavity was measured. Thus, the individual magnitudes of higher order modes could typically not be identified. However, the measurements could be performed quicker as less complex data acquisition and analyzing algorithms were needed. Moreover, the main interest lay on the value of the fractional  $\text{TEM}_{00}$  content. Thus, to obtain only the sum of the fractional contents of all higher order modes did not impose a problem. The measurements were performed in reflection due to slight drifts of the fiber output pointing at high power levels. As these drifts correlated with changes in input pump power, they can be mainly attributed to thermally induced movements of the fiber tip. These could most probably be overcome by more sophisticated fiber end cooling techniques or the use of end caps for improved mechanical stability.

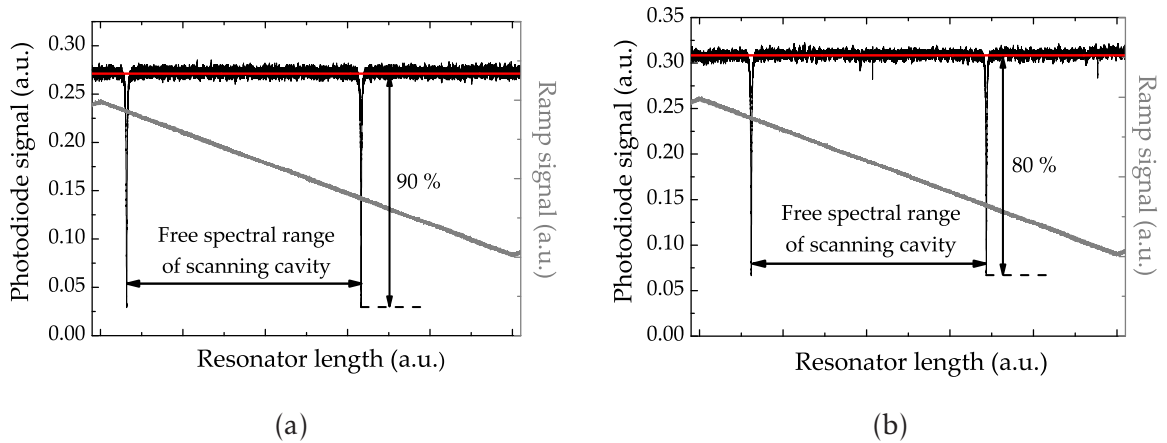


**Figure 5.14:** Signal reflected by the mode scanning cavity at (a) 22 W and (b) 50 W of output power. Also shown are the DC level of the photodiode signal (red) and the ramp signal used to tune the cavity length (gray).

The measured mode scanning signals at output power levels of 22 W and 50 W are shown in Fig. 5.14. These and two more values have also been included into Fig. 5.12(a). At 22 W of output power, a fractional  $\text{TEM}_{00}$  content of 90 % was measured. This value slightly dropped to about 80 % for 50 W of output power. At higher output power levels no mode content measurements could be performed as the mode-matching to the scanning cavity was too susceptible to the increasing pointing drifts. However, it was verified that still no significant degradation of the beam profile or any mode instability effects (see, e.g., Ref. 107) occurred at full power as can also be seen in the right picture of Fig. 5.13.

The slight degradation of beam quality with rising output power might however be linked to an increase of residual higher order modes inside of the fiber. While the fundamental fiber mode was obviously still predominant, the beam started to move slightly when the fiber was touched at substantial pump power levels. This indicated interaction with either higher order core or cladding modes. Because of the large quantum defect and high pump power levels, it is likely that these effects were at least partly thermally induced. Nevertheless, it should be noted that the here presented beam profiles and fractional  $\text{TEM}_{00}$  contents still point to almost diffraction limited beam quality. A fractional  $\text{TEM}_{00}$  content of 80 %, e.g., typically still leads to  $M^2$  values very close to unity [100].

## 5.5 Summary of Experiments with Yb-free Er-doped Fibers

The experiments presented in this chapter were focussed on the power scaling of Yb<sup>3+</sup>-free Er<sup>3+</sup>-doped fiber amplifiers cladding pumped around 980 nm. First, power scaling experiments performed with conventional step index core fibers with low index polymer coatings were described and theoretically treated. It was shown that such systems can be operated at substantial pump power levels and significant thermal loads. The main requirement was the application of an adequate cooling technique. By this, an Yb<sup>3+</sup>-free Er<sup>3+</sup>-doped multi-mode cw fiber amplifier could be operated at more than 67 W of output power at 1570 nm. This was a nearly twenty times higher value than the previously reported record at this pump wavelength and a nearly seven times higher value than reported for a resonantly pumped amplifier. The power scaling was limited by the onset of parasitic laser processes around 1560 nm. This means that with a change of seed wavelength even higher output power levels and efficiency values could likely be obtained. The differential efficiency with respect to absorbed pump power was about 30 %. Due to a measured M<sup>2</sup> parameter of about 8, the following work focussed on Yb<sup>3+</sup>-free Er<sup>3+</sup>-doped fibers with smaller core size. The goal was now to reach a similar power level while preserving the predominant fundamental mode content of the preamplifier. The use of fibers with smaller core but similar cladding size also implied smaller heat loads per unit length.

Also the experiments with this near single-mode fiber were successful. An output power of 54 W at 1570 nm wavelength could be reached. The output power was limited by the amount of available pump power. If more pump power would have been available, the output power of the system would have been most likely limited by stimulated Brillouin scattering (SBS) prior to the onset of thermal problems. Thus, power scaling of the presented system to beyond 100 W seems feasible, if suitable SBS mitigation techniques are applied. However, it should be noted that also the pump coupling might need to be optimized to be able to obtain higher output power levels. The free space coupling of large amounts of pump power seems to have led to thermally induced movements of the fiber tip. Thus, either fiber end caps for increased mechanical robustness or cooled high power fused fiber couplers are likely to be needed for stable long-term operation at significant pump power levels. However, this would not impose a fundamental problem for the development of a completely



fiber based version of the presented amplifier system. The only drawback of this amplifier was that the  $\text{TEM}_{00}$  content of 75 % was still relatively low. Thus, some further optimization of the fiber design might be needed, before it can be used for GWD applications.

Finally, experiments with the – to the best of my knowledge – first  $\text{Er}^{3+}$ -doped LMA photonic crystal fiber were described. The fiber had a core diameter of 40  $\mu\text{m}$  and a core NA of  $< 0.04$ . In a single-frequency MOPA scheme, more than 70 W of output power at 1556 nm could be demonstrated. This was again the highest output power value ever reported from an  $\text{Yb}^{3+}$ -free  $\text{Er}^{3+}$ -doped fiber amplifier and also the highest value obtained with a 980 nm pumped  $\text{Yb}^{3+}$ -free  $\text{Er}^{3+}$ -doped fiber laser system. The output power scaling was limited by the amount of available pump power. The fractional  $\text{TEM}_{00}$  content of the output beam was analyzed with the non-confocal scanning ring cavity at various power levels. A slight degradation from 90 % fundamental mode content at moderate output power levels to about 80 % at high output power levels was measured. However, this did not lead to a significant change in the observed output beam profile. Therefore, the presented  $\text{Er}^{3+}$ -doped photonic crystal fiber MOPA system could almost maintain the output characteristics of a single-mode single-frequency laser source. Simultaneously, it seems to have the potential to be scalable to single-frequency output power levels beyond 100 W. This presumption is based on a comparison of fiber length and mode field diameter with the corresponding values and output power of Ref. 139. From this comparison, no safe threshold values can be obtained due to the differences in fiber dopants and core design, but the mode field diameters and fiber lengths do at least allow for a rough estimate of the SBS threshold. In conclusion, the  $\text{Er}^{3+}$ -doped PCF is thus a promising candidate for GWD laser sources around 1550 nm wavelength, although some more work regarding its detailed noise and SBS properties as well as its thermal stability remains for the future.

## 6 Conclusion

In the experiments performed for this thesis, several new developments towards gravitational wave detector laser sources around 1550 nm wavelength have been made.

A novel scheme to stabilize  $\text{Er}^{3+}:\text{Yb}^{3+}$ -codoped fiber amplifiers against parasitic ASE and laser processes at 1.0  $\mu\text{m}$  wavelength could be demonstrated. In this scheme, an auxiliary seed signal in the  $\text{Yb}^{3+}$ -ion emission band wavelength is used to extract excess energy from the  $\text{Yb}^{3+}$ -ions. The output power of a single-mode amplifier with 7  $\mu\text{m}$  core diameter has been increased from below 2 W to 8.7 W at 1556 nm with this approach. A stable amplification by more than 22 dB was demonstrated, which is a very high value for a large signal  $\text{Er}^{3+}:\text{Yb}^{3+}$ -codoped fiber amplifier and was only limited by the available pump power. In further experiments, the influence of different auxiliary seed wavelengths was investigated for the first time. A theoretical prediction could be verified that shorter auxiliary seed wavelengths and increased reabsorption contribute to the efficiency of the 1.5  $\mu\text{m}$  signal amplification.

In a different experiment with  $\text{Er}^{3+}:\text{Yb}^{3+}$ -codoped fibers, a non-confocal scanning ring cavity was used to analyze the fractional  $\text{TEM}_{00}$  content of the output beams of single-frequency fiber amplifiers. The amplifiers were based on  $\text{Er}^{3+}:\text{Yb}^{3+}$ -codoped large mode area fibers with pedestal or multifilament-core design. At output power levels of several watts, a commercial step-index pedestal-design fiber with 23  $\mu\text{m}$  core diameter showed a fractional  $\text{TEM}_{00}$  content exceeding 80 % and mode field areas of about 300  $\mu\text{m}^2$ . These values were surpassed by a recently developed multifilament-core fiber with a hexagonal core size of 31/28  $\mu\text{m}$ . This fiber delivered output beams amplified to multiple watts of power and a  $\text{TEM}_{00}$  content of up to 95 %. Simultaneously, it had a significantly larger calculated mode field area of about 720  $\mu\text{m}^2$ . Measurements of the fractional  $\text{TEM}_{00}$  content were performed for the first time on the novel and highly interesting multifilament-core fibers and also generally for the first time on large mode area fibers in the 1.5  $\mu\text{m}$  wavelength band.

## 6 Conclusion

In further experiments, it was demonstrated for the first time that 980 nm pumped  $\text{Yb}^{3+}$ -free  $\text{Er}^{3+}$ -doped fiber amplifiers can be operated at substantial pump power levels and significant thermal loads. The main requirement was the application of an adequate cooling technique. By this, an  $\text{Yb}^{3+}$ -free  $\text{Er}^{3+}$ -doped multi-mode cw fiber amplifier could be operated at more than 67 W of output power at 1570 nm. This was a nearly twenty times higher value than the previously reported record at this pump wavelength and a nearly seven times higher value than reported for a resonantly pumped amplifier.

With a near single-mode fiber with 20  $\mu\text{m}$  core diameter – and a similar fiber core composition as in the previously used multi-mode fiber – an output power of 54 W at 1570 nm wavelength could be reached. The output power was limited by the amount of available pump power. If more pump power would have been available, the output power of the system would have been most likely limited by stimulated Brillouin scattering (SBS) prior to the onset of thermal problems. Thus, power scaling of the presented system even to beyond 100 W seems feasible, if suitable SBS mitigation techniques are applied. The measured fractional  $\text{TEM}_{00}$  content of this amplifier was about 75 %. This means that significant mode filtering would still be required before a possible usage as GWD laser source.

In addition to the experiments with conventional step-index core  $\text{Yb}^{3+}$ -free  $\text{Er}^{3+}$ -doped fibers also experiments with the – to the best of my knowledge – first  $\text{Er}^{3+}$ -doped LMA photonic crystal fiber were performed. The fiber had a core diameter of 40  $\mu\text{m}$  and a core NA of  $< 0.04$ . In a single-frequency MOPA scheme more than 70 W of output power at 1556 nm could be demonstrated. This was again the highest output power value ever reported from an  $\text{Yb}^{3+}$ -free  $\text{Er}^{3+}$ -doped fiber amplifier and also the highest value obtained with a 980 nm pumped  $\text{Yb}^{3+}$ -free  $\text{Er}^{3+}$ -doped fiber laser system. The output power scaling was limited by the amount of available pump power. The fractional  $\text{TEM}_{00}$  content of the output beam was analyzed with the non-confocal scanning ring cavity at various power levels. A slight degradation from 90 % fundamental mode content at moderate output power levels to about 80 % at high output power levels was measured. However, this did not lead to a significant change in the observable output beam profile. Therefore, the presented  $\text{Er}^{3+}$ -doped photonic crystal fiber MOPA system could almost maintain the output characteristics of a single-mode single-frequency laser source. Simultaneously, it seems to have the potential to be scalable to single-frequency output power levels beyond 100 W.

In conclusion, it could be shown that  $\text{Er}^{3+}$ -doped fiber based master-oscillator power-amplifier systems are highly interesting candidates for the laser sources of the potential third generation interferometric gravitational wave detectors. Significant power scaling potential of  $\text{Er}^{3+}:\text{Yb}^{3+}$ -codoped fiber amplifiers by use of an auxiliary seed signal in the  $\text{Yb}^{3+}$ -ion emission band could be demonstrated with single-mode amplifiers. Also a transfer to large mode area amplifiers and thus higher power levels seems to be feasible in a straightforward way. Additionally, the novel multifilament-core design could be identified as highly interesting for  $\text{Er}^{3+}:\text{Yb}^{3+}$ -codoped fiber based systems requiring high peak or average power, low nonlinear effects and excellent beam quality. Finally, also the power scaling potential of  $\text{Yb}^{3+}$ -free  $\text{Er}^{3+}$ -doped large mode area fiber amplifiers pumped with highly reliable and mature high power diode lasers at 980 nm could be demonstrated for the first time. Conventional fibers with fluorinated low index polymer coatings as well as a newly developed photonic crystal fiber could be operated at significant output power levels and simultaneously near diffraction limited beam quality.



## 7 Outlook

For the performed experiments as well as for the general development of GWD laser sources around 1550 nm wavelength several interesting issues remain to be investigated in the future.

For  $\text{Er}^{3+}:\text{Yb}^{3+}$ -codoped amplifiers with auxiliary seed signal the detailed noise properties and transfer functions for seed and pump fluctuations are highly interesting for future investigations. Similar behavior of high power LMA fiber amplifiers can be expected. Thus, the demonstrated scheme shows also good prospects to allow for high power  $\text{Er}^{3+}:\text{Yb}^{3+}$ -codoped fiber amplifiers without the  $\text{Yb}^{3+}$ -ASE induced instabilities. The scheme is in principle also compatible with the highly interesting MFC fiber technology. This might allow to combine the two technologies and develop long term stable and reliable  $\text{Er}^{3+}:\text{Yb}^{3+}$ -codoped high power systems with very high SBS threshold and no problems related to parasitic emission from the codoped  $\text{Yb}^{3+}$ -ions.

Yet, several issues remain for the development of future MFC fibers. The composition of the fiber core may need to be optimized to increase the amplification efficiency and to make strictly single-mode MFC fibers with possibly even larger mode field areas. Also, the possibility to splice MFC fibers to each other or to conventional step-index fibers remains to be thoroughly investigated. In addition to this, MFC fibers also have interesting characteristics with regard to stimulated Brillouin scattering. Due to the different spatially distributed fiber dopants, the fibers typically have two distinct Brillouin gain peaks in the frequency domain. Also this property will surely be of interest for future research efforts, because it might allow for SBS threshold values of multiple kW in fibers with a length of several meters.

Also for the presented systems based on step-index  $\text{Yb}^{3+}$ -free  $\text{Er}^{3+}$ -doped fibers several issues remain to be addressed in the future. The pump coupling of the current systems might need to be optimized to be able to obtain higher output power levels. The free space coupling of large amounts of pump power seems to have led to

thermally induced movements of the fiber tip. Thus, either fiber end caps for increased mechanical robustness or cooled high power fused fiber couplers are likely to be needed for stable long-term operation at significant pump power levels. Also fibers with slightly lower core NA would be interesting for future experiments, to further improve the beam quality and fractional  $TEM_{00}$  content of the amplifier output. With application of SBS mitigation techniques, output power levels in excess of 100 W might be possible with  $Yb^{3+}$ -free  $Er^{3+}$ -doped fiber amplifiers step-index LMA fiber amplifiers. Naturally, also the measurement of the SBS threshold and its dependence on different effects would be an interesting topic for further research. Another point of interest will be the pumping of  $Yb^{3+}$ -free  $Er^{3+}$ -doped fiber amplifiers at 1530 nm instead of 980 nm wavelength. With increasing available pump power, brightness and laser diode efficiency, this pump wavelength will become more and more attractive. This is mostly due to the significantly lower quantum defect and by a factor of two higher pump absorption. Thus, pumping at 1530 nm allows for shorter and more efficient fiber amplifiers with simultaneously lowered fiber heating per unit length.

For the  $Er^{3+}$ -doped LMA photonic crystal fiber, additionally the influence of fiber heating and internal stresses on the possible beam quality will be of special interest. Also the development of a new core composition for increased optical-to-optical amplification efficiency and possibly even larger core diameters would be feasible according to the fiber manufacturer. Larger core diameters would allow for further increase of the SBS threshold and/or larger pump cladding diameters for decreasing the requirements on the pump source brightness. As for all photonic crystal fibers also the developments of monolithic pump and signal couplers would be highly interesting. However, such developments are challenging because of the air-hole structures used in current PCF designs. Until a reliable solution for the problems with monolithic coupler technology is found, free space coupling will be necessary for PCF systems.



## Table of Acronyms

**cw** abbreviation for "continuous wave"

**GWD** Gravitational Wave Detector

**LIGO** Laser Interferometer Gravitational Wave Observatory

**MOPA** Master-Oscillator Power-Amplifier

**NPRO** Non-Planar Ring Oscillator

**YAG** Yttrium Aluminum Garnet

**NA** Numerical Aperture

**LMA** Large Mode Area

**ASE** Amplified Spontaneous Emission

**SBS** Stimulated Brillouin Scattering

**PCF** Photonic Crystal Fiber

**LCF** Leakage Channel Fiber

**LPF** Large Pitch Fiber

**FWHM** Full Width at Half Maximum

**CCC** Chirally Coupled Core

**MFC** Multifilament Core

**MCF** Multi-Core Fiber

**FBG** Fiber Bragg Grating

**TFB** Tapered Fiber Bundle

**WDM** Wavelength Division Multiplexer

## *7 Outlook*

**DFB** Distributed Feedback

**OSA** Optical Spectrum Analyzer

**ECDL** External Cavity Diode Laser

## Bibliography

- [1] B. Willke, N. Uehara, E. K. Gustafson, R. L. Byer, P. J. King, S. U. Seel and R. L. Savage, Jr. “Spatial and temporal filtering of a 10-W Nd:YAG laser with a Fabry–Perot ring-cavity premode cleaner”. *Optics Letters*, vol. 23, no. 21, pp. 1704–1706, 1998
- [2] L. Winkelmann, O. Puncken, R. Kluzik, C. Veltkamp, P. Kwee, J. Poeld, C. Bogan, B. Willke, M. Frede, J. Neumann, P. Wessels and D. Kracht. “Injection-locked single-frequency laser with an output power of 220 W”. *Applied Physics B: Lasers and Optics*, vol. 102, no. 3, pp. 529–538, 2011
- [3] B. Willke, K. Danzmann, M. Frede, P. King, D. Kracht, P. Kwee, O. Puncken, R. L. Savage, Jr., B. Schulz, F. Seifert, C. Veltkamp, S. Wagner, P. Weßels and L. Winkelmann. “Stabilized lasers for advanced gravitational wave detectors”. *Classical and Quantum Gravity*, vol. 25, no. 11, p. 114040, 2008
- [4] L. Winkelmann, O. Puncken, C. Veltkamp, R. Kluzik, M. Frede, J. Neumann, D. Kracht and P. Weßels. “210 W Single-Frequency Laser with 88% of Output Power in TEM<sub>00</sub> Mode for Advanced LIGO”. In “Frontiers in Optics”, p. JTUA2. Optical Society of America, 2009
- [5] M. Punturo et al. “The third generation of gravitational wave observatories and their science reach”. *Classical and Quantum Gravity*, vol. 27, no. 8, p. 084007, 2010
- [6] N. Mavalvala, D. McClelland, G. Mueller, D. Reitze, R. Schnabel and B. Willke. “Lasers and optics: looking towards third generation gravitational wave detectors”. *General Relativity and Gravitation*, vol. 43, no. 2, pp. 569–592, 2011
- [7] M. Frede, B. Schulz, R. Wilhelm, P. Kwee, F. Seifert, B. Willke and D. Kracht. “Fundamental mode, single-frequency laser amplifier for gravitational wave detectors”. *Optics Express*, vol. 15, no. 2, pp. 459–465, 2007

## *Bibliography*

- [8] T. J. Kane and R. L. Byer. “Monolithic, unidirectional single-mode Nd:YAG ring laser”. *Optics Letters*, vol. 10, no. 2, pp. 65–67, 1985
- [9] M. Hildebrandt, M. Frede, P. Kwee, B. Willke and D. Kracht. “Single-frequency master-oscillator photonic crystal fiber amplifier with 148 W output power”. *Optics Express*, vol. 14, no. 23, pp. 11071–11076, 2006
- [10] C. Spiegelberg, J. Geng, Y. Hu, Y. Kaneda, S. Jiang and N. Peyghambarian. “Low-Noise Narrow-Linewidth Fiber Laser at 1550 nm (June 2003)”. *Journal of Lightwave Technology*, vol. 22, no. 1, p. 57, 2004
- [11] A. Tünnermann, T. Schreiber and J. Limpert. “Fiber lasers and amplifiers: an ultrafast performance evolution”. *Applied Optics*, vol. 49, no. 25, pp. F71–F78, 2010
- [12] J. D. Jones and P. Urquhart. “An injection-locked erbium fibre laser”. *Optics Communications*, vol. 76, no. 1, pp. 42 – 46, 1990
- [13] T. C. Teyo, V. Sinivasagam, M. K. Abdullah and H. Ahmad. “An injection-locked erbium-doped fibre ring laser”. *Optics & Laser Technology*, vol. 31, no. 7, pp. 493 – 496, 1999
- [14] M. Frede, R. Wilhelm, M. Brendel, C. Fallnich, F. Seifert, B. Willke and K. Danzmann. “High power fundamental mode Nd:YAG laser with efficient birefringence compensation”. *Optics Express*, vol. 12, no. 15, pp. 3581–3589, 2004
- [15] O. Puncken, H. Tünnermann, J. J. Morehead, P. Weßels, M. Frede, J. Neumann and D. Kracht. “Intrinsic reduction of the depolarization in Nd:YAG crystals”. *Optics Express*, vol. 18, no. 19, pp. 20461–20474, 2010
- [16] D. Garbuzov, I. Kudryashov and M. Dubinskii. “Resonantly diode laser pumped 1.6- $\mu$ m-erbium-doped yttrium aluminum garnet solid-state laser”. *Applied Physics Letters*, vol. 86, no. 13, 131115, 2005
- [17] J. Kim, D. Shen, J. Sahu and W. Clarkson. “Fiber-Laser-Pumped Er:YAG Lasers”. *IEEE Journal of Selected Topics in Quantum Electronics*, vol. 15, no. 2, pp. 361 –371, 2009
- [18] N. Ter-Gabrielyan, L. D. Merkle, E. R. Kupp, G. L. Messing and M. Dubinskii. “Efficient resonantly pumped tape cast composite ceramic Er:YAG laser at 1645 nm”. *Optics Letters*, vol. 35, no. 7, pp. 922–924, 2010

- [19] N. Ter-Gabrielyan, L. D. Merkle, A. Ikesue and M. Dubinskii. “Ultralow quantum-defect eye-safe Er:Sc<sub>2</sub>O<sub>3</sub> laser”. *Optics Letters*, vol. 33, no. 13, pp. 1524–1526, 2008
- [20] G. P. Agrawal. *Nonlinear Fiber Optics*. Elsevier, fourth ed., 2007. ISBN 0-12-369516-3
- [21] J. C. Knight, T. A. Birks, P. S. J. Russell and D. M. Atkin. “All-silica single-mode optical fiber with photonic crystal cladding”. *Optics Letters*, vol. 21, no. 19, pp. 1547–1549, 1996
- [22] W. S. Wong, X. Peng, J. M. McLaughlin and L. Dong. “Breaking the limit of maximum effective area for robust single-mode propagation in optical fibers”. *Optics Letters*, vol. 30, no. 21, pp. 2855–2857, 2005
- [23] P. Yeh, A. Yariv and E. Marom. “Theory of Bragg fiber”. *Journal of the Optical Society of America*, vol. 68, no. 9, pp. 1196–1201, 1978
- [24] A. Argyros. “Guided modes and loss in Bragg fibres”. *Optics Express*, vol. 10, no. 24, pp. 1411–1417, 2002
- [25] L. Poladian, M. Straton, A. Docherty and A. Argyros. “Pure chiral optical fibres”. *Optics Express*, vol. 19, no. 2, pp. 968–980, 2011
- [26] A. E. Siegman. “Propagating modes in gain-guided optical fibers”. *Journal of the Optical Society of America A: Optics, Image Science, and Vision*, vol. 20, no. 8, pp. 1617–1628, 2003
- [27] C. J. Koester and E. Snitzer. “Amplification in a Fiber Laser”. *Applied Optics*, vol. 3, no. 10, pp. 1182–1186, 1964
- [28] D. Marcuse. “Gaussian approximation of the fundamental modes of graded-index fibers”. *Journal of the Optical Society of America B: Optical Physics*, vol. 68, no. 1, pp. 103–109, 1978
- [29] D. Gloge. “Weakly Guiding Fibers”. *Applied Optics*, vol. 10, no. 10, pp. 2252–2258, 1971
- [30] J. A. Buck. *Fundamentals of Optical Fibers*. Wiley Series in Pure and Applied Optics. Wiley & Sons, second ed., 2004. ISBN 0-47-122191-0
- [31] Website of Laserline GmbH, "[www.laserline.de](http://www.laserline.de)"

## *Bibliography*

- [32] E. Snitzer, H. Po, F. Hakimi, R. Tumminelli and B. McCollum. “Double Clad, Offset Core Nd Fiber Laser”. In “Optical Fiber Sensors”, p. PD5. Optical Society of America, 1988
- [33] D. J. Richardson, J. Nilsson and W. A. Clarkson. “High power fiber lasers: current status and future perspectives [Invited]”. *Journal of the Optical Society of America B: Optical Physics*, vol. 27, no. 11, pp. B63–B92, 2010
- [34] D. Nguyen, A. Chavez-Pirson, S. Jiang and N. Peyghambarian. “A Novel Approach of Modeling Cladding-Pumped Highly Er-Yb Co-Doped Fiber Amplifiers”. *IEEE Journal of Quantum Electronics*, vol. 43, no. 11, pp. 1018–1027, 2007
- [35] D. Kouznetsov, J. V. Moloney and E. M. Wright. “Efficiency of pump absorption in double-clad fiber amplifiers. I. Fiber with circular symmetry”. *Journal of the Optical Society of America B: Optical Physics*, vol. 18, no. 6, pp. 743–749, 2001
- [36] D. Kouznetsov and J. V. Moloney. “Efficiency of pump absorption in double-clad fiber amplifiers. II. Broken circular symmetry”. *Journal of the Optical Society of America B: Optical Physics*, vol. 19, no. 6, pp. 1259–1263, 2002
- [37] H. Po, E. Snitzer, R. Tumminelli, L. Zenteno, F. Hakimi, N. M. Cho and T. Haw. “Double Clad High Brightness Nd Fiber Laser Pumped by GaAlAs Phased Array”. In “Optical Fiber Communication Conference”, p. PD7. Optical Society of America, 1989
- [38] H. Zellmer, A. Tünnermann, H. Welling and V. Reichel. “Double-Clad Fiber Laser with 30 W Output Power”. In “Optical Amplifiers and Their Applications”, p. FAW18. Optical Society of America, 1997
- [39] A. Siegman and S. Townsend. “Output beam propagation and beam quality from a multimode stable-cavity laser”. *IEEE Journal of Quantum Electronics*, vol. 29, no. 4, pp. 1212–1217, 1993
- [40] A. E. Siegman. “How to (Maybe) Measure Laser Beam Quality”. In “DPSS (Diode Pumped Solid State) Lasers: Applications and Issues”, p. MQ1. Optical Society of America, 1998

- [41] M.-A. Lapointe, S. Chatigny, M. Piché, M. Cain-Skaff and J.-N. Maran. “Thermal effects in high-power CW fiber lasers”. *Proceedings of SPIE*, vol. 7195, no. 1, 71951U, 2009
- [42] J. L. Mrotek, M. J. Matthewson and C. R. Kurkjian. “Diffusion of Moisture Through Optical Fiber Coatings”. *Journal of Lightwave Technology*, vol. 19, no. 7, p. 988, 2001
- [43] J. Sahu, C. Renaud, K. Furusawa, R. Selvas, J. Alvarez-Chavez, D. Richardson and J. Nilsson. “Jacketed air-clad cladding pumped ytterbium-doped fibre laser with wide tuning range”. *Electronics Letters*, vol. 37, no. 18, pp. 1116–1117, 2001
- [44] K. Furusawa, A. Malinowski, J. Price, T. Monro, J. Sahu, J. Nilsson and D. Richardson. “Cladding pumped Ytterbium-doped fiber laser with holey inner and outer cladding”. *Optics Express*, vol. 9, no. 13, pp. 714–720, 2001
- [45] W. Wadsworth, R. Percival, G. Bouwmans, J. Knight and P. Russell. “High power air-clad photonic crystal fibre laser”. *Optics Express*, vol. 11, no. 1, pp. 48–53, 2003
- [46] J. Limpert, A. Liem, H. Zellmer and A. Tünnermann. “500 W continuous-wave fibre laser with excellent beam quality”. *Electronics Letters*, vol. 39, no. 8, pp. 645–647, 2003
- [47] N. A. Mortensen. “Air-clad fibers: pump absorption assisted by chaotic wave dynamics?” *Optics Express*, vol. 15, no. 14, pp. 8988–8996, 2007
- [48] C. Codemard, J. Sahu and J. Nilsson. “Tandem Cladding-Pumping for Control of Excess Gain in Ytterbium-Doped Fiber Amplifiers”. *IEEE Journal of Quantum Electronics*, vol. 46, no. 12, pp. 1860–1869, 2010
- [49] Website of IPG Photonics Corporation, "[www.ipgphotonics.com](http://www.ipgphotonics.com)"
- [50] V. Gapontsev, V. Fomin, A. Ferin and M. Abramov. “Diffraction Limited Ultra-High-Power Fiber Lasers”. In “Advanced Solid-State Photonics”, p. AWA1. Optical Society of America, 2010
- [51] Y.-C. Jeong, A. J. Boyland, J. K. Sahu, S.-H. Chung, J. Nilsson and D. N. Payne. “Multi-kilowatt Single-mode Ytterbium-doped Large-core Fiber Laser”. *Journal of the Optical Society of Korea*, vol. 13, no. 4, pp. 416–422, 2009



## *Bibliography*

- [52] Y. Jeong, J. Nilsson, J. Sahu, D. Payne, R. Horley, L. Hickey and P. Turner. “Power Scaling of Single-Frequency Ytterbium-Doped Fiber Master-Oscillator Power-Amplifier Sources up to 500 W”. *IEEE Journal of Selected Topics in Quantum Electronics*, vol. 13, no. 3, pp. 546–551, 2007
- [53] S. Gray, A. Liu, D. T. Walton, J. Wang, M.-J. Li, X. Chen, A. B. Ruffin, J. A. DeMeritt and L. A. Zenteno. “502 Watt, single transverse mode, narrow linewidth, bidirectionally pumped Yb-doped fiber amplifier”. *Optics Express*, vol. 15, no. 25, pp. 17044–17050, 2007
- [54] C. Zhu, I.-N. Hu, X. Ma and A. Galvanauskas. “Single-frequency and single-transverse mode Yb-doped CCC fiber MOPA with robust polarization SBS-free 511W output”. In “Advanced Solid-State Photonics”, p. AMC5. Optical Society of America, 2011
- [55] T. Miya, Y. Terunuma, T. Hosaka and T. Miyashita. “Ultimate low-loss single-mode fibre at 1.55  $\mu\text{m}$ ”. *Electronics Letters*, vol. 15, no. 4, pp. 106–108, 1979
- [56] Website of Corning Incorporated, "[www.corning.com](http://www.corning.com)"
- [57] E. Desurvire, D. Bayart, B. Desthieux and S. Bigo. *Erbium-Doped Fiber Amplifiers : Device and System Developments*. Lavoisier, 2002. ISBN 0-47-141903-6
- [58] P. Moulton, G. Rines, E. Slobodtchikov, K. Wall, G. Frith, B. Samson and A. Carter. “Tm-Doped Fiber Lasers: Fundamentals and Power Scaling”. *IEEE Journal of Selected Topics in Quantum Electronics*, vol. 15, no. 1, pp. 85–92, 2009
- [59] G. D. Goodno, L. D. Book and J. E. Rothenberg. “Low-phase-noise, single-frequency, single-mode 608 W thulium fiber amplifier”. *Optics Letters*, vol. 34, no. 8, pp. 1204–1206, 2009
- [60] J. W. Dawson, M. J. Messerly, R. J. Beach, M. Y. Shverdin, E. A. Stappaerts, A. K. Sridharan, P. H. Pax, J. E. Heebner, C. W. Siders and C. Barty. “Analysis of the scalability of diffraction-limited fiber lasers and amplifiers to high average power”. *Optics Express*, vol. 16, no. 17, pp. 13240–13266, 2008
- [61] M. Laroche, S. Girard, J. K. Sahu, W. A. Clarkson and J. Nilsson. “Accurate efficiency evaluation of energy-transfer processes in phosphosilicate  $\text{Er}^{3+}\text{-Yb}^{3+}$

- codoped fibers". *Journal of the Optical Society of America B: Optical Physics*, vol. 23, no. 2, pp. 195–202, 2006
- [62] R. Paschotta, J. Nilsson, A. Tropper and D. Hanna. "Ytterbium-doped fiber amplifiers". *IEEE Journal of Quantum Electronics*, vol. 33, no. 7, pp. 1049–1056, 1997
- [63] W. Miniscalco. "Erbium-doped glasses for fiber amplifiers at 1500 nm". *Journal of Lightwave Technology*, vol. 9, no. 2, pp. 234–250, 1991
- [64] S. Jackson, A. Sabella and D. Lancaster. "Application and Development of High-Power and Highly Efficient Silica-Based Fiber Lasers Operating at 2  $\mu\text{m}$ ". *IEEE Journal of Selected Topics in Quantum Electronics*, vol. 13, no. 3, pp. 567–572, 2007
- [65] P. Blixt, J. Nilsson, T. Carlnäs and B. Jaskorzynska. "Concentration-dependent upconversion in  $\text{Er}^{3+}$ -doped fiber amplifiers: Experiments and modeling". *IEEE Photonics Technology Letters*, vol. 3, no. 11, pp. 996–998, 1991
- [66] E. Maurice, G. Monnom, B. Dussardier and D. B. Ostrowsky. "Clustering-induced nonsaturable absorption phenomenon in heavily erbium-doped silica fibers". *Optics Letters*, vol. 20, no. 24, p. 2487, 1995
- [67] A. V. Kir'yánov, Y. O. Barmenkov and N. N. Il'ichev. "Excited-state absorption and ion pairs as sources of nonlinear losses in heavily doped Erbium silica fiber and Erbium fiber laser". *Optics Express*, vol. 13, no. 21, pp. 8498–8507, 2005
- [68] M. Wießell. "Untersuchungen an Erbium-dotierten Faserverstärkern". Diplomarbeit, Leibniz Universität Hannover, 2009
- [69] K. Tankala, B. Samson, A. Carter, J. Farroni, D. Machewirth, N. Jacobson, U. Manyam, A. Sanchez, M.-Y. Cheng, A. Galvanauskas, W. Torruellas and Y. Chen. "New developments in high power eye-safe LMA fibers". *Proceedings of SPIE*, vol. 6102, 610206, 2006
- [70] D. C. Brown and H. J. Hoffman. "Thermal, stress, and thermo-optic effects in high average power double-clad silica fiber lasers". *IEEE Journal of Quantum Electronics*, vol. 37, no. 2, pp. 207–217, 2001
- [71] R. Kashyap and K. Blow. "Observation of catastrophic self-propelled self-focusing in optical fibres". *Electronics Letters*, vol. 24, no. 1, pp. 47–49, 1988

## *Bibliography*

- [72] D. P. Hand and P. S. J. Russell. "Solitary thermal shock waves and optical damage in optical fibers: the fiber fuse". *Optics Letters*, vol. 13, no. 9, pp. 767–769, 1988
- [73] S. Todoroki. "Origin of periodic void formation during fiber fuse". *Optics Express*, vol. 13, no. 17, pp. 6381–6389, 2005
- [74] I. A. Bufetov, A. A. Frolov, E. M. Dianov, V. E. Fortov and V. P. Efremov. "Dynamics of fiber fuse propagation". In "Proc. Technical Digest Optical Fiber Communication Conference OFC/NFOEC", p. OThQ7. 2005
- [75] S. Yanagi, S. Asakawa, M. Kobayashi, Y. Shuto and R. Nagase. "Fiber fuse terminator". In "The 5th Pacific Rim Conference on Lasers and Electro-Optics, 2003. CLEO/Pacific Rim 2003.", p. 386. 2003
- [76] K. S. Abedin and M. Nakazawa. "Real time monitoring of a fiber fuse using an optical time-domain reflectometer". *Optics Express*, vol. 18, no. 20, pp. 21315–21321, 2010
- [77] J. Limpert, T. Schreiber, A. Liem, S. Nolte, H. Zellmer, T. Peschel, V. Guyenot and A. Tünnermann. "Thermo-optical properties of air-clad photonic crystal fiber lasers in high power operation". *Optics Express*, vol. 11, no. 22, pp. 2982–2990, 2003
- [78] G. Canat, L. Lombard, S. Jetschke, S. Unger, J. Kirchhof, H.-R. Müller, A. Durécu, V. Jolivet and P. Bourdon. "Er-Yb-Doped LMA Fiber Structures for High Energy Amplification of Narrow Linewidth Pulses at 1.5  $\mu\text{m}$ ". In "Conference on Lasers and Electro-Optics 2007. CLEO 2007.", p. CTuBB1. Optical Society of America, 2007
- [79] Website of Nufern, "[www.nufern.com](http://www.nufern.com)"
- [80] M. Hildebrandt, M. Frede and D. Kracht. "Narrow-linewidth ytterbium-doped fiber amplifier system with 45 nm tuning range and 133 W of output power". *Optics Letters*, vol. 32, no. 16, pp. 2345–2347, 2007
- [81] M. E. Fermann. "Single-mode excitation of multimode fibers with ultrashort pulses". *Optics Letters*, vol. 23, no. 1, pp. 52–54, 1998

- [82] B. Morasse, S. Chatigny, C. Desrosiers, Éric Gagnon, M.-A. Lapointe and J.-P. de Sandro. “Simple design for singlemode high power CW fiber laser using multimode high NA fiber”. *Proceedings of SPIE*, vol. 7195, 719505, 2009
- [83] K. K. Chen, J. H. V. Price, S. ul Alam, J. R. Hayes, D. Lin, A. Malinowski and D. J. Richardson. “Polarisation maintaining 100W Yb-fiber MOPA producing  $\mu$ J pulses tunable in duration from 1 to 21 ps”. *Optics Express*, vol. 18, no. 14, pp. 14385–14394, 2010
- [84] W. Torruellas, Y. Chen, B. McIntosh, J. Farroni, K. Tankala, S. Webster, D. Hagan, M. J. Soileau, M. Messerly and J. Dawson. “High peak power ytterbium-doped fiber amplifiers”. p. 61020N. *SPIE*, 2006
- [85] J. P. Kopolow, L. Goldberg, R. P. Moeller and D. A. Kliner. “Polarization-maintaining, double-clad fiber amplifier employing externally applied stress-induced birefringence”. *Optics Letters*, vol. 25, no. 6, pp. 387–389, 2000
- [86] R. Schermer and J. Cole. “Improved Bend Loss Formula Verified for Optical Fiber by Simulation and Experiment”. *IEEE Journal of Quantum Electronics*, vol. 43, no. 10, pp. 899–909, 2007
- [87] R. T. Schermer. “Mode scalability in bent optical fibers”. *Optics Express*, vol. 15, no. 24, pp. 15674–15701, 2007
- [88] J. M. Fini. “Intuitive modeling of bend distortion in large-mode-area fibers”. *Optics Letters*, vol. 32, no. 12, pp. 1632–1634, 2007
- [89] T. Eidam, S. Hanf, E. Seise, T. V. Andersen, T. Gabler, C. Wirth, T. Schreiber, J. Limpert and A. Tünnermann. “Femtosecond fiber CPA system emitting 830 W average output power”. *Optics Letters*, vol. 35, no. 2, pp. 94–96, 2010
- [90] F. Jansen, F. Stutzki, H.-J. Otto, M. Baumgartl, C. Jauregui, J. Limpert and A. Tünnermann. “The influence of index-depressions in core-pumped Yb-doped large pitch fibers”. *Optics Express*, vol. 18, no. 26, pp. 26834–26842, 2010
- [91] J. Knight, T. Birks, R. Cregan, P. Russell and P. de Sandro. “Large mode area photonic crystal fibre”. *Electronics Letters*, vol. 34, no. 13, pp. 1347–1348, 1998
- [92] Website of NKT Photonics A/S, "[www.nktpotonics.com](http://www.nktpotonics.com)"

## *Bibliography*

- [93] O. Schmidt, J. Rothhardt, T. Eidam, F. Röser, J. Limpert, A. Tünnermann, K. P. Hansen, C. Jakobsen and J. Broeng. “Single-polarization ultra-large-mode-area Yb-doped photonic crystal fiber”. *Optics Express*, vol. 16, no. 6, pp. 3918–3923, 2008
- [94] R. F. Cregan, J. C. Knight, P. S. J. Russell and P. J. Roberts. “Distribution of Spontaneous Emission from an Er<sup>3+</sup>-Doped Photonic Crystal Fiber”. *Journal of Lightwave Technology*, vol. 17, no. 11, p. 2138, 1999
- [95] A. Cucinotta, F. Poli, S. Selleri, L. Vincetti and M. Zoboli. “Amplification Properties of Er<sup>3+</sup>-Doped Photonic Crystal Fibers”. *Journal of Lightwave Technology*, vol. 21, no. 3, p. 782, 2003
- [96] C.-H. Liu, G. Chang, N. Litchinitser, D. Guertin, N. Jacobsen, K. Tankala and A. Galvanauskas. “Chirally Coupled Core Fibers at 1550-nm and 1064-nm for Effectively Single-Mode Core Size Scaling”. In “Conference on Lasers and Electro-Optics, 2007. CLEO 2007”, p. CTuBB3. 2007
- [97] H.-W. Chen, T. Sosnowski, C.-H. Liu, L.-J. Chen, J. R. Birge, A. Galvanauskas, F. X. Kärtner and G. Chang. “Chirally-coupled-core Yb-fiber laser delivering 80-fs pulses with diffraction-limited beam quality warranted by a high-dispersion mirror based compressor”. *Optics Express*, vol. 18, no. 24, pp. 24699–24705, 2010
- [98] L. Dong, H. A. McKay, L. Fu, M. Ohta, A. Marcinkevicius, S. Suzuki and M. E. Fermann. “Ytterbium-doped all glass leakage channel fibers with highly fluorine-doped silica pump cladding”. *Optics Express*, vol. 17, no. 11, pp. 8962–8969, 2009
- [99] F. Stutzki, F. Jansen, T. Eidam, A. Steinmetz, C. Jauregui, J. Limpert and A. Tünnermann. “High average power large-pitch fiber amplifier with robust single-mode operation”. *Optics Letters*, vol. 36, no. 5, pp. 689–691, 2011
- [100] S. Wielandy. “Implications of higher-order mode content in large mode area fibers with good beam quality”. *Optics Express*, vol. 15, no. 23, pp. 15402–15409, 2007
- [101] A. E. Siegman. “Gain-guided, index-antiguidded fiber lasers”. *Journal of the Optical Society of America B: Optical Physics*, vol. 24, no. 8, pp. 1677–1682, 2007

- [102] Y. Chen, T. McComb, V. Sudesh, M. Richardson and M. Bass. “Very large-core, single-mode, gain-guided, index-antiguided fiber lasers”. *Optics Letters*, vol. 32, no. 17, pp. 2505–2507, 2007
- [103] W. Hageman, Y. Chen, X. Wang, L. Gao, G. U. Kim, M. Richardson and M. Bass. “Scalable side-pumped, gain-guided index-antiguided fiber laser”. *Journal of the Optical Society of America B: Optical Physics*, vol. 27, no. 12, pp. 2451–2459, 2010
- [104] G. Canat, R. Spittel, S. Jetschke, L. Lombard and P. Bourdon. “Analysis of the multifilament core fiber using the effective index theory”. *Optics Express*, vol. 18, no. 5, pp. 4644–4654, 2010
- [105] M. M. Vogel, M. Abdou-Ahmed, A. Voss and T. Graf. “Very-large-mode-area, single-mode multicore fiber”. *Optics Letters*, vol. 34, no. 18, pp. 2876–2878, 2009
- [106] J. M. Fini. “Large-mode-area multicore fibers in the single-moded regime”. *Optics Express*, vol. 19, no. 5, pp. 4042–4046, 2011
- [107] C. Jauregui, T. Eidam, J. Limpert and A. Tünnermann. “The impact of modal interference on the beam quality of high-power fiber amplifiers”. *Optics Express*, vol. 19, no. 4, pp. 3258–3271, 2011
- [108] P. Russell. “Photonic Crystal Fibers”. *Science*, vol. 299, no. 5605, pp. 358–362, 2003
- [109] N. Andermahr and C. Fallnich. “Interaction of transverse modes in a single-frequency few-mode fiber amplifier caused by local gain saturation”. *Optics Express*, vol. 16, no. 12, pp. 8678–8684, 2008
- [110] N. Andermahr and C. Fallnich. “Modeling of transverse mode interaction in large-mode-area fiber amplifiers”. *Optics Express*, vol. 16, no. 24, pp. 20038–20046, 2008
- [111] R. Y. Chiao, C. H. Townes and B. P. Stoicheff. “Stimulated Brillouin Scattering and Coherent Generation of Intense Hypersonic Waves”. *Physical Review Letters*, vol. 12, no. 21, pp. 592–595, 1964

## *Bibliography*

- [112] R. G. Smith. “Optical Power Handling Capacity of Low Loss Optical Fibers as Determined by Stimulated Raman and Brillouin Scattering”. *Applied Optics*, vol. 11, no. 11, pp. 2489–2494, 1972
- [113] E. Ippen and R. Stolen. “Stimulated Brillouin scattering in optical fibers”. *Applied Physics Letters*, vol. 21, no. 11, pp. 539–541, 1972
- [114] R. W. Boyd. *Nonlinear Optics*. Academic Press, second ed., 2003. ISBN 0-12-121682-9
- [115] M. Hildebrandt, S. Buesche, P. Weßels, M. Frede and D. Kracht. “Brillouin scattering spectra in high-power single-frequency ytterbium doped fiber amplifiers”. *Optics Express*, vol. 16, no. 20, pp. 15970–15979, 2008
- [116] I. Dajani, C. Zeringue, T. J. Bronder, T. Shay, A. Gavrielides and C. Robin. “A theoretical treatment of two approaches to SBS mitigation with two-tone amplification”. *Optics Express*, vol. 16, no. 18, pp. 14233–14247, 2008
- [117] C. Zeringue, C. Vergien and I. Dajani. “Pump-limited, 203 W, single-frequency monolithic fiber amplifier based on laser gain competition”. *Optics Letters*, vol. 36, no. 5, pp. 618–620, 2011
- [118] I. Dajani, C. Zeringue, C. Lu, C. Vergien, L. Henry and C. Robin. “Stimulated Brillouin scattering suppression through laser gain competition: scalability to high power”. *Optics Letters*, vol. 35, no. 18, pp. 3114–3116, 2010
- [119] M. D. Mermelstein, A. D. Yablon and C. Headley. “Suppression of Stimulated Brillouin Scattering in an Er-Yb Fiber Amplifier Utilizing Temperature-Segmentation”. In “*Optical Amplifiers and Their Applications*”, p. TuD3. Optical Society of America, 2005
- [120] S. Yoo, C. A. Codemard, Y. Jeong, J. K. Sahu and J. Nilsson. “Analysis and optimization of acoustic speed profiles with large transverse variations for mitigation of stimulated Brillouin scattering in optical fibers”. *Applied Optics*, vol. 49, no. 8, pp. 1388–1399, 2010
- [121] A. Kobayakov, M. Sauer and D. Chowdhury. “Stimulated Brillouin scattering in optical fibers”. *Advances in Optics and Photonics*, vol. 2, no. 1, pp. 1–59, 2010



- [122] C. E. Dilley, M. A. Stephen and M. P. Savage-Leuchs. “High SBS-threshold, narrowband, erbium codoped with ytterbium fiber amplifier pulses frequency-doubled to 770 nm”. *Optics Express*, vol. 15, no. 22, pp. 14389–14395, 2007
- [123] J. W. Dawson, M. J. Messerly, J. E. Heebner, P. H. Pax, A. K. Sridharan, A. L. Bullington, R. J. Beach, C. W. Siders, C. P. J. Barty and M. Dubinskii. “Power scaling analysis of fiber lasers and amplifiers based on non-silica materials”. *Proceedings of SPIE*, vol. 7686, 768611, 2010
- [124] A. Wetter, M. Faucher, B. Sévigny and N. Vachon. “High core and cladding isolation termination for high-power lasers and amplifiers”. *Proceedings of SPIE*, vol. 7195, 719521, 2009
- [125] Website of nLight Corporation, "[www.nlight.net](http://www.nlight.net)"
- [126] M. Dubinskii, J. Zhang and V. Ter-Mikirtychev. “Record-efficient, resonantly-pumped, Er-doped singlemode fibre amplifier”. *Electronics Letters*, vol. 45, no. 8, pp. 400–401, 2009
- [127] J. W. Nicholson, M. F. Yan, P. Wisk, J. Fleming, F. DiMarcello, E. Monberg, T. Taunay, C. Headley and D. J. DiGiovanni. “Raman fiber laser with 81 W output power at 1480 nm”. *Optics Letters*, vol. 35, no. 18, pp. 3069–3071, 2010
- [128] S. Ramachandran, J. Fini, M. Mermelstein, J. Nicholson, S. Ghalmi and M. Yan. “Ultra-large effective-area, higher-order mode fibers: a new strategy for high-power lasers”. *Laser & Photonics Review*, vol. 2, no. 6, pp. 429–448, 2008
- [129] J. W. Nicholson, J. M. Fini, A. M. DeSantolo, E. Monberg, F. DiMarcello, J. Fleming, C. Headley, D. J. DiGiovanni, S. Ghalmi and S. Ramachandran. “A higher-order-mode Erbium-doped-fiber amplifier”. *Optics Express*, vol. 18, no. 17, pp. 17651–17657, 2010
- [130] J.-Y. Vinet. “On Special Optical Modes and Thermal Issues in Advanced Gravitational Wave Interferometric Detectors”. *Living Reviews in Relativity*, vol. 12, no. 5, p. 123, 2009
- [131] J. Zhang, V. Fromzel and M. Dubinskii. “Power and Efficiency Scaled Resonantly Cladding-Pumped Er-doped LMA Fiber Lasers”. In “Latin America Optics and Photonics Conference”, p. ME2. Optical Society of America, 2010

## *Bibliography*

- [132] S. G. Grubb, R. S. Cannon, T. W. Windhorn, S. W. Vendetta, P. A. Leilabady, D. W. Anthon, K. L. Sweeney, W. L. Barnes, E. R. Taylor and J. E. Townsend. “High-Power Sensitized Erbium Optical Fiber Amplifier”. In “Optical Fiber Communication”, p. PD7. Optical Society of America, 1991
- [133] J. Townsend, W. Barnes, K. Jedrzejewski and S. Grubb. “Yb<sup>3+</sup> sensitised Er<sup>3+</sup> doped silica optical fibre with ultrahigh transfer efficiency and gain”. *Electronics Letters*, vol. 27, no. 21, pp. 1958–1959, 1991
- [134] E. Snitzer and R. Woodcock. “Yb<sup>3+</sup>-Er<sup>3+</sup> Glass Laser”. *Applied Physics Letters*, vol. 6, no. 3, pp. 45–46, 1965
- [135] E. F. Artem’ev, A. G. Murzin, Y. K. Fedorov and V. A. Fromzel’. “Some characteristics of population inversion of the <sup>4</sup>I<sub>13/2</sub> level of erbium ions in ytterbium-erbium glasses”. *Soviet Journal of Quantum Electronics*, vol. 11, no. 9, p. 1266, 1981
- [136] G. Vienne, J. Caplen, L. Dong, J. Minelly, J. Nilsson and D. Payne. “Fabrication and characterization of Yb<sup>3+</sup>:Er<sup>3+</sup> phosphosilicate fibers for lasers”. *Journal of Lightwave Technology*, vol. 16, no. 11, pp. 1990–2001, 1998
- [137] G. Canat, Y. Jaouën and J.-C. Mollier. “Performance and limitations of high brightness Er<sup>3+</sup>-Yb<sup>3+</sup> fiber sources”. *Comptes Rendus Physique*, vol. 7, no. 2, pp. 177 – 186, 2006. High power fiber lasers and amplifiers
- [138] E. Maurice, G. Monnom, B. Dussardier and D. B. Ostrowsky. “Clustering effects on double energy transfer in heavily ytterbium-erbium-codoped silica fibers”. *Journal of the Optical Society of America B: Optical Physics*, vol. 13, no. 4, p. 693, 1996
- [139] Y. Jeong, S. Yoo, C. Codemard, J. Nilsson, J. Sahu, D. Payne, R. Horley, P. Turner, L. Hickey, A. Harker, M. Lovelady and A. Piper. “Erbium:Ytterbium Codoped Large-Core Fiber Laser With 297-W Continuous-Wave Output Power”. *IEEE Journal of Selected Topics in Quantum Electronics*, vol. 13, no. 3, pp. 573–579, 2007
- [140] Y. Jeong, J. K. Sahu, D. B. S. Soh, C. A. Codemard and J. Nilsson. “High-power tunable single-frequency single-mode erbium:ytterbium codoped large-core fiber master-oscillator power amplifier source”. *Optics Letters*, vol. 30, no. 22, pp. 2997–2999, 2005

- [141] A. Yusim, J. Barsalou, D. Gapontsev, N. S. Platonov, O. Shkurikhin, V. P. Gapontsev, Y. A. Barannikov and F. V. Shcherbina. "100 Watt, single-mode, CW, linearly polarized all-fiber format 1.56 $\mu$ m laser with suppression of parasitic lasing effects". Proceedings of SPIE, vol. 5709, pp. 69–77, 2005
- [142] B. Morasse, S. Agger, C. Hovington, S. Chatigny, Éric Gagnon, J.-P. de Sandro and C. Poulsen. "10W ASE-free single mode high power double cladding Er<sup>3+</sup>-Yb<sup>3+</sup> amplifier". Proceedings of SPIE, vol. 6453, 645324, 2007
- [143] P. Wysocki, T. Wood, A. Grant, D. Holcomb, K.-W. Chang, M. Santo, L. Braun and G. Johnson. "High Reliability 49 dB Gain, 13 W PM Fiber Amplifier at 1550 nm with 30 dB PER and Record Efficiency". In "Optical Fiber Communication Conference and Exposition and The National Fiber Optic Engineers Conference", p. PDP17. Optical Society of America, 2006
- [144] A. Shirakawa, H. Suzuki, M. Tanisho and K. Ueda. "Yb-ASE-Free Er Amplification in Short-Wavelength Filtered Er:Yb Photonic-Crystal Fiber". In "Optical Fiber Communication Conference and Exposition and The National Fiber Optic Engineers Conference", p. OThN2. Optical Society of America, 2008
- [145] G. A. Sefler, W. D. Mack, G. C. Valley and T. S. Rose. "Secondary energy transfer and nonparticipatory Yb<sup>3+</sup> ions in Er<sup>3+</sup>-Yb<sup>3+</sup> high-power amplifier fibers". Journal of the Optical Society of America B: Optical Physics, vol. 21, no. 10, pp. 1740–1748, 2004
- [146] G. C. Valley. "Modeling Cladding-Pumped Er/Yb Fiber Amplifiers". Optical Fiber Technology, vol. 7, no. 1, pp. 21–44, 2001
- [147] M. Federighi and F. Di Pasquale. "The effect of pair-induced energy transfer on the performance of silica waveguide amplifiers with high Er<sup>3+</sup>/Yb<sup>3+</sup> concentrations". IEEE Photonics Technology Letters, vol. 7, no. 3, pp. 303–305, 1995
- [148] B.-C. Hwang, S. Jiang, T. Luo, J. Watson, G. Sorbello and N. Peyghambarian. "Cooperative upconversion and energy transfer of new high Er<sup>3+</sup>- and Yb<sup>3+</sup>-Er<sup>3+</sup>-doped phosphate glasses". Journal of the Optical Society of America B: Optical Physics, vol. 17, no. 5, pp. 833–839, 2000
- [149] R. Paschotta. Manual of "RP Fiber Power V2.0" (Version: 2009-03-06). RP Photonics Consulting GmbH, Waldstr. 17, 78073 Bad Dürkheim, Germany

## *Bibliography*

- [150] J. Lincoln, W. Barnes, W. Brocklesby and J. Townsend. “Spectroscopic evaluation of the vibrational coupling of  $\text{Er}^{3+}$  ions in phospho-aluminosilicate fibres and an explanation of compositional variations in Er-Yb 1.5  $\mu\text{m}$  amplifier performance”. *Journal of Luminescence*, vol. 60-61, pp. 204 – 207, 1994. International Conference on Luminescence
- [151] S. Grubb, W. Humer, R. Cannon, T. Windhorn, S. Vendetta, K. Sweeney, P. Leilabady, W. Barnes, K. Jedrzejewski and J. Townsend. “+21 dBm Erbium Power Amplifier Pumped by a Diode-Pumped Nd:YAG Laser”. *IEEE Photonics Technology Letters*, vol. 4, no. 6, pp. 553–555, 1992
- [152] Q. Han, J. Ning and Z. Sheng. “Numerical Investigation of the ASE and Power Scaling of Cladding-Pumped Er-Yb Codoped Fiber Amplifiers”. *IEEE Journal of Quantum Electronics*, vol. 46, no. 11, pp. 1535 –1541, 2010
- [153] R. Paschotta. “Fiber Amplifiers - Short Course”. In “Cleo Europe 2011”, 2009
- [154] Q. Han, Y. He, Z. Sheng, W. Zhang, J. Ning and H. Xiao. “Numerical characterization of Yb-signal-aided cladding-pumped Er:Yb-codoped fiber amplifiers”. *Opt. Lett.*, vol. 36, no. 9, pp. 1599–1601, 2011
- [155] P. Cheo and G. King. “Clad-pumped Yb,Er codoped fiber lasers”. *IEEE Photonics Technology Letters*, vol. 13, no. 3, pp. 188–190, 2001
- [156] U. Röpke, H. Bartelt, S. Unger, K. Schuster and J. Kobelke. “Two-dimensional high-precision fiber waveguide arrays for coherent light propagation”. *Optics Express*, vol. 15, no. 11, pp. 6894–6899, 2007
- [157] G. Canat, S. Jetschke, S. Unger, L. Lombard, P. Bourdon, J. Kirchhof, V. Jolivet, A. Dolfi and O. Vasseur. “Multifilament-core fibers for high energy pulse amplification at 1.5  $\mu\text{m}$  with excellent beam quality”. *Optics Letters*, vol. 33, no. 22, pp. 2701–2703, 2008
- [158] P. Wessels and C. Fallnich. “Highly sensitive beam quality measurements on large-mode-area fiber amplifiers”. *Optics Express*, vol. 11, no. 25, pp. 3346–3351, 2003
- [159] P. Kwee, F. Seifert, B. Willke and K. Danzmann. “Laser beam quality and pointing measurement with an optical resonator”. *Review of Scientific Instruments*, vol. 78, no. 7, 073103, 2007

- [160] J. Nicholson, J. Jasapara, A. Desantolo, E. Monberg and F. Dimarcello. “Characterizing the Modes of a Core-Pumped, Large-Mode Area Er Fiber Using Spatially and Spectrally Resolved Imaging”. In “Conference on Lasers and Electro-Optics/International Quantum Electronics Conference”, p. CWD4. Optical Society of America, 2009
- [161] R. Scarmozzino, A. Gopinath, R. Pregla and S. Helfert. “Numerical techniques for modeling guided-wave photonic devices”. *IEEE Journal of Selected Topics in Quantum Electronics*, vol. 6, no. 1, pp. 150–162, 2000
- [162] N. A. Mortensen. “Effective area of photonic crystal fibers”. *Opt. Express*, vol. 10, no. 7, pp. 341–348, 2002
- [163] J. L. Gouët, L. Lombard and G. Canat. “Multifilament core fiber mode content and other properties using  $S^2$  characterization”. In “Fiber Laser Applications”, p. FThE6. Optical Society of America, 2011
- [164] G. Canat, L. Lombard, P. Bourdon, V. Jolivet, O. Vasseur, S. Jetschke, S. Unger and J. Kirchhof. “Measurement and modeling of Brillouin scattering in a multifilament core fiber”. In “Conference on Lasers and Electro-Optics 2009. CLEO/QELS 2009.”, p. JTuB3. 2009
- [165] M. Dubinskii and V. V. Ter-Mikirtychev. “Scalable, Single-Frequency, Er-only Doped Fiber Amplifier Cladding-Pumped by Multimode 980-nm Diode Lasers”. In “Advanced Solid-State Photonics”, p. WE24. Optical Society of America, 2008
- [166] M. Dubinskii, J. Zhang and I. Kudryashov. “Power scaling of resonantly cladding-pumped, Yb-free, Er-doped LMA fiber lasers”. *Laser Physics*, vol. 19, pp. 902–905, 2009
- [167] E. Lallier and D. Papillon-Ruggeri. “High energy pulsed eye-safe fiber amplifier”. In “CLEO/Europe and EQEC 2011 Conference Digest”, p. CJ1.5. Optical Society of America, 2011
- [168] J. Zhang, V. Fromzel and M. Dubinskii. “Resonantly cladding-pumped Yb-free Er-doped LMA fiber laser with record high power and efficiency”. *Optics Express*, vol. 19, no. 6, pp. 5574–5578, 2011

## *Bibliography*

- [169] H. D. Baehr and K. Stephan. *Wärme- und Stoffübertragung*. Springer Berlin / Heidelberg, fourth ed., 2004
- [170] J. Jasapara, M. Andrejco, A. DeSantolo, A. Yablon, Z. Várallyay, J. Nicholson, J. Fini, D. DiGiovanni, C. Headley, E. Monberg and F. DiMarcello. “Diffraction-Limited Fundamental Mode Operation of Core-Pumped Very-Large-Mode-Area Er Fiber Amplifiers”. *IEEE Journal of Selected Topics in Quantum Electronics*, vol. 15, no. 1, pp. 3 –11, 2009
- [171] R. S. Quimby. “Output saturation in a 980-nm pumped erbium-doped fiber amplifier”. *Applied Optics*, vol. 30, no. 18, pp. 2546–2552, 1991

## Publications in Peer-Reviewed Journals

- [172] A. Ruehl, V. Kuhn, D. Wandt and D. Kracht. “Normal dispersion erbium-doped fiber laser with pulse energies above 10 nJ”. *Optics Express*, vol. 16, no. 5, pp. 3130–3135, 2008
- [173] V. Kuhn, P. Weßels, J. Neumann and D. Kracht. “Stabilization and power scaling of cladding pumped Er:Yb-codoped fiber amplifier via auxiliary signal at 1064 nm”. *Optics Express*, vol. 17, no. 20, pp. 18304–18311, 2009
- [174] V. Kuhn, S. Unger, S. Jetschke, D. Kracht, J. Neumann, J. Kirchhof and P. Weßels. “Experimental Comparison of Fundamental Mode Content in Er:Yb-Codoped LMA Fibers with Multifilament- and Pedestal-Design Cores”. *J. Lightwave Technol.*, vol. 28, no. 22, pp. 3212–3219, 2010
- [175] V. Kuhn, D. Kracht, J. Neumann and P. Weßels. “Dependence of Er:Yb-Codoped 1.5  $\mu\text{m}$  Amplifier on Wavelength-Tuned Auxiliary Seed Signal at 1  $\mu\text{m}$  Wavelength”. *Optics Letters*, vol. 35, no. 24, pp. 4105–4107, 2010
- [176] V. Kuhn, D. Kracht, J. Neumann and P. Wessels. “67 W of Output Power from an Yb-Free Er-Doped Fiber Amplifier Cladding Pumped at 976 nm”. *IEEE Photon. Technol. Lett.*, vol. 23, no. 7, pp. 432–434, 2011
- [177] V. Kuhn, D. Kracht, J. Neumann and P. Weßels. “Er-doped photonic crystal fiber amplifier with 70 W of output power”. *Opt. Lett.*, vol. 36, no. 16, pp. 3030–3032, 2011



## Publications in Conference Proceedings

- [178] A. Ruehl, V. Kuhn, D. Wandt and D. Kracht. “Passively Mode-Locked Erbium-Doped Fiber Oscillator with Pulse Energies above 10 nJ”. In “Advanced Solid-State Photonics”, p. WB21. Optical Society of America, 2008
- [179] V. Kuhn, D. Wandt, A. Rühl and D. Kracht. “Erbium-Faserlaser im positiven Dispersionsbereich mit Pulsenergien über 10 nJ”. In “DPG Frühjahrstagung”, p. Q46.2. Darmstadt, 2008
- [180] A. Ruehl, V. Kuhn, D. Wandt and D. Kracht. “10 nJ-Normal Dispersion Erbium-Doped Fiber Laser Exhibiting Spectral Filtering”. In “Conference on Lasers and Electro-Optics/Quantum Electronics and Laser Science Conference and Photonic Applications Systems Technologies”, p. CTuFF5. Optical Society of America, 2008
- [181] M. Wießell, V. Kuhn, P. Weßels and J. Neumann. “Einfrequenter Erbium-Faserverstärker als Laserquelle für Gravitationswellendetektoren”. In “DPG Frühjahrstagung”, p. Q12.3. Hamburg, 2009
- [182] V. Kuhn, P. Weßels, J. Neumann and D. Kracht. “Suppression of Parasitic Laser Processes in Cladding Pumped Er:Yb-Codoped Fiber Amplifier via Auxiliary Signal at 1.0  $\mu\text{m}$ ”. In “Advanced Solid-State Photonics (ASSP)”, p. AWB13. San Diego, CA, 2010
- [183] V. Kuhn, D. Wandt, A. Rühl and D. Kracht. “Leistungskalierung Er:Yb-kodotierter Faserverstärker durch Injektion eines Hilfssignals bei 1,0  $\mu\text{m}$ ”. In “DPG Frühjahrstagung”, p. Q12.10. Hannover, 2010
- [184] V. Kuhn, S. Unger, S. Jetschke, D. Kracht, J. Neumann, J. Kirchhof and P. Weßels. “Experimental Comparison of TEM<sub>00</sub> Mode Content in Er:Yb-Codoped LMA Fibers with Cores based on Multifilament- and Pedestal-Designs”. In “Europhoton”, p. TuP7. Hamburg, 2010

- [185] V. Kuhn, D. Kracht, J. Neumann and P. Weßels. “Yb-free Er-doped 976 nm Pumped Large Mode Area Fiber Amplifier with 67 W of Output Power”. In “Advanced Solid State Photonics (ASSP)”, p. ATuB5. Istanbul, 2011
- [186] V. Kuhn, D. Kracht, J. Neumann and P. Weßels. “Yb-free Er-doped 980nm Pumped Single-Frequency Fiber Amplifier with Output Power of 54W and Near-Diffraction Limited Beam Quality”. In “CLEO/Europe and EQEC 2011 Conference Digest”, p. CJ7.5. München, 2011
- [187] V. Kuhn, D. Kracht, J. Neumann and P. Weßels. “Er-doped single-frequency photonic crystal fiber amplifier with 70 W of output power for gravitational wave detection”. In “Fiber Lasers IX: Technology, Systems, and Applications”, pp. 8237–19. 2012. (accepted for oral presentation at Photonics West 2012 and publication in Proceedings of SPIE)

# Curriculum Vitae

## Personal Data

Name: Vincent Kuhn  
Date of birth: February 12<sup>th</sup> 1984  
Place of birth: Hannover  
Nationality: German  
Marital status: Married

## Education

1990 - 1994 Grundschule Georgsstraße, Garbsen  
1994 - 1996 Orientierungsstufe Berenbostel, Garbsen  
1996 - 2003 Geschwister-Scholl-Gymnasium Berenbostel, Garbsen  
06/2003 Abitur

## University Education

10/2003 - 06/2008 Physics at Leibniz University Hannover  
06/2008 Degree "Diplom-Physiker",  
Title of the thesis: "Erbium-dotierter Femtosekunden-Faserlaser mit positiver Resonatordispersion"

## Professional Affiliations

07/2008 - 12/2011 Research Scientist at the Laser Zentrum Hannover e.V., Laser Development Department, Single-Frequency Lasers Group  
07/2011 - 08/2011 Intern at Mitsubishi Electric Corporation, Information Technology R&D Center in Kamakura City, Japan  
from 01/2012 Research Scientist at TRUMPF Laser GmbH + Co. KG

Reviewer for Optics Letters and IEEE Journal of Quantum Electronics.

Member of Deutsche Physikalische Gesellschaft (DPG) and Optical Society of America (OSA).

## **Awards**

12/2011

Award for best publication of the Laser Zentrum Hannover e.V. (LZH) in the year 2011 for "Er-doped photonic crystal fiber amplifier with 70 W of output power", *Opt. Lett.*, vol. 36, no. 16, pp. 3030–3032, 2011. Awarded by board of directors of the LZH.

## Danksagung

Zunächst möchte ich mich bei Herrn Prof. Karsten Danzmann für die Übernahme der Betreuung dieser Arbeit bedanken. Zudem gilt mein Dank auch Herrn Prof. Michael Oestreich für die Übernahme des Korreferats. Bei Dr. Dietmar Kracht und Dr. Jörg Neumann bedanke ich mich für die Möglichkeit meine Arbeiten im Laser Zentrum Hannover e.V. (LZH) durchführen zu können. Außerdem gilt mein Dank auch allen Personen die zum Zustandekommen des Exzellenzclusters "Centre for Quantum Engineering and Space-Time Research" (QUEST) beigetragen haben, in dessen Rahmen ich meine Arbeiten durchgeführt habe.

Mein besonderer Dank gilt Dr. Peter Weßels für seine freundliche und unkomplizierte Art und besonders auch für seine zahlreichen Anregungen und anschaulichen Einsichten die sehr zum Gelingen dieser Arbeit beigetragen haben. Desweiteren bedanke ich mich auch bei allen anderen Mitgliedern der Gruppe "Single-Frequency Lasers", sowie der Abteilung "Lasersentwicklung" des LZH für die gute Zusammenarbeit und angenehme Arbeitsatmosphäre.

Zudem möchte ich meinen Eltern und meiner gesamten Familie danken, die mich immer unterstützt und mir mein Studium ermöglicht haben. Schließlich gilt mein größter Dank meiner Frau Leonore für ihre Geduld und Unterstützung, insbesondere in den sehr ereignisreichen letzten Monaten in denen es für uns beide viel zu planen, erledigen und erfreulicherweise auch feiern gab.